LAWRENCE
LIVERMORE
NATIONAL
LABORATORY

UCRL-LR-139216

Fluorescence Lifetime Measurements of Boronate Derivatives to Determine Glucose Concentration

J. H. Gable

June 1, 2000

This work was performed under the auspices of the U.S. Department of Energy by University of California, Lawrence Livermore National Laboratory under Contract W-7405-Eng-48.

Fluorescence Lifetime Measurements of Boronate Derivatives to Determine Glucose Concentration

BY

JENNIFER HARDER GABLE

B.S. (University of California, Los Angeles) 1993
M.S. (University of California, Davis) 1995

DISSERTATION

Submitted in partial satisfaction of the requirements for the degree of

DOCTOR OF PHILOSOPHY

in

Applied Science

in the

OFFICE OF GRADUATE STUDIES

of the

UNIVERSITY OF CALIFORNIA

Davis

Approved:

_____

_____

_____

_____

Committee in Charge

2000

Jennifer Harder Gable
June 2000
Engineering, Applied Science

Fluorescence Lifetime Measurements of Boronate Derivatives to Determine Glucose Concentration

Abstract

A novel investigation into the fluorescence lifetimes of molecules, both established and newly designed, was performed. These molecules are the basis of a continuous, minimally invasive, glucose sensor based on fluorescence lifetime measurements. This sensor, if coupled with an automated insulin delivery device, would effectively create an artificial pancreas allowing for the constant monitoring and control of glucose levels in a person with diabetes. The proposed sensor includes a fluorescent molecule that changes its' fluorescence properties upon binding selectively and reversibly to glucose. One possible sensor molecule is N-methyl-N-(9-methylene anthryl)-2-methylenephenylboronic acid (AB). The fluorescence intensity of AB was shown to change in response to changing glucose concentrations. (James, 1994) James proposed that when glucose binds to AB the fluorescence intensity increases due to an enhancement of the N→B dative bond which prevents photoinduced electron transfer (PET). PET from the amine (N) to the fluorophore (anthracene) quenches the fluorescence. The dative bond between the boron and the amine can prevent PET by involving the lone pair of electrons on the amine in interactions with the boron rather than allowing them to be transferred to the fluorophore.

Results of this research show the average fluorescence lifetime of AB also changes with glucose concentration. It is proposed that fluorescence is due to two components: 1) AB with an enhanced N→B interaction, and no PET, and 2) AB with a weak N→B interaction, resulting in fluorescence quenching by PET. Lifetime measurements of AB as a function of both the pH of the solvent and glucose concentration in the solution were made to characterize this two component system and investigate the nature of the N→B bond. Measurements of molecules similar to AB were also performed in order to isolate behavior of specific AB constituents. These molecules are 9-(Methylaminomethyl)-anthracene (MAMA), and N-benzyl-N-methyl-N-methyl anthracene (AB-B). Fluorescence lifetime measurements confirmed the two species of AB, with and without PET. Fluorescence lifetimes were approximately 11 nsec without PET and 3 nsec with PET. The degree of the interaction between the N and the B atoms was also determined by fluorescence lifetime measurements. Electron transfer rates of AB were measured to be on the order of 10^8 sec^{-1}. Analysis of AB as a glucose sensor shows it has the potential for measuring glucose concentrations in solution with less than 5% error. Two novel glucose sensing molecules, Chloro-oxazone boronate (COB) and Napthyl-imide boronate (NIB), were synthesized. Both molecules have a N→B dative bond similar to AB, but with longer wavelength fluorophores. COB and NIB were found to be unacceptable for use as glucose sensor molecules due to the small changes in average fluorescence lifetime.

ACKNOWLEDGEMENTS

Fluorescence Lifetime Measurements of Boronate Derivatives to Determine Glucose Concentration

List of Figures and Tables

LIST OF FIGURES AND TABLES

Chapter I

INTRODUCTION

This chapter begins with a description of the glucose sensor under investigation and the approach taken in its development. Next is an overview of diabetes, and reasons why a continuous glucose sensor is necessary for better maintenance of this disease. Then brief descriptions of other current sensor research methods are given for continuous glucose sensors that lend themselves to integration with an insulin pump. A comparison is then given of the advantages and disadvantages of the sensor design used in this research and other designs.

1.1 Sensor Description

The molecule used in the glucose sensor design described in this work was first developed by Tony James et al. (James, 1994). James created anthracene monoboronic acid, referred to as AB in this research, to measure glucose concentrations in the physiological range. This sensor design functions by determining the relative amounts of two molecular populations: AB and ABG (AB with glucose bound). When glucose is bound to the sensor molecule, the anthracene moiety fluoresces (Figure 1.1). Without glucose the anthracene fluorescence of AB is quenched by intramolecular photoinduced electron transfer (PET) as depicted in Figure 1.2. Consequently, the amount of fluorescence is directly related to the concentration of ABG, or the amount of glucose bound to the sensor molecules.

1.1.1 Photoinduced Electron Transfer (PET)

The mechanism causing the fluorescence intensity and lifetime changes of AB is intramolecular photoinduced electron transfer (PET). This is the transfer of an electron from one part of the molecule to another through the overlap of electron orbitals. The molecular design of AB can be divided into three sections: 1) the fluorophore (electron acceptor), 2) the switch (electron donor) that can turn off the fluorescence, and 3) the glucose receptor that controls electron donation. In the case of AB the fluorophore is anthracene, the electron donor/switch is the amine (with its lone pair of electrons), and the glucose receptor is the boronic acid. When glucose is bound, the boronic acid prevents electrons from being transferred to the fluorophore through interaction with the amine electrons. This effectively turns off the PET mechanism and increases the fluorescence intensity (Figure 1.1).

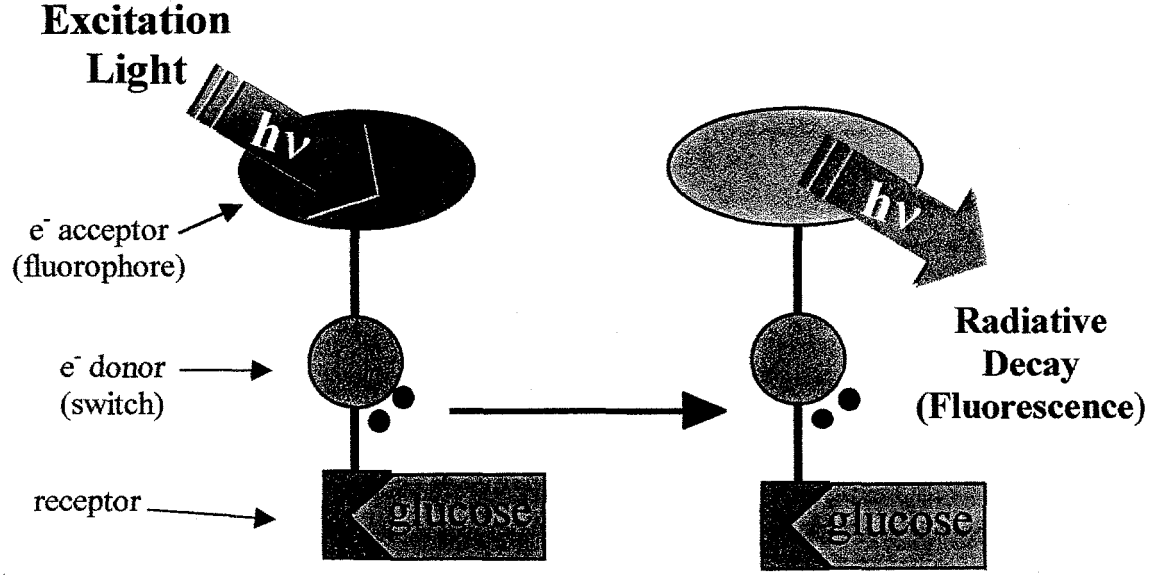

Figure 1.1 – Fluorescence of the sensor molecule when glucose is bound (ABG).

When glucose is not bound to the receptor, an electron from the amine donor is free to be transferred to the excited fluorophore via intramolecular PET, quenching the fluorescence (Figure 1.2).

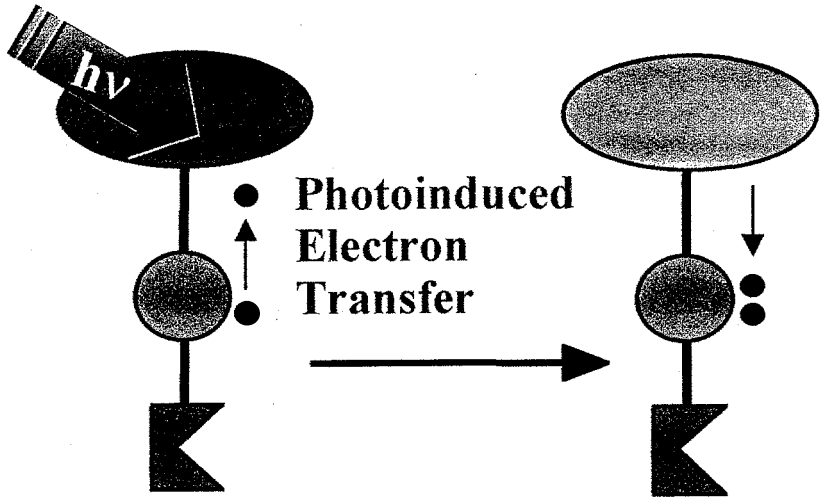

Figure 1.2 – The fluorescence of the sensor molecule (AB) is quenched by photoinduced electron transfer (PET).

The specific interactions between the receptor and the switch of AB will be explained in Chapter Two, and a more detailed discussion of PET follows in Chapter Three.

1.1.2 Fluorescence Lifetimes

Although James reported AB as a glucose sensor molecule based on fluorescence intensity changes, new measurements made here show the fluorescence lifetime also changes with glucose concentration. Fluorescence lifetimes are defined by the average time a fluorophore spends in the excited state before emitting a photon. Measurements of AB and ABG reveal two different and unique fluorescence lifetimes, τ_{AB} and τ_{ABG}

respectively. The fluorescence lifetime of ABG is longer than that of AB because the fluorescence of AB is quenched by PET. However, a small fraction of AB molecules also display the same, unquenched, lifetime as ABG. For the purpose of this introduction, only the shorter, quenched, lifetime of AB will be employed. The dual fluorescence of AB must be taken into account, and will be discussed in detail the next chapter. The total fluorescence as a function of time (F(t)) is a combination of fluorescence from both lifetime components. The contribution (α_{AB} or α_{ABG}) of each fluorescence lifetime component (τ_{AB} or τ_{ABG}) is proportional to the concentration of its relative species ([AB] or [ABG]), as displayed in Equations 1.1 and 1.2.

$$F(t) = (\alpha_{AB})e^{-t/\tau_{AB}} + (\alpha_{ABG})e^{-t/\tau_{ABG}} \quad 1.1$$

$$\frac{\alpha_{AB}}{\alpha_{ABG}} = \frac{[AB]}{[ABG]} \quad 1.2$$

Equations 1.1 and 1.2 will be derived and discussed in Chapter Three. The sensor studied here is based on measuring the change in the average fluorescence lifetime of AB with varying glucose concentrations. Generally, in biosensor design lifetime changes are advantageous over fluorescence intensity changes due to the intrinsic properties of the measurement. Fluorescence lifetimes are independent of the details of the excitation source or the measured fluorescence intensity, providing for more robust sensor design. This will be examined in further detail in Chapter Three.

1.1.3 Sensor Design Challenges

Molecules must have certain characteristics to be acceptable for long term sensing. First of all, they must selectively bind to glucose to avoid false readings. The

receptor of AB binds to other sugars as well as glucose. Fructose, galactose and glucose are the three main sugars found in the blood and interstitial fluid. However, concentrations of glucose in the blood range from 2.2 mM (40mg/dL) to over 11 mM (~200mg/dL), while both galactose and fructose exist in concentrations below 0.1 mM (James, 1994(a)) and can therefore be neglected. The binding of glucose to the sensor molecule must also be reversible. Measurements done by myself and other researchers from the Medical Technology Program (MTP) at Lawrence Livermore National Laboratory (LLNL) have shown that the binding of glucose to AB is reversible on short time scales (< 1sec).

To create a minimally invasive glucose sensor, AB can be incorporated into a biocompatible membrane implanted a few millimeters under the skin surface. Glucose from the interstitial fluid is able to diffuse into the membrane and come into contact with the glucose receptors of AB. The glucose measurement is made using transdermal illumination and fluorescence detection, requiring the excitation and emission wavelengths of the fluorophore to pass through the skin without significant attenuation. The transmission of light through 2.5 mm of skin has been measured by another researcher from the MTP at LLNL. Light transmission was measured through the skin at the web of the hand between the thumb and forefinger. Although skin color and thickness effect the measurement, Figure 1.3 shows a typical example of how light transmission increases at longer wavelengths due to the decrease in light absorption in the tissue.

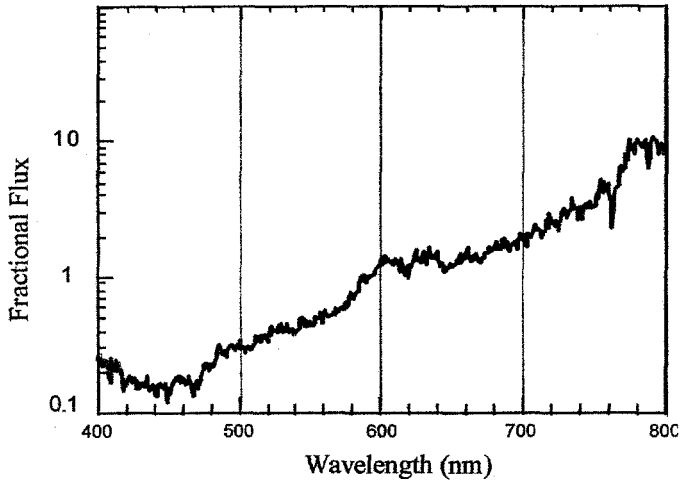

Figure 1.3 – Transmission of light through the skin at the web of the hand (2.5 mm thick).

The excitation and emission wavelengths of AB are 367 nm and 412 nm, respectively. Figure 1.3 shows that wavelengths near 400 nm are too short to travel through a few millimeters of skin without significant attenuation. Therefore it would be desirable to replace the anthracene of AB with another fluorophore with excitation and emission wavelengths between 600 nm and 800 nm. This would allow for the use of excitation light from commercially available LEDs, and for reasonable transmission of excitation and emission light through the skin. It is important to note, although this graph does not show it, as the wavelength increases above 1000 nm absorption by water decreases the transmission of light through skin. (Delpy, 1994)

1.1.4 Research Goals

The goal of this research is to investigate changes in the fluorescence lifetime of the anthracene boronate (AB) molecule as a function of glucose concentration and to understand the mechanisms driving PET. This will also determine its ability to measure

glucose concentration in a minimally invasive glucose sensor for diabetics. Knowledge gained from measurements of AB will be used to create a molecule with a longer wavelength fluorophore, suitable for transdermal sensing. The fluorescence characterization of the new molecule is beyond the scope of this work. To understand the PET mechanism of AB, two other molecules, referred to as MAMA and AB-B, were also investigated. These molecules have a structure similar to AB, but without certain components, allowing for the isolation of the contributions from each component of AB. MAMA consists of the fluorophore and the switch of AB, but lacks the receptor needed for binding glucose and the link between the receptor and the switch. AB-B is one step closer to AB, lacking the glucose receptor but including the link between the receptor and switch. Although MAMA and AB-B do not have a glucose receptor to control PET from the amine donor, hydrogen ions can be used to control the electron transfer. Hydrogen ions bind to the amine (switch) and prevent the transfer of electrons with PET. Therefore, examination of the fluorescence lifetimes of molecules with and without PET was done using a common technique of varying the pH of the solution. This also provides for a measurement of the maximum switching potential of AB to be compared with the fluorescent switching measured as a function of glucose. It is desirable for the degree of fluorescent switching with glucose to approach the value of fluorescent switching found with pH.

Both AB and AB-B have poor solubility in water and were therefore examined in solutions of methanol and water to increase solubility. MAMA, however, is soluble in water and can therefore be examined in 100% aqueous solution. To predict how AB would respond to a completely aqueous environment (*in vivo*), MAMA was examined in

solutions with varying amounts of methanol (0 – 100%) to establish the changes in fluorescence due to the methanol in solution. Measurements of AB-B and AB were made in 50% methanol and 50% aqueous solution (by volume) to guarantee complete solubility.

Electrochemistry measurements were also made on MAMA, AB-B and AB. This provided measurements of the energy of the oxidation of the switch and the reduction of the fluorophore. The energy difference between the oxidation and the reduction is important in understanding the rate at which PET occurs. This rate can also be calculated using fluorescence lifetime values, and is related to the change in the fluorescence lifetime when glucose binds to AB. Based on electrochemical and fluorescence measurements, two novel molecules (NIB and COB) with longer wavelength fluorophores were synthesized. Preliminary measurements made on these molecules show changes in fluorescence properties upon binding to glucose.

AB is the model system for future glucose sensor molecules. Understanding the details and mechanisms responsible for the fluorescence lifetime changes of AB with glucose concentration is the first step in creating a better sensor molecule – one that has longer excitation and emission wavelengths. This minimally invasive sensor design has the potential of continually measuring the glucose levels of a diabetic patient.

1.2 Diabetes Mellitus

Diabetes mellitus literally means "excessive excretion of sweet urine." (Lehninger, 1993) High blood sugar levels, resulting in high levels of sugar in the urine, are caused in this disease by the body's inability to produce or effectively use insulin, a

hormone used to regulate glucose levels. The accumulation of sugar in the blood is the cause of many serious long term complications including heart disease, kidney disease, and blindness. In 1995 an estimated total of 15.7 million people in the United States (or approximately 5.9% of the population) had a form of diabetes, with approximately one third of the cases undiagnosed. (National Institute of Diabetes and Digestive and Kidney Diseases (NIDDK), 1999) Diabetes is typically divided into three classifications: 1) type 1 diabetes, also referred to as insulin-dependent diabetes mellitus (IDDM), 2) type 2 diabetes, or noninsulin-dependent diabetes mellitus (NIDDM), and 3) gestational diabetes. Persons with type 1 diabetes lack the ability to produce insulin, while persons with type 2 produce either do not produce enough insulin, or cannot use insulin effectively. Approximately 93% of diagnosed cases of diabetes are type 2. Gestational diabetes manifests during pregnancy but retreats after childbirth, and is only seen in 2-5% of all pregnancies. In 1992 medical costs, both direct and indirect, for the treatment of diabetes and its complications totaled $98.2 billion. (NIDDK, 1999)

1.3 Motivation

Normal blood glucose values range from 70 mg/dL to 120 mg/dL. If blood glucose levels become too low, hypoglycemia can cause a diabetic to pass out and eventually die if not treated. However, if blood glucose levels rise too high due to an insufficient supply of insulin, hyperglycemia can occur. This can lead to ketoacidosis (diabetic coma) or contribute to long term complications such as eye, kidney, nerve and cardiovascular disease. (American Diabetes Association (ADA), 2000) The Diabetes Control and Complications Trial (DCCT) Research Group conducted a study on the

long-term effect of tight glucose control in diabetics. Subjects attempted to keep their glucose levels within the normal range, and less than 180 mg/dL after meals, by testing at least four times per day. This study showed that by attempting to maintain glucose levels within the normal range, the risk of long term complications commonly occurring in diabetics is reduced. The risk of eye disease was 76% lower, kidney disease reduced by 50%, nerve disease was 60% lower, and cardiovascular disease had a 35% reduced risk. (DCCT Research Group,1993)

Currently, the most common home testing devices require the patient to extract a drop of blood (typically from the fingertip) and place in onto a paper strip treated with chemicals. The glucose in the blood reacts with the oxygen and is catalyzed by the glucose oxidase enzyme to produce hydrogen peroxide. (Lehninger, 1993)

$$\text{D-Glucose} + O_2 \xrightarrow{\text{glucose oxidase}} \text{D-Gluconate} + H_2O_2 \qquad 1.3$$

The hydrogen peroxide produced in this reaction causes the paper strip to change color through a reaction with tetramethylbenzidine and peroxidase. (King, 1993)

$$H_2O_2 + \underset{\textit{reduced, colorless}}{\text{Tetramethylbenzidine}} \xrightarrow{\text{Peroxidase}} H_2O + \underset{\textit{oxidized, blue}}{\text{Tetramethylbenzidine}} \qquad 1.4$$

This change in color, measured by a change in the reflectance at a specific wavelength of light, is optically monitored over time, resulting in a glucose measurement with 3-5% accuracy in the laboratory. However, many problems with these sensors occur outside of a controlled environment causing the average accuracy of a measurement to become higher than 10% in home use. The factors inhibiting the accuracy of the glucose meters at home include temperature changes, the need for constant calibration, improper test strip use, and abnormal concentrations of haematocrit in the blood. (Lifescan, 1994) An

important limitation of this method is the inability to continuously monitor changing glucose levels. A single measurement of glucose does not tell the diabetic if blood sugar levels are increasing, constant, or decreasing. A continuous sensor would measure present glucose levels as well as upward or downward trends, allowing for tighter control. A sensor of this kind could be integrated with an insulin pump to provide closed loop control of the glucose levels of a diabetic person.

External insulin pumps are available for diabetics, and implanted pumps are currently in human trials. (MiniMed, 1999) When injected, insulin lowers the blood glucose levels of an insulin-dependent diabetic by aiding in the absorption of glucose by cells in the body (Lehninger, 1993). With the development of a continuous glucose monitoring device, it would be easier for diabetics to maintain their blood sugar levels within a range approaching the normal physiological range of 70 mg/dL to 120 mg/dL. The glucose sensor could communicate with the insulin pump, controlling the rising glucose levels of a diabetic after eating, effectively creating an artificial pancreas. This would have enormous impact on the diabetic community. The following section describes some glucose sensing methods currently under investigation. The scope of the methods described here has been limited to sensors with the potential for continuous monitoring, and capable of being integrated with an insulin pump. For a complete review of glucose sensor research on methods not requiring blood extraction, the reader is referred to a review article by J. N. Roe and B. R. Smoller (Roe, 1998). For a more in-depth review of optical glucose measurement techniques, a special issue of the IEEE-LEOS Newsletter includes a series of articles describing techniques based on infrared light, Raman spectroscopy, and the rotation of polarized light. (Waynant, 1998)

Although the infrared, Raman, and polarized light techniques are non-invasive, the need for large detectors, large lasers, or awkward geometries make it difficult to implement these techniques in a sensor for continuous measurements of glucose.

1.4 Electrochemical Sensors

Continuous, minimally invasive electrochemical sensors have been developed based on the same reaction used in the test strips of the glucose sensors currently on the market (Equation 1.3). Hydrogen peroxide is the detected quantity, providing an indirect measurement of glucose concentration. Many electrochemical glucose sensors have been designed using the same basic principles. Two of these designs are discussed here, and the reader is referred to the literature (Troupe, 1998; Anzai, 1998; Tamada, 1999) for more examples.

The successful design of one particular electroenzymatic sensor is built upon a flexible substrate. This allows for the device to be comfortably placed through the skin and remain in the subcutaneous tissue for a short time without discomfort. The working electrode of the device is plated with platinum-black and coated with glucose oxidase. The sensor electrodes are covered with a biocompatible membrane three orders of magnitude more permeable to oxygen than glucose. By making sure that excess O_2 is present, glucose becomes the limiting factor in the enzymatic equation (Equation 1.3), eliminating the effects caused by varying oxygen concentrations. (Mastrototaro, 1991)

This approach to electrochemical measurements is the basis for the continuous glucose monitoring system from MiniMed Inc. This device uses a flexible substrate inserted into the subcutaneous tissue, and may remain in place for three days making

glucose measurements every five minutes. It recently received approval by the Food and Drug Administration (FDA) for limited use by physicians. (Mastrototaro, 1998; MiniMed, 1999)

Another electrochemical sensor uses a platinum electrode coated with Teflon. Near the end of the electrode is a section with glucose oxidase in a layered structure of cellulose acetate and Nafion. The area with the glucose oxidase is then coated with polyurethane to protect the sensor while allowing for glucose to diffuse in. Around the outside of the Teflon is a silver and silver chloride coating creating the cathode. Experiments with this device showed a difference between blood glucose and subcutaneous glucose values. Results showed that when the blood glucose levels are increasing, the subcutaneous glucose values are slightly delayed compared to the values in the blood. However, when blood glucose values are decreasing due to an injection of insulin, subcutaneous glucose values drop faster than blood glucose measurements because of the consumption of glucose by cells in the tissue. This "push-pull" relationship is attributed to the glucose kinetics *in vivo*. (Thomé-Duret, 1996) The relationship between blood glucose and subcutaneous glucose is very important to understand if subcutaneous glucose sensors are to replace blood glucose measurement devices in the future.

1.5 Optical Sensors

1.5.1 Fluorescence Resonance Energy Transfer

A technique developed extensively by J. Lakowicz for measuring glucose, or other analytes, is fluorescence resonance energy transfer (FRET). One fluorophore, the

donor, is excited at a wavelength that only weakly excites fluorescence in a second, acceptor fluorophore. If the donor and acceptor fluorophore molecules are near each other, the donor will transfer some of its absorbed excitation energy to the acceptor. Typical distances at which energy transfer is 50% efficient (i.e. the Förster distance) are from 20 to 50 Å. (Lakowicz, 1983) The energy is transferred via a non-radiative dipole-dipole interaction between the two fluorophores. The absorbed energy promotes the acceptor fluorophore to an excited state, which can result in fluorescent decay. The fluorescent emission of the acceptor is at a longer wavelength than that of the donor. Competitive binding assays coupled with FRET donor and acceptor fluorophores have been designed to measure glucose. This method is minimally invasive, requiring molecules with fluorescent tags to be inside the body where glucose can interact with them. One disadvantage to this design is that the molecules must remain free to move about in order for the FRET to be switched on and off.

A sensor design using competitive binding was created at the Center for Fluorescence Spectroscopy (CFS) at the University of Maryland. A Conconavalin-A (Con-A) molecule, which is a lectin – a protein that specifically binds to a sugar (Alberts, 1994), is tagged with a donor fluorophore, and a sugar (i.e. α-D-Mannoside) molecule is tagged with an acceptor fluorophore. The sugar has a specific binding site on Con-A and competes with native glucose molecules for this binding site. When the tagged sugar binds to Con-A and the donor fluorophore is excited and energy is transferred to the acceptor on the sugar causing it to fluoresce. When physiological glucose binds to Con-A, the donor fluorphore on the Con-A will fluoresce while the acceptor fluorophore on the sugar will not. Instead of looking at the change in fluorphore intensity as a function

of wavelength to measure the glucose concentration, the change in fluorescence lifetime corresponding to the fraction of bound and unbound labeled sugar molecules is measured. (Lakowicz, 1993) Another variation on this method developed by Lakowicz uses Con-A labeled with Ruthenium metal-ligand complex, a fluorescent dye, as the donor and insulin linked to the sugar maltose and labeled with a Malachite Green fluorophore as the acceptor. (Tolusa, 1997)

A similar glucose sensing scheme patented by Chick et al. uses a donor fluorophore (e.g. fluorescein) linked to a macromolecule (e.g. glycosylated serum albumin) which can bind to glucose-binding ligands. The acceptor fluorophore (e.g. rhodamine) is attached to the lectin (e.g. Con-A) which has a specific binding site for glucose. The labeled glucose competes with the native glucose in the body for the binding site. If physiological glucose concentrations are low, a larger fraction of glucose molecules attached to donor fluorophores will bind to the lectin bringing the donor and acceptor fluorophores within range for FRET to occur. For high physiological glucose concentrations, the reverse occurs, reducing the amount of FRET. (Chick, 1994)

1.5.2 Fluorescence Intensity

Multianalyte fiber optic biosensors have been developed at Tufts University by D. Walt, et al. One such sensor is capable of simultaneous measurements of glucose and oxygen. At one end of the fiber bundle polymer matrices with analyte sensing molecules are deposited. To measure glucose, both an oxygen sensor and a glucose sensor are deposited onto the fibers. The oxygen sensor mechanism is based on changes in fluorescence intensity due to collisional quenching of a ruthenium complex ($Ru(Ph_2phen)_3^{2+}$) by oxygen that permeates the polydimethylsiloxane copolymer. The

glucose sensor is similar to the oxygen sensor, but is coated with a layer of poly(hydoxyethylmethacrylate) in which glucose oxidase is covalently bound. Glucose diffuses into this layer and reacts with the glucose oxidase (Equation 1.3) and oxygen. The oxygen not consumed by the glucose reaction is then detected in the underlying layer with the ruthenium complex. Excitation light is sent to the sensor via the fiber bundle, which also collects the fluorescent light. The fiber bundle is then imaged with a CCD camera and the ratio of signal between the oxygen sensor and the glucose sensor results in a quantitative, and spatially resolved, measurement of glucose concentration. (Healey, 1997; Steemers, 1999)

1.5.3 Fluorescence Lifetimes

An example of a fluorescent lifetime sensor that does not use FRET as the sensing mechanism was developed at the University of Maryland by Lakowicz. The sensor measures glucose by measuring the change in the fluorescence lifetime of a mutant glucose/galactose binding protein (GGBP) labeled with a fluorophore. The fluorophore is a naphanene derivative (ANS-26), and shows a decrease in fluorescence intensity and lifetime when glucose is bound to the ANS26-GGBP molecule. However, the change in lifetime with glucose was only a few percent of the 5 nsec average lifetime, so another fluorophore was added to the sensor in order to enhance the measurement of the small lifetime change. A metal-ligand complex with a long fluorescence lifetime (~1000 nsec), $[Ru(bpy)_3]^{2+}$, was coated on the outside of the sample cuvette containing the sensor molecule (ANS26-GGBP) and glucose. The fluorescence of the metal-ligand complex is insensitive to glucose, but increases the average measured lifetime of the system. This system has not yet been demonstrated, but theoretically this sensor design should have

enough sensitivity to measure physiological glucose levels. (D'Auria, 1999; Tolosa, 1999)

1.5.4 Scattering

Glucose has been measured using the diffraction of light from polymerized crystalline colloidal arrays (PCCAs) that swell with changes in glucose concentration. The PCCA is polymerized within a hydrogel film that includes glucose oxidase molecules. When the glucose oxidase reacts with glucose (Equation 1.3) it is reduced creating a negatively charged molecule. This negative charge causes the hydrogel to expand due to the influx of positively charged ions, which raises the osmotic pressure. The swelling of the hydrogel increases the spacing between the spherical polystyrene colloids in the hydrogel. Therefore the angle at which light is diffracted increases according to Bragg's law:

$$m\lambda = 2nd\sin\theta \qquad 1.5$$

where θ is the angle of diffraction, n is the refractive index of the PCCA/hydrogel system, d is the spacing between the spheres (~200 nm), λ is the wavelength of light, and m is the order of diffraction. The hydrogel can be coated on the end of a fiber optic, creating a minimally invasive, and continuous glucose sensor. (Asher, 1998)

1.6 Summary and Overview

Table 1.1 summarizes the glucose sensing techniques previously discussed. The most common strength is the basis of the measurement on fluorescence lifetimes.

Weaknesses in methods other than the one described in this work, are intrinsic to the method and cannot be overcome.

Method Description	Strengths	Weaknesses
Fluorescence Lifetime of AB (*Section 1.1*)	• Single molecule • Based on lifetime changes • Molecule can be covalently liked to polymer	• Short excitation/emission wavelengths • Influenced by other molecules binding to glucose site
Fluorescence Resonance Energy Transfer (*Section 1.5.1*)	• Based on lifetime changes	• Multiple molecules must remain free to move • Influenced by other molecules binding to glucose site
Fluorescence Intensity (*Section 1.5.2*)	• Incorporated into fiber optic	• Based on fluorescence intensity • Influenced by other molecules binding to glucose site
Fluorescence Lifetimes (*Section 1.5.3*)	• Single molecule • Based on lifetime changes	• Small change in lifetime • Influenced by other molecules binding to glucose site
Scattering (*Section 1.5.4*)	• Incorporated into fiber optic	• Based on angle of scattered light intensity

Table 1.1 – Summary of current research on continuous glucose sensors.

The sensor molecule discovered by James, anthracene boronate (AB), is attractive because, unlike the FRET sensors, it does not need to be free to move in solution and interact with molecules other than glucose. It can therefore be covalently linked to a polymer, which in turn can be implanted beneath the skin. AB is a smaller, simpler

molecule than other fluorescent sensor molecules, such as enzymes or biomolecules, resulting in a better chance of survival in the body.

The next chapter will provide a brief introduction to sensor designs incorporating AB, as well as a description of the PET mechanism. Other molecules that were investigated to aid in the understanding AB will be introduced, along with related potential sensor molecules that were synthesized having longer excitation and emission wavelengths. Chapter Three will present the equations used in modeling the kinetics of the AB reactions, the theory of fluorescence and how it is influenced by the kinetics, and an examination of PET and the theories used to calculate the rate of electron transfer. This rate can be determined using a combination of fluorescence and electrochemistry, and is important in understanding the fluorescence properties of AB. With the background established, the experimental methods are described in Chapter Four. Chapter Four will also include the equations used in frequency domain lifetime measurements and curve fitting used in the analysis of lifetime data. Results from measurements of AB and related molecules will be presented in Chapter Five. Here, the mechanisms involved in AB will be explained and trends seen in the measurements will be examined. The fluorescence of AB must be characterized and understood to optimize a sensor design based on fluorescence lifetimes. The goal of this project is to characterize the fluorescent lifetime properties of AB and understand the mechanisms behind its ability to sense glucose. In Chapter Six, results from two novel sensor molecules will be shown. Finally, Chapter Seven summarizes the accomplishments of this sensor work and provides recommendations for future research.

REFERENCES

American Diabetes Association (ADA), http://www.diabetes.org/, 2000.

The Diabetes Control and Complications Trial (DCCT) Research Group. The Effect of Intensive Treatment of Diabetes on the Development and Progression of Long-Term Complications in Insulin-Dependent Diabetes Mellitus, *The New England Journal of Medicine* 329(14): 977-986, 1993.

Anzai, J, H. Takeshita, et al. Layer-by-Layer Construction of Enzyme Multilayers on an Electrode for the Preparation of Glucose and Lactate Sensors: Elimination of Ascorbate Interference by Means of an Ascorbate Oxidase Multilayer. *Anal. Chem.* 70(4): 811-917, 1998.

Asher, S.A. and J.H. Holtz. Glucose Sensing Intelligent Polymerized Crystalline Colloidal Arrays. *LEOS Newsletter* 12(2): 32-34, 1998.

Chick, et al. Method and Device for Detecting and Quantifying Glucose in Body Fluids. US Patent #5,342,789. Aug. 30, 1994.

D'Auria, S., et al. The Fluorescence Emission of the Apo-glucose Oxidase from *Aspergillus niger* as Probe to Estimate Glucose Concentrations. *Biochemical and Biophysical Research Communications* 263: 550-553, 1999.

Delpy, D. Optical spectroscopy for diagnosis. *Physics World*, 34-39. August 1994.

Healey, B.G., L. Li, and D.R. Walt. Multianalyte biosensors on optical imaging bundles. *Biosensors & Bioelectronics* 12 (6): 521-529, 1997.

James, T.D., et al. Novel Photoinduced Electron-transfer Sensor for Saccharides based on the Interaction of Boronic Acid and Amine. *J. Chem. Soc., Chem. Commun.*: 477-478, 1994.

James, T.D., K.R.A.S. Sandanayake, and S. Shinkai. A Glucose-Selective Molecular Fluorescence Sensor. *Angew. Chem. Int. Ed. Engl.* 33 (21): 2207-2209, 1994. (a)

King, T.W. In Vitro Development of a Noninvasive Polarimetric Glucose Sensor for Diabetic Home Monitoring. Master's Thesis, Texas A&M University, August 1993.

Lakowicz, J.R.. Principles of Fluorescence Spectroscopy. Plenum Press, New York, 1983.

Lifescan Inc., a Johnson & Johnson company. http://lifescan.com/, or One Touch Basic Blood Glucose Monitoring System, Owner's Booklet. AW 054-128-02A, 1994.

Mastrototaro, J., et al. Clinical Results from a Continuous Glucose Sensor Multi-Center Study. *Diabetes* 47: A61 Suppl. 1, 1998.

Mastrototaro, J.J., K.W. Johnson, et al. An electroenzymatic glucose sensor fabricated on a flexible substrate. *Sensors and Actuators B* 5: 139-144, 1991.

MiniMed Inc., http://www.minimed.com/, 1999.

NIDDK (National Institute of Diabetes and Digestive and Kidney Diseases) http://www.niddk.nih.gov/, 1999.

Roe, J.N., and B.R. Smoller. Bloodless Glucose Measurements. *Critical Reviews in Therapeutic Drug Carrier Systems* 15(3): 199-241, 1998.

Steemers, F.J. and D.R. Walt. Multi-Analyte Sensing: From Site-Selective Deposition to Randomly-Ordered Addressable Optical Fiber Sensors. *Mikrochim. Acta* 131: 99-105, 1999.

Tamada, J.A., S. Garg, et al. Noninvasive Glucose Monitoring: Comprehensive Clinical Results. *JAMA* 282(19): 1839-1844, 1999.

Thomé-Duret, V., et al. Use of a Subcutaneous Glucose Sensor to Detect Decreases in Glucose Concentration Prior to Observation in Blood. *Analytical Chemistry* 68(21): 3822-3826, 1996

Tolusa, L., et al. Lifetime-Based Sensing of Glucose Using Energy Transfer with a Long Lifetime Donor. *Analytical Biochemistry* 250: 102-108, 1997.

Tolusa, L., et al. Glucose Sensor for Low-Cost Lifetime-Based Sensing Using a Genetically Engineered Protein. *Analytical Biochemistry* 267: 114-120, 1999.

Troupe, C.E., I.C. Drummond, et al. Diamond-based glucose sensors. *Diamond and Related Materials* 7: 575-580, 1998.

Waynant, R.W. and V.M Chenault. Overview of Non-Invasive Fluid Glucose Measurement Using Optical Techniques to Maintain Glucose Control in Diabetes Mellitus. *LEOS Newsletter* 12(2): 3-6, 1998

Chapter II

SENSOR DESIGN

This chapter begins with a description of the possible sensor device architectures. Next, a detailed introduction to the model sensor molecule (AB) is presented along with an explanation of the N→B dative bond. Understanding the characteristics of this bond provides important insight into the ability of AB to change its fluorescence properties with glucose concentration and will be discussed further in Chapters Five and Seven. Finally, structures of all molecules used in this research will be presented.

2.1 Device Architecture

Two glucose sensor designs incorporating the anthracene boronate (AB) molecules have been examined. One design uses a fiber optic for light delivery, while the other is based on an implanted membrane using transdermal light delivery and detection. Both designs rely on the fluorescence of a glucose sensitive sensor molecule to measure glucose concentration in the interstitial fluid. (Van Antwerp, 1999)

2.1.1 Fiber Optic

A semi-invasive sensor design, similar to the electrochemical sensor developed by MiniMed, uses a fiber optic cable with a biocompatible polymer membrane attached at one end. This membrane may be dip coated onto the fiber, or physically attached to the end of the fiber. The sensor molecule is covalently linked throughout this polymer membrane (Figure 2.1).

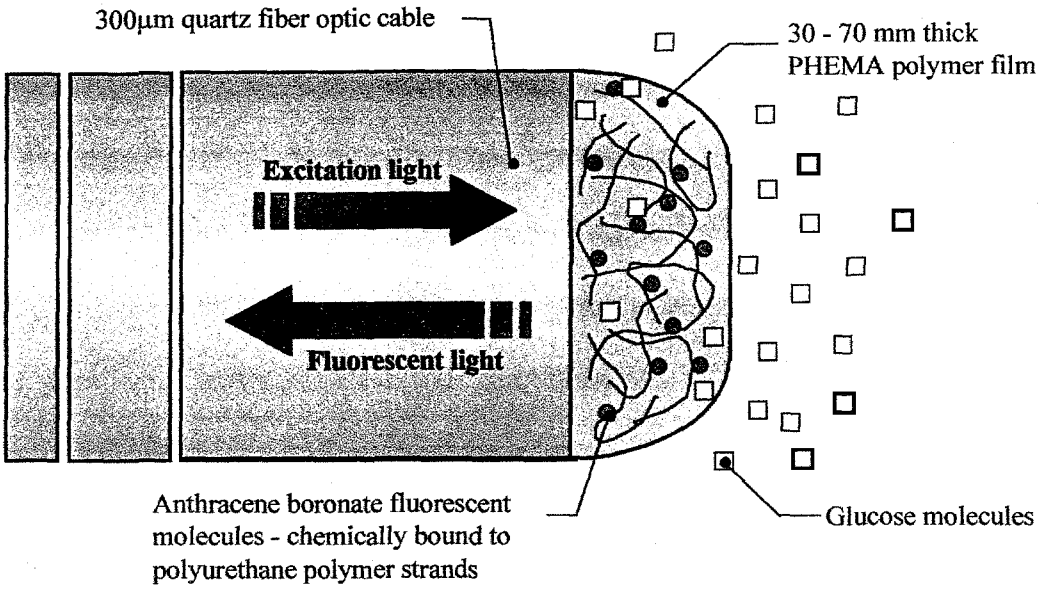

Figure 2.1 – Schematic of fiber optic glucose sensor design.

The fiber is inserted a few millimeters into the skin using a hollow needle to create the small incision needed for insertion. The needle is removed, leaving the sensor in the subcutaneous tissue where interstitial fluid diffuses into the membrane and interacts with the sensor molecule. Excitation light is delivered via the fiber from a light source such as a light emitting diode (LED). The fluorescent light emitted by the sensor molecule is collected using the same fiber, then passed through a high-pass filter to remove any excitation light collected with the fluorescence. Due to the invasive nature of the fiber optic beneath the skin, this sensor can typically remain in one place for a up to three days with minimal threat of infection.

2.1.2 Implanted

The less-invasive sensor design consists of a polymer membrane, a few millimeters in dimension, implanted in the subcutaneous tissue (Figure 2.2). The

membrane includes the fluorescent sensor molecule covalently linked to the polymer, and is part of a potentially long-term glucose sensor. Directly above the sensor membrane, on top of the skin, is a device that includes the light source, light detector, filter to reject source light incident on the detector, and a radio transmitter to relay the detector signal to a remote device. The fluorophores in the membrane are excited transdermally by the light source at the surface of the skin.

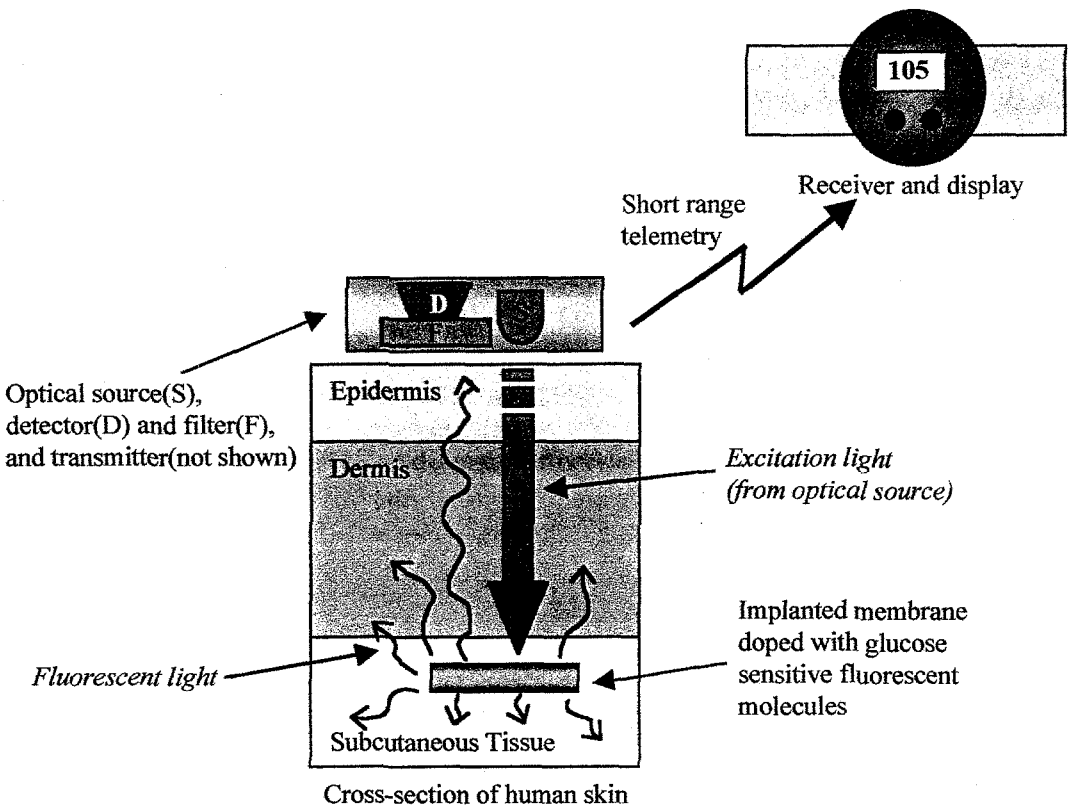

Figure 2.2 – Schematic of implanted glucose sensor design.

The fluorescence from the glucose sensitive sensor molecules in the membrane is measured by the detector in the device on the skin's surface. A signal proportional to the detected fluorescence is transmitted to a receiver, such as a wristwatch, and converted to a glucose concentration measurement and the result is displayed. As long as the

implanted membrane is not encapsulated by fibrous tissue (i.e. cut off from the interstitial fluid due to an immune response by the body against the foreign object) and the fluorophore remains stable, the implanted sensor could function for many years.

Another possible sensor configuration is similar to the fiber optic design, except that the entire device is implanted. This would eliminate the problem of transdermal excitation and detection. It is also possible that multiple fibers could be excited with the same source, thus yielding multiple measurements of glucose concentration. The exact geometry of this sensor has not yet been developed. Utilization of the fully implanted sensor would require minor surgery, as well as a long life battery or transdermal radio frequency power delivery to a passive implanted system.

2.2 Sensing Molecules

2.2.1 Anthracene Boronate (AB)

The sensor molecule identified by James et al. is anthracene monoboronic acid, or anthracene boronate (AB). James et al. suggested that when glucose binds to the boronic acid moiety ($B(OH)_2$) it increases the electronegativity of the boron atom, strengthening the dative bond (N→B) with the amine (N). (James, 1994) A dative bond similar to the one in AB has a bond dissociation energy on the order of 10 kcal/mol (Toyota, 1990) which is weaker than a covalent bond (a C-C bond has a dissociation energy of 83 kcal/mol), yet stronger than a hydrogen bond or van der Waals interaction which have dissociation energies of less than 5 kcal/mol. (Lehninger, 1993) This enhanced bond reduces the probability of one of the amine lone pair electrons transferring via PET to the photoexcited anthracene and quenching the fluorescence (Figure 2.3).

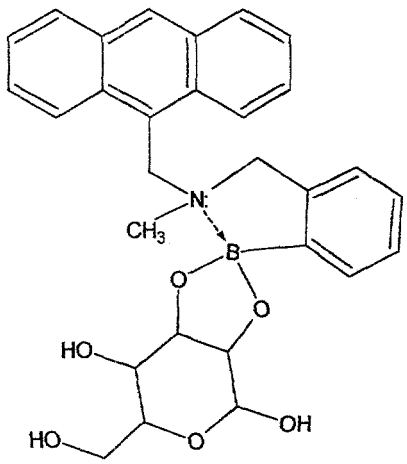

Figure 2.3 – AB with glucose bound to the boronic acid. The N→B dative bond is enhanced, effectively eliminating quenching of the fluorophore by PET.

Without glucose the electronegativity of the boron atom decreases and the N→B is not as strong, but it remains a dative bond (Figure 2.4). The probability increases for the transfer of an electron from the lone pair of the amine to the anthracene after photoexcitation. If transferred, the electron will reduce the amount of fluorescence, and shorten the fluorescent lifetime.

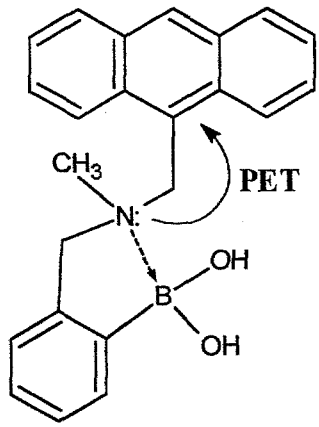

Figure 2.4 – AB without glucose bound to the boronic acid. The electrons on the amine are now free to be transferred via PET to quench the fluorescence of the anthracene.

The interaction between the amine and the boron controls the electron transfer. The characteristics of the N→B dative bond as well as the rate of electron transfer were investigated using fluorescence and electrochemical measurement techniques and will be discussed in detail at the end of Chapter Five.

2.2.2 N→B Interactions

In trivalent boron (BX_3) three bonds are created by sp^2 hybrid orbitals which form a planar molecule with bonds separated by 120 degrees. The remaining $2p_z$ orbital is left vacant and is perpendicular to the plane, ready to accept electrons from the lone electron pair of the sp^3 orbital of an amine such as ammonia (NH_3). If this orbital forms a covalent bond, the molecule changes from a trigonal to a tetrahedral character. The angle between B-X bonds in a uniform trigonal molecule (BX_3) is 120 degrees, while the angle

between bonds in a uniform tetrahedral molecule (BX_4) is 109.5 degrees (Figure 2.5). (Toyota, 1992)

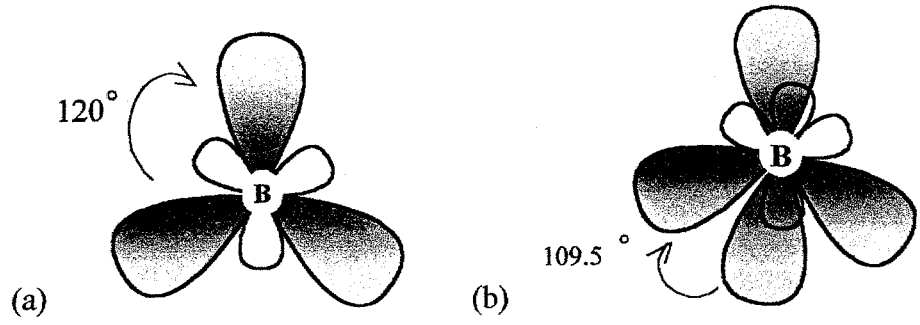

Figure 2.5 – Orbitals for (a) trigonal boron (BX_3) and (b) tetrahedral boron (BX_4).

In a dative bond, the boron atom is a combination of both trigonal and tetrahedral. The nature of the dative bond can be quantified in a parameter known as the tetrahedral character (THC).

$$\mathrm{THC}[\%] = \frac{120^\circ - [(\theta_1 + \theta_2 + \theta_3)^\circ / 3]}{120^\circ - 109.5^\circ} \times 100 \qquad 2.1$$

Angles measured between bonds using x-ray analysis are labelled θ_1, θ_2, and θ_3. (Toyota, 1992)

The intramolecular coordinative, or dative, bond between boron and nitrogen has been studied extensively in many different compounds. (Carboni, 1999; Steinberg, 1964; Brotherton, 1970; Toyota, 1990, 1992, 1999; Höpfl, 1999) The boron atom acts as a Lewis acid (or electron acceptor) in its interaction with the more basic amine (electron donor). (Toyota, 1992) A molecule with boron and nitrogen environments resembling those in AB, 2-[2-(dimethylaminomethyl) phenyl-4,4-diphenyl-1,3,2-dioxaborolane (Toyota-1), (Figure 2.6),

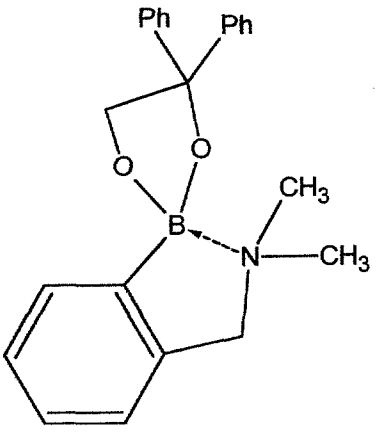

Figure 2.6 - 2-[2-(dimethylaminomethyl)phenyl-4,4-diphenyl-1,3,2-dioxaborolane(Toyota-1). (Toyota, 1990, 1992, 1999)

was determined to have a N-B bond length of 1.756 Å. Typical bond lengths of N-B bonds range from 1.66 to 1.76 Å. (Toyota, 1992) The length of a carbon-carbon single covalent bond is approximately 1.54 Å (Lehninger, 1993). As bond length increases, the boron complex shifts from tetrahedral to trigonal planar and the strength of the interaction with the donor decreases. (Höpfl, 1999) The energy barrier to dissociation of the N→B bond in Toyota-1 was measured to be 9.7 kcal/mol with NMR lineshape analysis. (Toyota, 1990) Thermal energy is 0.59 kcal/mol, suggesting that the strength of the N→B bond is large enough to be present in every AB molecule. X-ray crystallography showed the THC of Toyota-1 is 51%. (Toyota, 1999) This would suggest that the orbital overlap between the amine and the boron is approximately halfway between no bond and a complete, covalent, bond. In a molecule like AB, this would allow for a finite probablility of electron transfer in all molecules even though the N→B dative bond exists.

The nature of the N→B bond is complex. The THC may provide a way of characterizing the bond strength and determining the amount of electron transfer in AB alone in solution. This is important because a higher probability of electron transfer in AB may translate into a greater potential for increased fluorescence with glucose. The THC of AB will be examined in Chapter Five.

2.2.3 Fluorophore Candidates

To examine the PET as well as the N→B bond more closely, we began by studying precursors to the final, glucose sensitive molecule, AB. The fluorophore of AB is anthracene, and has been studied extensively in the literature (Platt, 1949; Klevens, 1949; Ramasesha, 1993; Tanaka, 1995; McVey, 1976). To examine the effect of the amine substituent on anthracene, 9-(Methylaminomethyl)-anthracene (MAMA) was studied (Figure 2.7). This molecule was investigated using different solvents and different pH solutions.

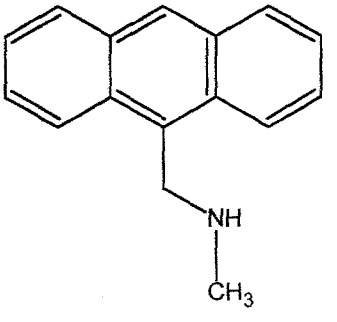

Figure 2.7 – MAMA (9-(Methylaminomethly)-anthracene)

Next, with the help of the synthetic chemistry group at LLNL, we examined MAMA with the phenyl ring attached, but not the boronic acid. This molecule was

labeled AB-B (Figure 2.8), and was also investigated in various solvents and at different pH levels.

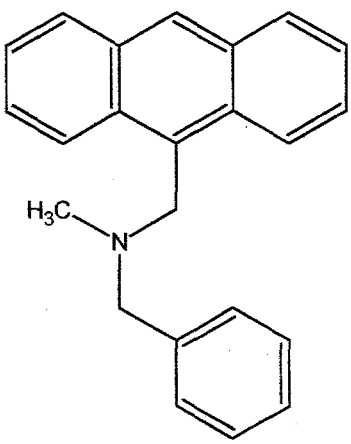

Figure 2.8 – AB-B (N-benzyl-N-methyl-N-methyl anthracene)

Finally, the molecule developed by T. James et al. (Figure 2.9) was synthesized and its fluorescence properties were measured under various conditions. Studies were performed to determine the sensitivity and fluorescent properties of anthracene boronate (AB) as a function of glucose concentration as well as pH and solvent variation.

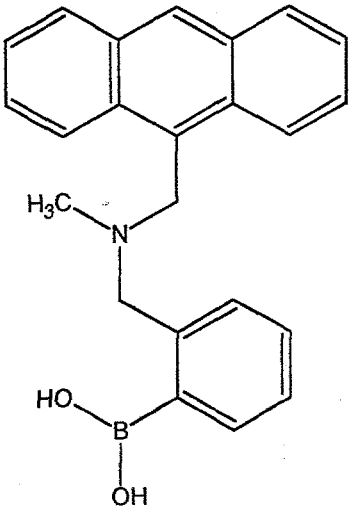

Figure 2.9 – AB (N-methyl-N-(9-methylene anthryl)-2-methylenephenylboronic acid)

The LLNL team of chemists is also synthesizing many new molecules to develop a sensor with a longer wavelength fluorophore. The first sensor molecule developed was based on oxazine 170. This molecule, chloro-oxazone boronate, or COB (Figure 2.10), was synthesized with the help of chemists from the University of New Orleans, Louisiana.

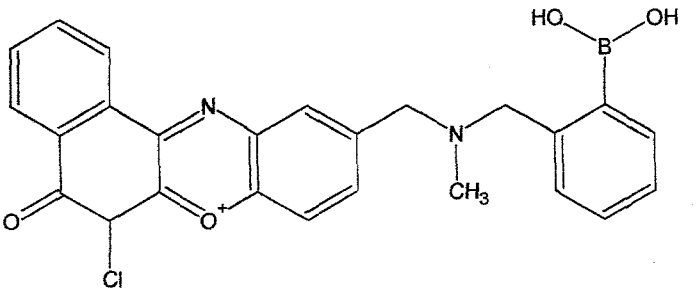

Figure 2.10 – COB (6-Chloro-10methyl-5Hbenzo[a]phenoxazin-5-one)

Another class of longer wavelength fluorophores under investigation is based on naphthylimide chemistry. The first compound in this class to be synthesized with the boronic acid moiety was naphthylimide boronate, or NIB. To further classify this compound, the name NIB-2T will be used (Figure 2.11). The 2 refers to the two carbon linker from the electron donating amine to the amine of the fluorophore, and the T refers to the tertiary nature of that same amine on the fluorophore.

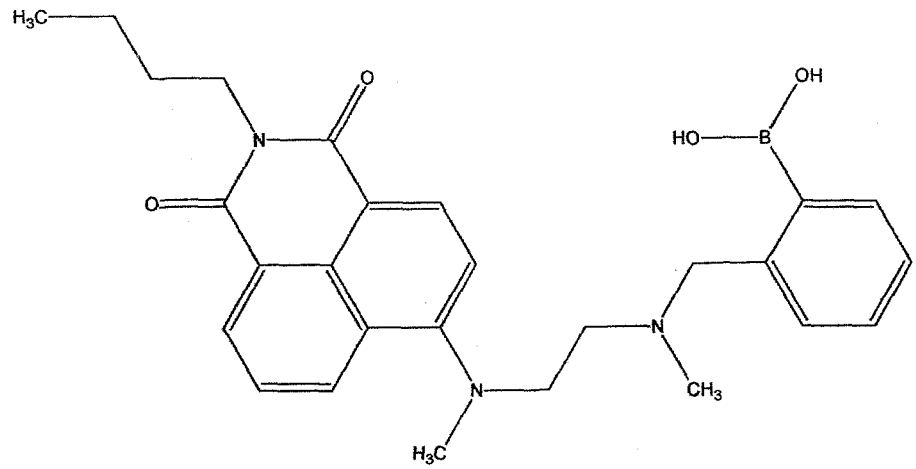

Figure 2.11 – NIB-2T

Derivatives and slightly modified versions of NIB-2T were also synthesized. These variations allowed us to break down the functional parts of NIB as we did with the AB. A variation that includes the phenyl ring, but not the boronic acid, is NIB-B-2S (Figure 2.12). In this molecule, the linker is still two carbons in length, but the amine that was tertiary is now secondary.

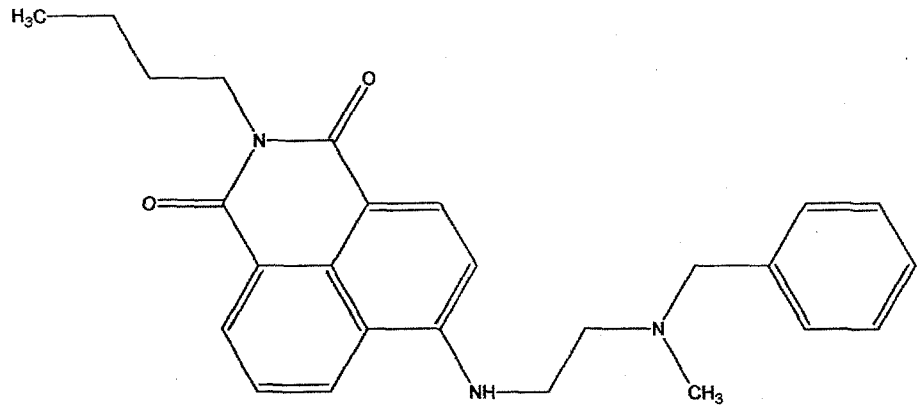

Figure 2.12 – NIB-B-2S

Other variations were synthesized, including one with three carbon chains between the fluorophore and the electron donating amine. These variations were tested using steady state fluorescence techniques and found to have a lower relative fluorescence yield than the molecules with two carbon linkers. Since this would reduce the achievable sensitivity of a glucose measurement, these molecules were not examined further.

REFERENCES

Brotherton, R.J., and H. Steinberg, ed. Progress in Boron Chemistry 3. Pergamon Press, Oxford, 1970.

Carboni, B. and L. Monnier. Recent Developments in the Chemistry of Amine- and Phosphine-Boranes. *Tetrahedron* 55: 1197-1248, 1999.

Höpfl, H. The tetrahedral character of the boron atom newly defined – a useful tool to evaluate the N→B bond. *Journal of Organometallic Chemistry* 581: 129-149, 1999.

James, T.D., et al. Novel Photoinduced Electron-transfer Sensor for Saccharides based on the Interaction of Boronic Acid and Amine. *J. Chem. Soc., Chem. Commun.*: 477-478, 1994.

Klevens, H.B. and J.R. Platt. Spectral Resemblances of Cata-Condensed Hydrocarbons. *J. of Chem. Phys.* 17 (5): 470-472, 1949.

Leninger, A.L., D.L. Nelson, and M.M. Cox. Principles of Biochemistry, second edition. Worth Publishers, New York, 1993.

McVey, J.K., D.M. Shold, and N.C. Yang. Direct observation and characterization of anthracene excimer in solution. *J. of Chem. Phys.* 65 (8), 3375-3376, 1976.

Platt, J.R. Classification of Spectra of Cata-Condensed Hydrocarbons. *J. of Chem. Phys.* 17 (5): 484-495, 1949.

Ramasesha, S., D.S. Galvão, and Z.G. Soos. Exact Eigenstates of the Pariser-Parr-Pople Model for Anthracene. *J. Phys. Chem.* 97: 2823-2829, 1993.

Steinberg, H. and A.L. McCloskey, ed. Progress in Boron Chemistry 1. Pergamon Press, New York, 1964.

Tanaka, F., M. Okamoto, and S. Hirayama. Pressure and Temperature Dependences of the Rate Constant for S_1—T_2 Intersystem Crossing of Anthracene Compounds in Solution. *J. Phys. Chem.* 99: 525-530, 1995.

Toyota, S., and M. Oki. Structure of Intramolecular Boron-Amine Complexes and Proposal of Tetrahedral Character for Correlation between Molecular Structure and Barrier to Dissociation of the N-B Bonds. *Bull. Chem. Soc. Jpn.* 65: 1832-1840, 1992.

Toyota, S., et al. Effect of Benyzlic Methyl Groups on Kinetic Basicity of Amine Ligand in *o*-Boron Substituted *N,N*-Dimethylbenzylamines. *Bull. Chem. Soc. Jpn.* 72: 1879-1885, 1999.

Van Antwerp, W.P., J.J. Mastrototaro, S.M. Lane, J.H. Satcher, Jr., C.B. Darrow, T.A. Peyser, and J. Harder. Detection of Biological Molecules Using Boronate-Based Chemical Amplification and Optical Sensors. U.S. Patent Number 6,002,954. Dec. 14, 1999.

Chapter III

THEORY

The concepts presented in this chapter are important in understanding the physics and chemistry of the sensor design at the molecular level. Equations set forth in this chapter are used to estimate the efficiency and feasibility of the potential sensor molecules. Kinetics of the reactions between sensor molecules and glucose lead to equations that relate the concentrations of each species of sensor molecule to the fluorescence properties of the molecule. A brief description of fluorescence, both steady state and lifetime, is given to support the basic relationships derived for fluorescence of the sensor molecule. Following the theory of kinetics and fluorescence is an introduction to photoinduced electron transfer (PET). Understanding PET and its effect on fluorescence is essential to improving the design of the glucose sensor. Finally, electron transfer theories are presented as a way of predicting the rate of electron transfer from the electrochemical properties of the sensor molecules.

3.1 Reaction Kinetics

Knowing the reactions taking place and their rates is essential to understanding a molecule's ability to measure glucose. The equations for anthracene boronate (AB) are presented here. Two basic forms of AB are assumed to exist in our model: 1) AB, the simplest form as depicted in the previous chapter, and 2) ABG (AB bound to glucose). Each of these species is affected by pH. At low pH, the protons in solution attach to the amine, binding with the lone pair of electrons and preventing PET. This creates both

ABH and ABGH. At high pH, the hydroxilization of the boron changes it to a tetrahedral form (C-B$(OH)_3$) which prevents interaction with the amine, thus allowing PET.

It is assumed that in AB and similar sensor molecules, two fluorescence components exist. These components are the fluorescent sensor molecule with and without fluorescence quenching by PET. For MAMA the two components are simply MAMA with protonation of the amine (MAMAH) and without protonation (MAMA). MAMA is quenched by PET, while MAMAH is not. For the most part MAMA and AB-B are unaffected by OH^- anions because they lack a boron atom, or binding site for OH^-. AB-B is similar to MAMA in the sense that AB-B is quenched by PET, while AB-BH is not. However, AB is slightly more complicated than either MAMA or AB-B. The fluorescence of AB, ABOH and ABGOH is quenched by PET, while the fluorescence of $AB_{N\text{-}B}$ (AB with an enhanced N→B bond), ABH, ABG, and ABGH is not. The quenching probability is related to the nature of the N→B dative bond and will be examined in detail in Chapter Five. The fluorescence characteristics of the unquenched species of AB (i.e. $AB_{N\text{-}B}$) are indistinguishable from the fluorescence characteristics of ABH. Therefore, for simplicity, the following chapter will not include $AB_{N\text{-}B}$ as a separate species. This does not effect the derivations of the equations, and it will be added as a separate component when essential. Chapter Five will describe the dual fluorescence of AB in detail, including an estimation for the probability of PET.

3.1.1 Reaction Equations

For simplicity the reactions of AB are written without the H or OH reactants of the solution.

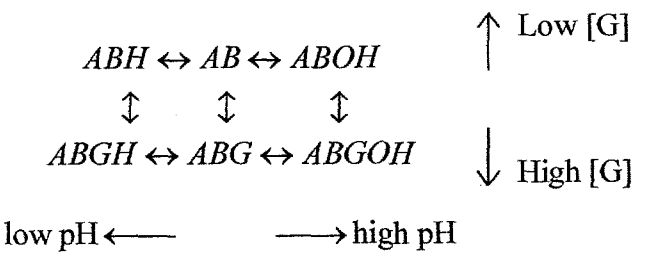

From this set of reactions a list of the primary equilibrium constants can be defined.

$$K_H = \frac{1}{K_a} = \frac{[ABH]}{[AB][H]} \qquad 3.1$$

$$K_{OH} = \frac{1}{K_b} = \frac{[ABOH]}{[AB][OH]} \qquad 3.2$$

$$K_G = \frac{[ABG]}{[AB][G]} \qquad 3.3$$

Note that K_b does not exist for molecules without the boronic acid moiety, such as MAMA and AB-B. We have assumed that each reaction is independent, so that the above constants can be written similarly for the other reactions in the diagram above. From conservation of mass, equations relating the concentrations of each species are written. Initial concentrations of AB and G are written as $[AB]_0$ and $[G]_0$, respectively.

$$[AB]_0 = [AB]+[ABH]+[ABOH]+[ABG]+[ABGH]+[ABGOH] \qquad 3.4$$

$$[G]_0 = [G]+[ABG]+[ABGH]+[ABGOH] \qquad 3.5$$

Combining equations 3.1 through 3.5 leads to expressions for [AB] and [G].

$$[AB] = \frac{[AB]_0}{(1 + K_H[H] + K_{OH}[OH])(1 + K_G[G])} \quad 3.6$$

$$[G] = \frac{[G]_0(1 + K_H[H] + K_{OH}[OH])}{1 - K_G([AB]_0 - [G]_0)(1 + K_H[H] + K_{OH}[OH])} \quad 3.7$$

These equations are particularly useful in describing the theoretical relative fluorescence intensities discussed in Section 3.2.2.

3.1.2 Acidity

The acidity of a molecule is a measure of its proton donating ability. The acidity of the amine in these sensor molecules is very important in determining the amount of fluorescence increase that can be obtained with the addition of glucose. If the pK_a is much higher than the physiological pH (7.4) then the sensor molecule will be protonated and binding to glucose will have little or no effect on the fluorescence. As the pK_a decreases below 7.4 the percentage of protonated molecules at pH 7.4 decreases. Thus a pK_a less than 7.4 is necessary for a molecule to be successful in a physiological glucose sensor.

Through careful pH titrations, or, as in this case, fluorescence measurements in a range of pH values, the dissociation constant (K_a) can be determined. The point on the titration curve where the concentration of the proton acceptor (AB) equals that of the proton donor (ABH) is the pK_a value. The Henderson-Hasselbalch equation is used to calculate the pK_a from pH values and concentrations of a weak acid (proton donor) and its conjugate base (proton acceptor). This can be written for AB, where ABH is the weak acid and AB is the conjugate base.

$$pK_a = pH - \log\left(\frac{[AB]}{[ABH]}\right) \qquad 3.8$$

Values of pK_a for compounds related to our sensor molecules are summarized in Table 3.1.

Compound	pK_a
AB in solution of buffered saline with 33% MeOH (James, 1994)	2.9
Anthrylboronic acid (Yoon, 1992)	8.8
NH_4^+ in water (Lehninger, 1993)	9.25

Table 3.1 - pK_a values for molecules related to AB

Measurements by James et al. on AB in a solution of buffered saline with 33% methanol found the pK_a to be 2.9. Following the argument above, since the pK_a is less than the physiological pH of 7.4, it is determined that AB will work as a sensor molecule in a physiological environment (assuming that the fluorescence properties change sufficiently). The pK_a can be used as a screening tool, rejecting candidate molecules with pK_a values above 7.4.

3.2 Fluorescence

Fluorescence by the sensor molecule allows for a measurement of glucose concentration. Previous work (James, 1994) has demonstrated that the intensity of fluorescence is dependent upon glucose concentration for AB. However, *measured* fluorescence intensity is dependent upon many experimental factors other than glucose. Geometry changes between the source, fluorophore, and detector will change the

measured intensity, as will fluctuations in the excitation source and variations in the optical properties of materials in the light path. Photobleaching or leaching of the fluorophore from the polymer substrate will cause the fluorescence intensity to decrease. In a sensor, these problems will all result in errors in measured glucose concentration. However, such problems associated with fluorescence intensity do not affect fluorescence lifetime measurements, because the lifetime of the fluorophore is not dependent upon the *measured* fluorescence intensity. The fluorescence lifetime is a measure of intrinsic decay rates of the fluorophore as will be described in this section. This important distinction makes fluorescence lifetime sensors more appropriate for robust sensor measurements.

Upon absorption of a photon by a molecule, an electron may be promoted from the ground state to a higher molecular orbital. As the molecule returns to the lower energy ground state, the excited electron decays to a lower energy level by either radiative or nonradiative means. Decay through radiative means is known as fluorescence. The average time that the electron spends in the excited state before decaying to a lower energy level is the characteristic, or intrinsic lifetime. The observed fluorescence lifetime is a function of both the intrinsic lifetime and the quantum yield of the fluorescence (Equation 3.13). The observed lifetime is found by measuring the average time it takes for an ensemble of molecules to radiatively decay from the excited state to the ground state.

3.2.1 Decay Paths

Assume that the molecule of interest, anthracene boronate (AB), is excited by a photon from the ground state energy level, S_0 to the first excited singlet energy level, S_1.

In a simplified model, the possible pathways of deexcitation from S_1 are characterized by the decay rates: k_{NR}, k_{FL}, k_{ET}, and k_{ISC} (Figure 3.1).

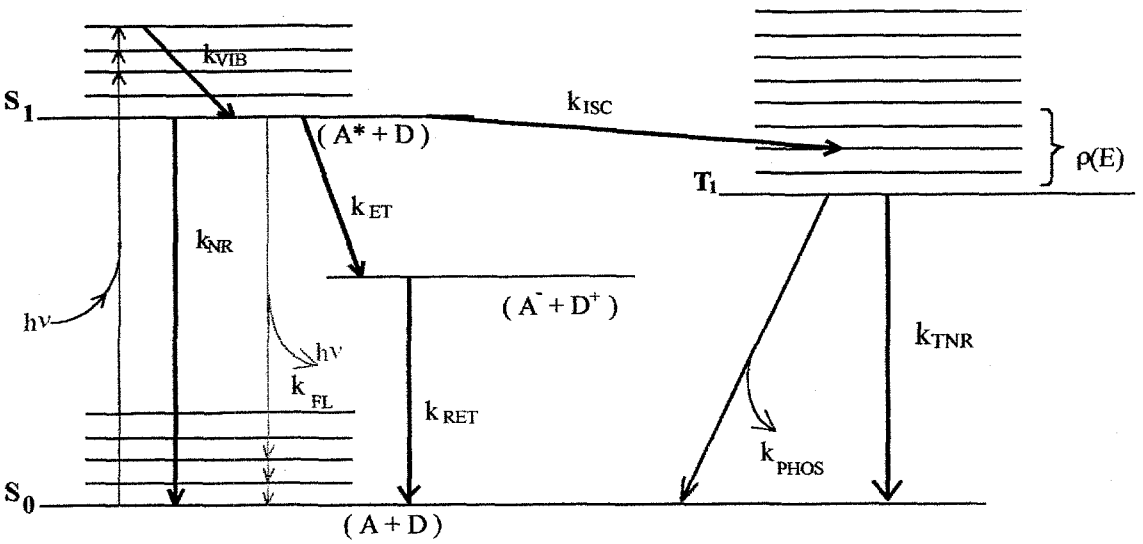

Figure 3.1 - Jablonski diagram of possible pathways for a molecule involved in PET. S_0 is the ground singlet state, S_1 is the first excited singlet state, and T_1 is the first triplet state. k_{NR} is the non-radiative decay rate, k_{FL} is the fluorescent decay rate, k_{ET} is the rate of decay from photoinduced electron transfer, k_{ISC} is the rate of decay due to intersystem crossing, k_{RET} is the rate of return from the charge transfer (A^-+D^+) state to S_0, k_{PHOS} is the rate of phosphorescence from the triplet (T_1) state, and k_{TNR} is the rate of non-radiative decay from the triplet state. A and D represent the electron acceptor and the donor, respectively. Photon energy is shown by hν, and ρ(E) represents the group of vibrational energy levels within the T_1 with energy less than or equal to the energy of S_1.

In the Jablonski diagram above (Figure 3.1) k_{NR} is the non-radiative decay rate, k_{FL} is the fluorescent decay rate, k_{ET} is the rate of decay from photoinduced electron transfer, and k_{ISC} is the rate of decay due to intersystem crossing from the first singlet state to the first (or in some rare cases, second or higher) triplet state (T_1). k_{RET} is the rate of return from the charge transfer (A^-+D^+) state to the ground (S_0) state, k_{PHOS} is the rate of phosphorescence from the triplet (T_1) state, and k_{TNR} is the rate of non-radiative decay from the triplet state. The decay rates will be discussed further in this section.

The first step in the Jablonski diagram above is the absorption of a photon (hν) by the molecule. This occurs at a rate defined by the Einstein absorption coefficient. For the case of unpolarized, isotropic radiation in the dipole approximation the rate of absorption is

$$B_{1\leftarrow 0} = \frac{\pi I(\omega_{10})}{3\hbar^2 c\varepsilon_0}\left|D_{10}\right|^2 \qquad 3.8$$

where $I(\omega_{10})$ is the intensity of incoming light at the frequency corresponding to the energy level difference between the ground state and the excited state, and $\mathbf{D}_{10}$ is the dipole matrix element between these two states.

$$\boldsymbol{D}_{10} = \langle S_1 | \boldsymbol{D} | S_0 \rangle \qquad 3.9$$

The wave functions of the excited and ground states (ignoring vibrational states) are denoted by S_1 and S_0, respectively, and **D** is the dipole operator. (Bransden, 1989) Typically, the rate of absorption is around 10^{15} sec^{-1}. (Lakowicz, 1983)

After absorbing a photon into the manifold of vibrational states above the excited state, a quick relaxation of the molecule occurs through vibrational transitions. k_{VIB} is the rate of relaxation through the upper state vibrational levels down to the lowest vibrational

level of S_1. This process, known as internal conversion, usually occurs in times of order 10^{-12} sec. During this time, changes in bond lengths and angles as well as the sphere of solvent around the molecule contribute to lowering the overall energy. (Lakowicz, 1983)

From the excited state, S_1, several decay paths exist. The nonradiative decay pathway (k_{NR}) from S_1 to S_0 occurs mainly through collisions with other molecules. This results in a transfer of energy from the excited molecule to: 1) translational or rotational energy (kinetic), 2) excitation of another molecule, and/or 3) breakage of bonds. (Levine, 1975)

Spontaneous emission, or in the case of spontaneous singlet decay, fluorescence emission, is labeled by k_{FL} . k_{FL} is equal to A_{01}, the Einstein coefficient for spontaneous emission from state 1 to state 0.

$$A_{0\leftarrow 1} = k_{FL} = \frac{\omega_{10}^3}{3\pi c^3 \hbar \varepsilon_0} |\boldsymbol{D}_{10}|^2 \qquad 3.10$$

It is important to note that in equations 3.8 and 3.10 vibrational states were ignored yielding the approximation that $\omega_{10} = \omega_{01}$. In actuality, the absorbed photon is of greater energy than the emitted photon, due to the energy loss during the relaxation through the vibrational transitions to the lowest vibrational level of the excited state. This phenomenon of the emitted photon being of less energy than the absorbed photon is known as Stoke's shift. (Bransden, 1989)

The fluorescence decay rate is equal to the reciprocal of the intrinsic fluorescence lifetime

$$k_{FL} = \frac{1}{\tau_0} \qquad 3.12$$

of the excited state (S_1). It is important to note that τ_0 is not the same as the observed lifetime (τ_F), except when the quantum yield (Q_F) is equal to one, due to the following relationship.

$$\tau_F = \frac{\tau_0}{Q_F} \tag{3.13}$$

The intrinsic lifetime of the excited state is the average time that the electron remains in that state. If broadening mechanisms are ignored, the natural linewidth of the excited state emission as a function of frequency is described by a Lorentzian

$$I(\omega) = I_0 \frac{\gamma/\pi}{(\omega - \omega_{10}) + \gamma^2} \tag{3.14}$$

where 2γ is the full width at half maximum, and $2\gamma = 1/\tau_0$. (Louden, 1983; Bransden, 1989) The Heisenburg uncertainty principle, $\Delta E \Delta t \geq \hbar$, which results from the Fourier transform relationship between frequency (or energy) and time, can be applied to the emission lineshape to determine the distribution in time. This results in an exponential expression describing the lifetime of the excited state. (Loudon,1983)

$$I(t) = \int_{-\infty}^{\infty} I(\omega) e^{i\omega t} d\omega = \alpha e^{-t/\tau_0} \tag{3.15}$$

where α is a constant. The average over time of the exponential distribution is simply

$$\begin{aligned} \langle \tau \rangle &= \frac{\int_0^\infty tN(t)dt}{\int_0^\infty N(t)dt} \\ &= \frac{\int_0^\infty t\left(N_0 e^{-t/\tau_0}\right)dt}{\int_0^\infty N_0 e^{-t/\tau_0} dt} \\ &= \tau_0 \end{aligned} \tag{3.16}$$

where N(t) is the number of molecules in the excited state at time t, and N_0 is the number of molecules initially in the excited state. (Lakowicz, 1983) However, this is only true for an ideal case with a single exponential. In most cases, the lifetime is a sum of exponentials.

$$I(t) = \sum_i \alpha_i e^{-t/\tau_i} \qquad 3.17$$

This will be discussed in detail later in this chapter.

The non-radiative electron transfer rate, k_{ET}, depends upon whether the electron is transferred through bonds or spatially, through overlapping, non-bonding, orbitals. The mechanism of PET will be discussed in more detail later in this chapter.

Decay through intersystem crossing (ISC) is quantum mechanically forbidden in the dipole approximation. However, when higher order terms are included in the Hamiltonian, decay from the excited single state to a triplet state is possible, although with reduced probability. The ISC rate can be written as

$$k_{ISC} = \left(\frac{2\pi}{\hbar}\right)\rho(E)\left|\langle S_1|H'|T_1\rangle\right|^2 \qquad 3.18$$

where the density of states, ρ(E), refers to the manifold of vibrational levels in the triplet state with energy less than or equal to the energy of S_1 (see Figure 3.1). The interaction Hamiltonian, H', includes a spin-orbit correction to the unperturbed (i.e. without the presence of a radiation field) Hamiltonian, H_0. The complete Hamiltonian is written $H = H_0 + W(\mathbf{r},t) + H'$, where

$$W(\boldsymbol{r},t) = -\mathcal{E} \cdot \boldsymbol{D} \qquad 3.19a$$

and

$$H' \propto \boldsymbol{L} \cdot \boldsymbol{S} \qquad 3.19b$$

W(**r**,t) is a time-dependent potential due to the applied electric field, **E**, and **D** is the dipole operator. (Steinfeld, 1985) The spin-orbit coupling term (**L** · **S**), represents an interaction between the orbital angular momentum, **L**, and the spin operator of the electron, **S**. (Bransden, 1989) Once in the triplet state the electron can non-radiatively decay (k_{TNR}) to S_0, phosphoresce (k_{PHOS}) from T_1 to S_0, or perhaps absorb thermal energy and return to S_1, provided that the energy difference between T_1 and S_1 is on the order of kT.

3.2.2 Quantum Yield and Fluorescence Lifetimes

The fluorescence quantum yield is defined as the ratio of the number of photons emitted to the number of photons absorbed. This can be written in terms of decay rates from the excited state.

$$Q_F = \frac{k_{FL}}{k_{FL}+k_{NR}+k_{ISC}+k_{ET}} \qquad 3.20$$

The observed lifetime can also be written in terms of the decay rates.

$$\tau_F = \frac{1}{k_{FL}+k_{NR}+k_{ISC}+k_{ET}} \qquad 3.21$$

Comparing Equations 3.20 and 3.21, and using Equation 3.12, leads to the expression for the quantum yield in terms of the observed lifetime, τ_F, and the intrinsic lifetime, τ_0, stated earlier (Equation 3.13)

$$Q_F = \frac{\tau_F}{\tau_0} \qquad 3.22$$

For AB this can be expressed as

$$Q_{AB} = \frac{k_{FL}}{k_{FL}+k_{NR}+k_{ISC}+k_{ET}} = \frac{\tau_{AB}}{\tau_0} \qquad 3.23$$

In the case where glucose binds to AB (denoted by ABG) the decay rates k_{FL}, k_{NR}, and k_{ISC} do not change, and the PET pathway is now unavailable, the quantum yield for ABG is

$$Q_{ABG} = \frac{k_{FL}}{k_{FL}+k_{NR}+k_{ISC}} = \frac{\tau_{ABG}}{\tau_0} \qquad 3.24$$

A direct relation between the lifetimes and quantum yields of AB and ABG can now be written.

$$\frac{\tau_{AB}}{\tau_{ABG}} = \frac{Q_{AB}}{Q_{ABG}} \qquad 3.25$$

If the protonation of AB (i.e. the creation of ABH) also eliminates the PET pathway, and the protonation of AB is independent of glucose binding, then the quantum yield for ABH and ABGH should equal that of ABG.

$$Q_{ABG} = Q_{ABH} = Q_{ABGH} \qquad 3.26$$

Equations 3.24 and 3.25 combined with the assumption that the intrinsic lifetime of AB does not change upon protonation or binding of glucose, leads to an equation equating the observed lifetimes of the three species that are not quenched by PET.

$$\tau_{ABG} = \tau_{ABH} = \tau_{ABGH} \qquad 3.27$$

The binding of OH to AB or ABG changes the boron to the form with a tetrahedral center (Figure 2.8b), eliminating the N→B bond. Therefore, the fluorescence of ABOH and ABGOH are quenched by PET.

$$Q_{AB} = Q_{ABOH} = Q_{ABGOH} \tag{3.28}$$

$$\tau_{AB} = \tau_{ABOH} = \tau_{ABGOH} \tag{3.29}$$

The rate of electron transfer, k_{ET}, can be derived from equations 3.23 and 3.24 above.

$$k_{ET} = \frac{1}{\tau_{AB}} - \frac{1}{\tau_{ABG}} \tag{3.30}$$

This will become important later when comparing the electron transfer rates measured by electrochemical methods. Note that Equation 3.30 can also be used for MAMA and AB-B by replacing the subscript AB with MAMA or AB-B, and ABG with MAMAH or AB-BH.

3.2.3 Steady State Fluorescence

Assuming all forms of AB are fluorescent to some degree, the steady-state equation for measured fluorescence intensity is

$$\begin{aligned} F = {} & \sigma_{AB}[AB] + \sigma_{ABG}[ABG] + \sigma_{ABH}[ABH] + \sigma_{ABOH}[ABOH] \\ & + \sigma_{ABGH}[ABGH] + \sigma_{ABGOH}[ABGOH] \end{aligned} \tag{3.31}$$

where $\sigma_i = D_i Q_i$, where D_i is a constant related to the absorption cross-section and spectral properties of the molecule as well as the detector response, and Q_i is the quantum yield of that particular species. Assuming the cross-section and the spectra for AB, ABH,

ABOH, ABG, ABGH and ABGOH are approximately equal, i.e. effects of H, OH and glucose are small compared to AB and therefore do not change spectral properties when bound to AB, we can assume $D_{AB} = D_{ABH} = D_{ABOH} = D_{ABG} = D_{ABGH} = D_{ABGOH} = D$. Using equations 3.26 and 3.28, equation 3.31 can now be written as

$$\begin{aligned} F = D\{&Q_{AB}[AB] + Q_{ABG}[ABG] + Q_{ABG}[ABH] \\ &+ Q_{AB}[ABOH] + Q_{ABG}[ABGH] + Q_{AB}[ABGOH]\} \end{aligned} \tag{3.32}$$

In fluorescence spectroscopy measurements, relative intensity is often used, as opposed to absolute intensity, to lessen the effects of source fluctuations and other instrumental and experimental artifacts. Dividing Equation 3.32 for F by the fluorescence intensity when $[G]_0 = 0$ (labeled F_0), yields the relative fluorescence intensity, R.

$$\begin{aligned} R = \frac{F}{F_0} &= \frac{\begin{aligned} &D\{Q_{AB}[AB] + Q_{ABG}[AB_{N-B}] + Q_{ABG}[ABG] + Q_{ABG}[ABH] \\ &+ Q_{AB}[ABOH] + Q_{ABG}[ABGH] + Q_{AB}[ABGOH]\} \end{aligned}}{D\{Q_{AB}[AB] + Q_{ABG}[AB_{N-B}] + Q_{ABG}[ABH] + Q_{AB}[ABOH]\}} \\ &= 1 + \left\{ \frac{Q_R([ABG] + [ABGH]) + [ABGOH]}{Q_R[ABH] + [AB] + [ABOH]} \right\} \end{aligned} \tag{3.33}$$

In Equation 3.33 $[AB_{N\text{-}B}]$ is the concentration of AB molecules with an enhanced N→B bond preventing PET. The difference in fluorescence between $[AB_{N\text{-}B}]$ and [ABH] or [ABG] in indistinguishable and therefore $[AB_{N\text{-}B}]$ is grouped with [ABH] in the relative intensity equation. The quantum yield of $AB_{N\text{-}B}$ is accordingly equal to Q_{ABG}, and Q_R is the ratio of quantum yields.

$$Q_R = \frac{Q_{ABG}}{Q_{AB}} \tag{3.34}$$

For determining relative intensity as a function of pH, rather than glucose, F is divided by F_2, the fluorescence intensity at pH = 2, assuming all AB is protonated.

$$R_{pH} = \frac{F}{F_2} = 1 + \left\{ \frac{Q_R[ABG] + [AB] + [ABOH] + [ABGOH]}{Q_R[AB]_0} \right\} \qquad 3.35$$

A useful measure of sensor efficiency is the fraction of fluorescence switching. For a fluorescent sensor molecule the switching fraction is defined as the relative increase in fluorescence with the addition of glucose.

$$SF = \frac{(F - F_0)}{F_0} \qquad 3.36$$

3.2.4 Fluorescence Lifetimes

In the time domain, the fluorescent decay from an infinitesimally short excitation pulse applied to a mixture of anthracene boronate molecules, both bound to glucose (ABG) and unbound (AB), is the sum of exponential decays. Using equations 3.27 and 3.29 for simplicity,

$$I(t) = (\alpha_{AB} + \alpha_{ABOH} + \alpha_{ABGOH}) e^{-t/\tau_{AB}} + (\alpha_{ABG} + \alpha_{ABH} + \alpha_{ABGH}) e^{-t/\tau_{ABG}} \qquad 3.37$$

where the α's are coefficients, with values between zero and one. These coefficients can be related to the concentration of fluorescing molecules by examining the steady state fluorescence intensity, F , given by

$$F = \sigma_{AB}([AB] + [ABOH] + [ABGOH]) + \sigma_{ABG}([ABG] + [ABH] + [ABGH]) \qquad 3.38$$

where [ ] denotes concentration and σ_i is proportional to the quantum yield, Q_i . With $Q_{ABG} > Q_{AB}$ the maximum fluorescence is obtained when ([AB]+[ABOH]+[ABGOH]) = 0, and the minimum when ([ABG]+[ABH]+[ABGH]) = 0. The ratio of maximum to minimum fluorescence is then

$$\frac{F_{max}}{F_{min}} = \frac{\sigma_{ABG}([ABG]+[ABH]+[ABGH])}{\sigma_{AB}([AB]+[ABOH]+[ABGOH])} \qquad 3.39$$

Integrating the equation for the time evolution of the fluorescence decay yields a steady state expression.

$$F = \int_0^\infty I(t)dt = (\alpha_{AB} + \alpha_{ABOH} + \alpha_{ABGOH})\tau_{AB} + (\alpha_{ABG} + \alpha_{ABH} + \alpha_{ABGH})\tau_{ABG} \qquad 3.40$$

The relative fluorescence intensity can also be found from lifetime measurements by dividing Equation 3.40 by the same equation at pH 2 (maximum fluorescence intensity).

$$R(\alpha,\tau) = \frac{(\alpha_{ABG} + \alpha_{ABH} + \alpha_{ABGH})\tau_{ABG} + (\alpha_{AB} + \alpha_{ABOH} + \alpha_{ABGOH})\tau_{AB}}{\left[(\alpha_{ABG} + \alpha_{ABH} + \alpha_{ABGH})\tau_{ABG} + (\alpha_{AB} + \alpha_{ABOH} + \alpha_{ABGOH})\tau_{AB}\right]_{pH=2}} \qquad 3.41$$

Maximum fluorescence intensity occurs when ($\alpha_{AB} + \alpha_{ABOH} + \alpha_{ABGOH}$) = 0, and the corresponding minimum occurs when ($\alpha_{ABG} + \alpha_{ABH} + \alpha_{ABGH}$) = 0.

$$\frac{F_{max}}{F_{min}} = \frac{\sigma_{ABG}([ABG]+[ABH]+[ABGH])}{\sigma_{AB}([AB]+[ABOH]+[ABGOH])} = \frac{(\alpha_{ABG} + \alpha_{ABH} + \alpha_{ABGH})\tau_{ABG}}{(\alpha_{AB} + \alpha_{ABOH} + \alpha_{ABGOH})\tau_{AB}} \qquad 3.42$$

Equation 3.42 uses the previous assumptions that the D_i's are equal, and that the ratio of quantum yields is equal to the ratio of the lifetimes for AB and ABG (Equation 3.25). This simplifies the ratio of fluorescence maximum and minimum to a relationship between concentrations and preexponential coefficients.

$$\frac{([ABG]+[ABH]+[ABGH])}{([AB]+[ABOH]+[ABGOH])} = \frac{(\alpha_{ABG} + \alpha_{ABH} + \alpha_{ABGH})}{(\alpha_{AB} + \alpha_{ABOH} + \alpha_{ABGOH})} \qquad 3.43$$

This simple, yet powerful, equation is only valid for a system with two lifetime components where the spectral properties of each are the same. For MAMA, as well as AB-B, only two species exist, therefore modification of Equation 3.43 is very straightforward.

$$\frac{[MAMAH]}{[MAMA]} = \frac{\alpha_{MAMAH}}{\alpha_{MAMA}} \qquad 3.44$$

The fractional contribution by one component to the total fluorescence of a multiexponential decay is expressed in the following equation.

$$f_i = \frac{\alpha_i \tau_i}{\sum_j \alpha_j \tau_j} \qquad 3.45$$

The pre-exponential factors, α_i, and the fluorescence lifetimes, τ_i, are from Equation 3.37.

The average fluorescence lifetime, or first moment, of a multiexponential decay function is expressed as

$$\langle \tau \rangle = \frac{\int_0^\infty t\left(\sum_i \alpha_i e^{-t/\tau_i}\right)dt}{\int_0^\infty \left(\sum_i \alpha_i e^{-t/\tau_i}\right)dt} = \frac{\sum_i \alpha_i \tau_i^2}{\sum_i \alpha_i \tau_i} = \sum_i f_i \tau_i \qquad 3.46$$

3.3 Photoinduced Electron Transfer (PET)

Photoinduced electron transfer occurs between two separate molecules (inter) as well as within a single molecule (intra). The most important difference between the two types is the effect of diffusion. In intermolecular electron transfer, the diffusion rate can control the rate of fluorescence quenching by electron transfer. The basic reactions can be written as

$$\begin{array}{ccccccc} D + A^* & \xleftrightarrow{k_{DIF},\, k_{-DIF}} & DA^* & \xleftrightarrow{k_{ET},\, k_{-ET}} & D^+A^- & \xrightarrow{k_{RET}} & D + A \\ \Big\downarrow \frac{1}{\tau_0} & & \Big\downarrow \frac{1}{\tau_F} & & & & \\ A & & DA & & & & \end{array} \qquad 3.47$$

where D represents the molecule that donates an electron to the acceptor molecule, A. The rate of diffusion bringing D closer to A is given by k_{DIF}, while they diffuse apart at a rate of k_{-DIF}. Forward and back electron transfer rates are given by k_{ET} and k_{-ET}, respectively, and k_{RET} is the rate the charge transfer complex returns to the ground state, where both molecules are neutral. Applying a steady state treatment to the above reaction network (i.e. setting the corresponding rate equations to zero and solving for [D], τ_F, and τ_0), the rate of fluorescence quenching of A^* is

$$k_q = \left(\frac{1}{[D]}\right)\left(\frac{1}{\tau_F} - \frac{1}{\tau_0} - 1\right) = \frac{k_{DIF}}{1 + \left(\frac{k_{-DIF}}{k_{ET}}\right)\left(1 + \frac{k_{-ET}}{k_{RET}}\right)} \qquad 3.48$$

where the first part of Equation 3.48 is the Stern-Volmer equation. (Kavarnos, 1993) A common assumption is that the rate of back electron transfer is very small compared to the rate of return, $k_{-ET} << k_{RET}$. This simplifies the equation above.

$$k_q = \frac{k_{DIF}}{1 + \left(\frac{k_{-DIF}}{k_{ET}}\right)} \qquad 3.49$$

For intramolecular systems diffusion is not a concern, and the reaction network is simplified.

$$DA^* \xleftarrow{k_{ET}, k_{-ET}} D^+A^- \xrightarrow{k_{RET}} DA \qquad 3.50$$

Using the steady state treatment on the reaction equations as before,

$$k_q = \frac{k_{ET}k_{RET}}{k_{-ET} + k_{RET}} \qquad 3.51$$

assuming that $k_{-ET} << k_{RET}$, Equation 3.51 is further simplified.

$$k_q = k_{ET} \qquad 3.52$$

A common architecture for a molecule exhibiting intramolecular PET is the donor-spacer-acceptor (typically denoted by D-A) design. (Bissell, 1993; de Silva, 1997) For the sensor molecules examined here, the electron donor is the lone pair on the amine, the acceptor is the fluorophore (e.g. anthracene), and the spacer is the carbon linker between them. The previous Jablonski diagram (Figure 3.1) includes notation relating the electronic states to the D-A design. The excited state, S_1, is labeled D-A* due to the excitation of the acceptor component. After electron transfer the molecule is in a charge transfer state denoted by D^+-A^-.

To create a picture of electron transfer, potential energy surfaces are commonly used. These surfaces are approximated by parabolic curves that show the energy as a function of nuclear position in the harmonic oscillator approximation, $P.E. = \frac{1}{2}kx^2$.

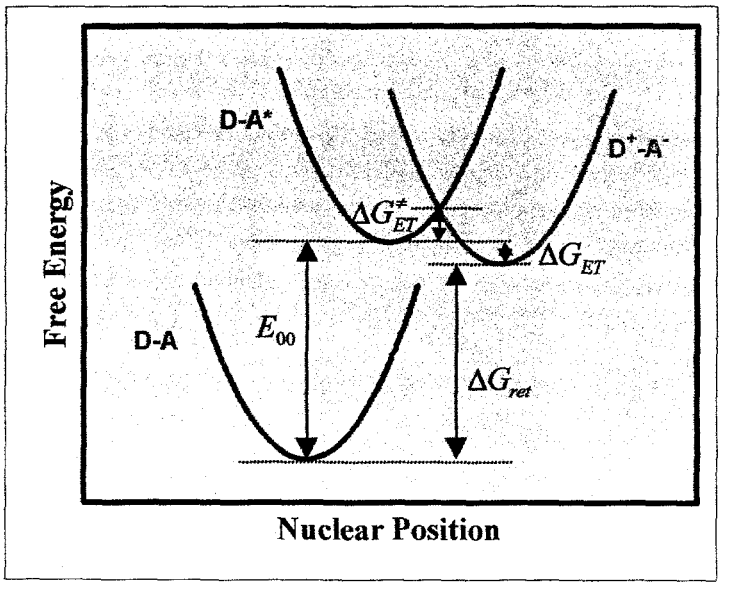

Figure 3.2 - Potential energy surfaces for the ground state, excited state, and charge transfer state of a molecule, D-A.

The energy of the zero order transition (from the lowest vibrational level in the ground state, D-A, to the lowest vibrational level in the excited state, D-A*) is E_{00}. The height of the energy barrier to electron transfer is $\Delta G_{ET}^{\neq}$, while the free energy difference between the excited state (D-A*) and the charge transfer state (D^+-A^-) is given by ΔG_{ET}. It follows that the return energy difference is $\Delta G_{ret} = E_{00} - \Delta G_{ET}$.

Transfer of an electron in PET can occur either through space (due to orbital overlap), or through bonds in the spacer. The number of bonds, and the flexibility of the molecule will affect the rate of transfer. Too many atoms in the spacer, and through bond transfer becomes too slow to compete with other decay paths. Too few atoms and the spatial requirements for orbital overlap are not met.(Kavarnos, 1993)

3.4 Electron Transfer Rate and Electrochemistry

Two theories of electron transfer are predominant in the literature. The more empirical theory, was developed by Rehm and Weller. (Rehm, 1970) It incorporates the adiabatic outersphere approximation, which assumes that the outer solvent sphere does not change during the electron transfer reaction. The molecules undergoing electron transfer are treated as rigid spheres. The equation for the electron transfer free energy barrier is

$$\Delta G_{ET}^{\neq} = \left[\left(\frac{\Delta G_{ET}}{2}\right)^2 + \left(\Delta G_{ET}^{\neq}(0)\right)^2\right]^{\frac{1}{2}} + \frac{\Delta G_{ET}}{2} \qquad 3.53$$

where $\Delta G_{ET}^{\neq}(0)$, the activation free enthalpy, was determined from experiments to be equal to 2.4 kcal/mol. (Rehm, 1970)

Marcus theory includes a more rigorous treatment of solvent effects as well as changes in the bond lengths due to molecular vibrations involved in electron transfer. This theory was developed using statistical mechanics, beginning with the potential energy surfaces in Figure 3.3.1.(Marcus, 1965) The free energy barrier in Marcus theory is

$$\Delta G_{ET}^{\neq} = \frac{\lambda}{4}\left[\left(\frac{\Delta G_{ET}}{\lambda}\right)+1\right]^2 \qquad 3.54$$

where $\lambda = \lambda_i + \lambda_o$, the inner- and outer-sphere solvent reorganization energies. (Kavarnos, 1993) The inner-sphere reorganization energy is due to changes in bond lengths of the reactant (R, or in this case, D-A^*) and the product (P, or D^+-A^-)

$$\lambda_i = \sum_n \left[\frac{f(R)_n f(P)_n}{f(R)_n + f(P)_n}\right](\Delta q_n)^2 \qquad 3.55$$

where $f(R)_n$ and $f(P)_n$ are the force constants for the nth vibration and Δq_n is the change in bond length between reactant and product state for the nth vibrational mode. (Kavarnos, 1993) This quantity is difficult to calculate, but it is large enough that it should not be neglected. One case involving stretching of metal-oxygen bonds yielded a λ_i of approximately 40 kcal/mol.(Marcus, 1965) This inner-sphere reorganizational energy will therefore be treated as a constant of the molecule, regardless of solvent. The outersphere solvent energy is dependant upon the dielectric properties of the solvent.

$$\lambda_0 = \Delta e^2\left(\frac{1}{2r_D} - \frac{1}{2r_A} + \frac{1}{d_{cc}}\right)\left(\frac{1}{n^2} - \frac{1}{\varepsilon_s}\right) \qquad 3.56$$

The difference in charge between product and reactant is given by Δe. The donor and acceptor molecules undergoing electron transfer are assumed to be spheres with radii r_D and r_A, with the distance between them, d_{cc}, equal to the sum of the radii. The solvent

dependence is in the last term where n is the index of refraction and ε_s is the dielectric constant. This term is valid for intramolecular as well as intermolecular electron transfer. (Marcus, 1965)

The most controversial difference between Rehm-Weller and Marcus theories is their predictions in what Marcus labeled "the inverted region." (Kavarnos, 1993) The inverted region occurs when

$$-\Delta G_{ET} > \lambda \qquad 3.57$$

At this point, and for increasing values of ΔG_{ET}, the rate of electron transfer is predicted to decrease. However, in the model by Rehm-Weller the electron transfer rate becomes constant. The existence of an inverted region has been seen experimentally for selected molecules, however it is often obscured by other kinetic processes. (Kavarnos, 1993)

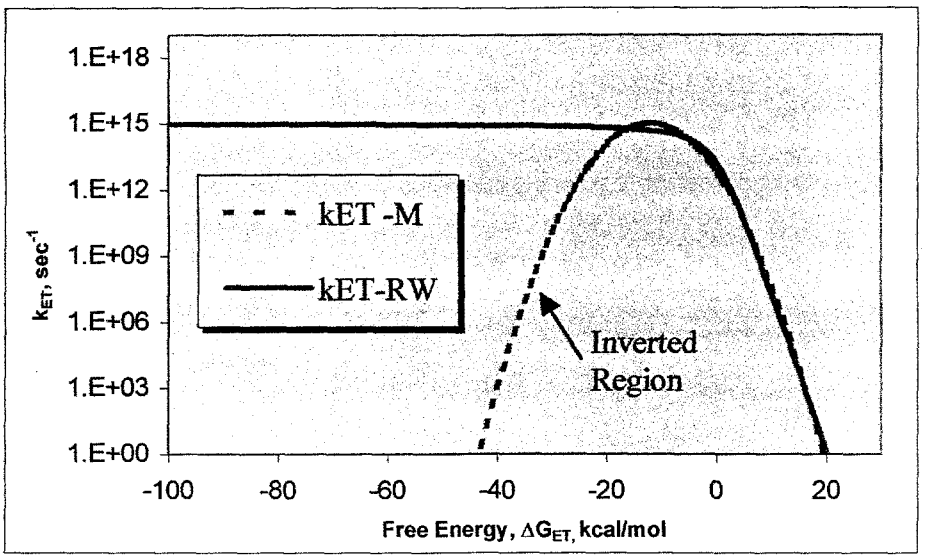

Figure 3.3 - Comparison between the electron transfer rate predicted by Rehm-Weller and Marcus. $k_{ET} \propto Exp(-\Delta G^{\neq}_{ET} / RT)$

Experimental values of ΔG_{ET} are measured using electrochemistry techniques. This allows for a direct measurement of the oxidation potential of the amine donor, denoted by $E^0(D/D^+)$ for the electromotive force (emf) of the removal of an electron, as well as the reduction potential of the acceptor fluorophore, denoted by $E^0(A^-/A)$ for the emf of the addition of an electron. These measurements are useful in predicting the ability of a newly synthesized sensor molecule to exhibit PET. For the case of intramolecular electron transfer, the free energy, ΔG_{ET}, is determined from the measured values by the Rehm-Weller equation. (Kavarnos, 1993)

$$\Delta G_{ET}[kcal/mol] = 23.06\left[E^0(D/D^+) - E^0(A^-/A)\right] - \Delta E_{00} \qquad 3.58$$

The energy difference between the ground state (D-A) and the excited state (D-A*) is given by ΔE_{00} and may be estimated using the average of the peak fluorescence excitation (λ_{ex}) and emission (λ_{em}) wavelengths.

$$\Delta E_{00} = \frac{hc}{\lambda_{00}} \approx \frac{2hc}{(\lambda_{ex} + \lambda_{em})} \qquad 3.59$$

In the following chapters, electrochemistry measurements will be used to determine the feasibility of electron transfer. If ΔG_{ET} is negative then the electron transfer is thermodynamically allowed. Also, the height of the electron transfer barrier, $\Delta G_{ET}^{\neq}$, (see Figure 3.2) will be determined in order to calculate of the electron transfer rate, $k_{ET} \propto Exp(-\Delta G_{ET}^{\neq} / RT)$.

REFERENCES

Bransden, B.H., and C.J. Joachain. Introduction to Quantum Mechanics. John Wiley & Sons Inc., New York, 1989.

Bissell, R.A. et al. Fluorescent PET (Photoinduced Electron Transfer) Sensors. *Topics in Current Chemistry* 168: 223-264. Springer-Verlag, Berlin, 1993.

de Silva, A.P. et al. Signaling Recognition Events with Fluorescent Sensors and Switches. *Chem. Rev.* 97: 1515-1566, 1997.

James, T.D., et al. Novel Photoinduced Electron-transfer Sensor for Saccharides based on the Interaction of Boronic Acid and Amine. *J. Chem. Soc., Chem. Commun.*: 477-478, 1994.

Kavarnos, G.J. Fundamentals of Photoinduced Electron Transfer. VCH Publishers, Inc., New York, 1993.

Lakowicz, J.R. Principles of Fluorescence Spectroscopy. Plenum Press, New York, 1983.

Leninger, A.L., D.L. Nelson, and M.M. Cox. Principles of Biochemistry, second edition. Worth Publishers, New York, 1993.

Levine, I.N. Molecular spectroscopy. Wiley, New York, 1975.

Loudon, R. The Quantum Theory of Light, second edition. Clarandon Press, Oxford, 1983.

Maiti, M., et al. Photophysics of 4-methoxy-benzo[b]thiophene in different environments. Its role in non-radiative transitions both as an electron and as an energy donor. *Journal of Luminescence* 82:259-276, 1999.

Marcus, R.A. On the Theory of Electron-Transfer Reactions. VI. Unified Treatment for Homogeneous and Electrode Reactions. *J. of Chem. Phys.* 43 (2): 679-701, 1965.

Rehm, D., and A. Weller. Kinetics of Fluorescence Quenching by Electron and H-Atom Transfer. *Israel Journal of Chemistry* 8: 259-271, 1970.

Steinfeld, J.I. Molecules and Radiation, second edition. The MIT Press, Massachusetts, 1985.

Yoon, J., and A.W. Czarnik. Fluorescent Chemosensors of Carbohydrates. A Means of Chemicaly Communicating the Binding of Polyols in Water Based on Chelation-Enhanced Quenching. *J. Am. Chem. Soc.* 114: 5874-5875, 1992.

Chapter IV

EXPERIMENTAL METHODS

This chapter will describe the materials and equipment used in the experiments as well as the experimental methods of data collection and analysis. The technique of measuring fluorescence lifetimes in the frequency domain will be presented along with the essential equations.

4.1 Sample Preparation

All of the sensor molecules, except for MAMA, were synthesized by researchers in the Chemistry and Materials Science (C&MS) group at LLNL. MAMA (9-(methylaminomethyl)-anthracene) is commercially available (Aldrich, 73356-19-1). Stock solutions of the sensor molecules were prepared in (99.9%) MeOH obtained from Aldrich. Buffer solutions were made by the C&MS group for pH 2 through 13. The buffers are 0.1 M in water and are composed of the following:

pH	Acid / Base
2.0	HCl / KCl
4.0	HOAc / NaOAc
5.0	HOAc / NaOAc
6.0	KH_2PO_4 / NaOH
8.0	KH_2PO_4 / NaOH
8.6	NH4Cl / NH3
9.2	$NaHCO_3$ / $Na2CO_3$
9.5	$NaHCO_3$ / $Na2CO_3$
10.0	$NaHCO_3$ / NaOH
11.0	$NaHCO_3$ / NaOH
12.0	Na_2HPO_4 / NaOH
13.0	KCl / NaOH

Table 4.1 - Composition of pH buffers.

where Ac represents acetate. Buffers at pH 7.4 were made from a powder purchased from Sigma (P-3813). This phosphate buffered saline (PBS) which includes 0.138 M NaCl and 0.0027 M KCl, was prepared according to directions at 0.01 M and was measured to have a pH value of 7.4 at 25° C. The D – (+) – Glucose (99.5%) was obtained from Sigma (EEC# 50-99-7) and was prepared at concentrations of 300 g/L in water.

Samples for all fluorescence measurements were made in standard 3 mL quartz cuvettes from either Starna Cells or NSG Precision Cells, Inc. Sensor molecule concentrations were kept in the micromolar range to avoid excimer formation and self-absorption. (McVey, 1976; Lakowicz, 1983) For lifetime measurements, glycogen and POPOP were used as standard compounds as explained in Section 4.4. The glycogen was obtained from Sigma (G-8751), type II from oyster, EEC#232-683-8. The POPOP (1,4-

bis(5-Phenyl-2-oxazolyl)benzene) was a laser grade fluorophore obtained from Exciton. For electrochemical measurements, acetonitrile (ACN) with 0.1 M Tetrabutylammonium Perchlorate (TBAP) was used as the solvent for the sensor molecules. The ACN (99%) was obtained from Aldrich, EEC#200-835-2, and the TBAP was from Sigma, EEC#217-655-5. Bubbling N_2 gas into solution is a common method for eliminating the free O_2 that can quench the fluorescence through collisions. (Koller, 1991) Unless otherwise stated, degassing of the samples by N_2 prior to taking a measurement was determined to have no significant effect on the fluorescence. All samples were held at 25° C using a Neslab temperature bath, model RTE-111.

4.2 Steady State Fluorescence

Steady state fluorescence and fluorescence lifetime measurements were performed with the same instrument. A Fluorolog-Tau-3-21 (Jobin Yvon Horiba, formerly SPEX, Instruments S.A., Inc.), fluorescence spectrometer was used with a double monochrometer in the excitation path, a single monochrometer in the emission path, and a Pockels cell to modulate the excitation intensity for lifetime measurements (Figure 4.1).

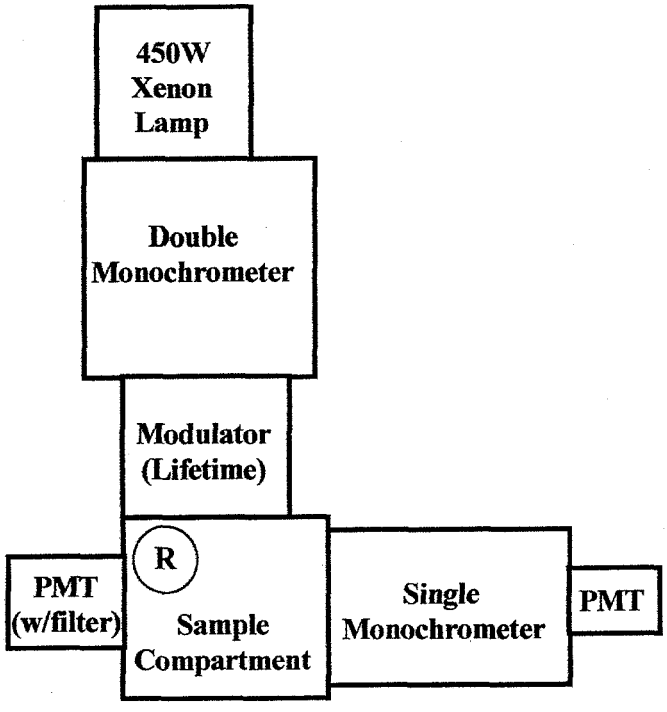

Figure 4.1 - Fluorolog Tau-3-21 (Jobin Yvon, Horiba)

The Xe lamp spectrum ranges from 250 nm to 900 nm. The double monochrometer has two 1200 groove/mm gratings blazed for optimal transmission at 330 nm. The modulator was taken out of the light path for steady state measurements, and will be described in the section on fluorescence lifetime measurements. A reference photodiode detector, R, measures the intensity of the excitation light just before it enters the sample compartment. The sample compartment holds standard 1 cm x 1 cm x 3 cm cuvettes and is connected to the temperature bath to regulate the sample temperature. The emission monochrometer has one 1200 groove/mm grating blazed at 500 nm. Hamamatsu (model R928P) photomultiplier tubes (PMTs) are used for photon detection.

4.3 Excitation/Emission Spectra

Fluorescence excitation spectra were acquired by varying the excitation wavelength while measuring the fluorescence at a single emission wavelength. Emission spectra were taken using a constant excitation wavelength and varying the detected fluorescence wavelength. Single excitation and emission wavelengths used were chosen to optimize the fluorescence output. The fluorescence signal is corrected for lamp fluctuations by dividing the measured signal by the signal from the reference detector. This also eliminates errors made by non-uniform reflections in the excitation monochrometer. Corrections for errors due to non-uniform reflection by the gratings in the emission monochrometer, as well as variations in detector sensitivity as a function of wavelength, were not made because they were negligible for the range of wavelengths used. Excitation and emission wavelengths are listed in Table 4.2 along with the band pass of the slits in the excitation and emission monochrometers. Band pass was chosen so that the fluorescent signal was at a maximum while remaining in the linear range of the detector. No changes were noted on the fluorescence emission as a function of excitation bandwidth.

Compound	Excitation (nm)	Emission (nm)	Slit Band Pass (nm)
MAMA	367.0	414.0	1.0
AB-B	370.6	418.0	1.5
AB	369.0	417.5	1.5
COB	440	545	3
NIB	425	548	Ex-3, Em-4

Table 4.2 - Excitation and emission wavelengths used for steady state fluorescence measurements. Slit band pass settings were the same for both excitation and emission scans, except where noted.

The total emission intensity was measured by integrating over the entire wavelength range of emission using the integration function in DataMax, the software package used to control the Fluorolog. Since all of the parameters were kept constant for each molecule, the relative intensity of each sample was obtained using the integrated area under the emission spectrum. Phosphorescence was not observed in any of the samples.

4.4 Fluorescence Lifetime Measurements

Measurements of fluorescence lifetimes were done in the frequency domain. This is also known as the phase-modulation technique. Instead of using a short pulse of light to excite fluorescence, as is commonly done, the sample is excited by a continuous beam of light with sinusoidally modulated intensity. The resultant fluorescence is also sinusoidally modulated, but reduced in intensity and with a phase lagging that of the incident light. This phase lag, as well as the ratio of demodulation, is a measure of the fluorescence lifetime. Figure 4.2 shows the relationship between sinusoidally modulated excitation light of the form

$$I(t) = A + B\sin(\omega t) \qquad 4.1$$

where A and B are constants describing the DC offset and modulation amplitude of the light, and $\omega = 2\pi f$ where f is the frequency of modulation in Hz. The resulting fluorescence light is of the form

$$F(t) = a + b\sin(\omega t - \phi) \qquad 4.2$$

where a and b are constants similar to A and B, and ϕ is the phase difference between the excitation light and the fluorescent light.

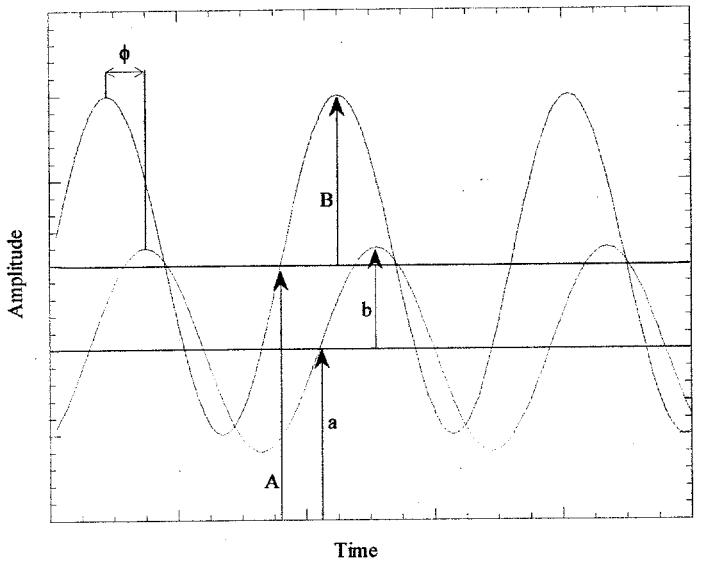

Figure 4.2 - The fluorescence (red) is phase shifted, ϕ, from the excitation light (blue). The amount of phase shift is correlated with the lifetime of the fluorophore.

During fluorescence lifetime measurements the light modulator was placed in the path of the excitation light. When the applied voltage is modulated, the intensity of the light passing through the Pockels cell is also modulated. The frequency of modulation can range from 0.1 to 310 MHz. To detect the modulated light, the PMTs are also modulated. By modulating the detectors at a frequency slightly (~ 12 kHz) different from the frequency of the incident and fluorescent light, a beat frequency is created which contains the desired phase and modulation information. This method of cross-correlation detection is described further in Appendix A.

A reference fluorophore with a known lifetime is used to minimize instrumental errors. For MAMA, AB-B, and AB the reference fluorophore was POPOP. POPOP in methanol has a known lifetime of 1.32 nsec. (Atzeni, 1997) The lifetime of POPOP was found to remain stable at temperatures ranging from 20° to 40° C. Reference fluorophores must have excitation and emission wavelengths similar to the fluorophore of interest. When such a fluorophore is not available, a scattering solution can be used as a reference. For the long-wavelength sensor molecules such as COB and NIB, glycogen was used as the reference compound. Glycogen is a polysaccharide with a large, but very compact structure (Lehninger, 1993) ideal for scattering light in solution. It does not fluoresce in the wavelength range used in these experiments and can therefore be used as a scatterer with a lifetime of zero. Glycogen was also used to verify the 1.32 nsec lifetime of POPOP. A Schott KV399 filter was used to eliminate the excitation light and collect all emission above 399 nm for lifetime measurements.

4.5 Frequency Domain Equations

The incident, or excitation, light used for frequency domain measurements was described by Equation 4.1, and the resulting fluorescent light by Equation 4.2. For a complete derivation of the frequency domain equations, the reader is referred to Appendix A. To measure the fluorescence lifetime the phase (ϕ) and demodulation (m) are measured while the modulation frequency is varied. For a single exponential decay, the equations relating the fluorescence lifetime to the phase and modulation are straightforward.

$$\tan\phi = \omega\tau \tag{4.3}$$

$$m \equiv \frac{B/A}{b/a} = \frac{1}{\sqrt{1+\omega^2\tau^2}} \tag{4.4}$$

However, for a multiexponential decay, the equations become more complex.

$$\tan\phi = N/D \tag{4.5}$$

$$m \equiv \frac{B/A}{b/a} = \sqrt{N^2 + D^2} \tag{4.6}$$

where N and D are

$$N = \sum_{i=1}^{n} f_i \sin\phi_i \cos\phi_i \tag{4.7}$$

$$D = \sum_{i=1}^{n} f_i \cos^2\phi_i \tag{4.8}$$

The total number of exponential components is n, f_i is the fractional intensity of the *i*th component, and ϕ_i is the phase shift from the *i*th component. (Lakowicz, 1983) Extracting the components of a multiexponential decay from the phase and modulation data is made manageable with computational curve fitting algorithms.

4.6 Curve fitting

One of the more commonly used programs for the analysis of phase-modulation data was developed at the University of Illinois, Globals Unlimited. (Beechem, 1998) This program uses a nonlinear minimization technique credited to Marquardt and Levenberg. Experimental data points ($data_i$) are compared to values from the exponential

fits (fit_i). The chi-square function (χ^2) is a measure of the agreement between data and theory.

$$\chi^2 = \sum_{i=1}^{n} \frac{(data_i - fit_i)^2}{\sigma_i^2 (N - m - 1)} \qquad 4.9$$

where σ_i is the standard deviation for each data point measured, N is the total number of data points, and m is number of fitting parameters. To extract the fluorescence lifetimes and pre-exponential coefficients fitting parameters are adjusted to minimize χ^2. A value of χ^2 much higher or lower than unity indicates that the data either does not fit the theoretical exponential equations or the standard deviations (errors in individual measurements) are incorrect. (Beechem, 1998)

The Globals Unlimited program allows for multiple experiments to be linked together, thereby placing constraints on the lifetime values or other parameters. For all data points shown in the next chapter at least two, and usually five, trials were performed in succession. With the temperature held constant, the lifetime values of the samples are not expected to change. Therefore, the lifetime values for each sample were linked together for all of the trials. For a step-by-step procedure of the analysis of lifetime data the reader is referred to Appendix C. Error analysis was performed on the data using the standard deviation of the values obtained for measurements on each sample without linking trials. Error bars are shown on graphs of fluorescence lifetime data unless the error is smaller than the data point used to plot the value. A more detailed description of the error analysis follows in Appendix B.

4.7 Electrochemistry

Researchers at the Medical Photonics Laboratory at LLNL made the electrochemical measurements using a Cypress Systems potentiostat. The electrochemical cell includes three electrodes: a glassy carbon working electrode, a platinum wire quasi-reference electrode, and a plantinum wire counter electrode. Solutions were degassed with a steady stream of nitrogen. Sensor molecule concentration was around 10^{-4} M in ACN with 0.1M TBAP as the supporting electrolyte. ACN was used as the solvent, rather than PBS and methanol, because it is aprotic, or unable to donate hydrogen ions, and thus does not interact with the molecule under investigation. Electrochemical measurements of oxidation or reduction potential are accurate to within ±0.5 kcal/mol.

REFERENCES

Atzeni, S.H., Ph.D. Jobin Yvon Horiba. *Personal communication*, 1997.

Beechem, J.M., E. Gratton, et al. Globals Unlimited, Technical Reference Manual, Revision 3. Board of Trustees, University of Illinois, 1998.

Koller, E. and O. Wolfbeis. Fiber Optic Chemical Sensors and Biosensors, Vol. I, CRC press, 1991.

Lakowicz, J.R.. Principles of Fluorescence Spectroscopy. Plenum Press, New York, 1983.

Leninger, A.L., D.L. Nelson, and M.M. Cox. Principles of Biochemistry, second edition. Worth Publishers, New York, 1993.

McVey, J.K., D.M. Shold, and N.C. Yang. Direct observation and characterization of anthracene excimer in solution. *J. of Chem. Phys.* 65 (8), 3375-3376, 1976.

Chapter V

RESULTS – Anthracene Derivatives

This chapter will present and discuss the fluorescence steady-state and lifetime measurements of MAMA, AB-B and AB. Steady-state fluorescence measurements were made to measure the pK_a of the molecule, as well as the switching fraction with glucose and pH. Fluorescence lifetime measurements were used to examine the N→B bond and measure the rate of electron transfer. Electrochemistry measurements also yielded an electron transfer rate. This rate was compared to the rate obtained from fluorescence measurements to assess the ability of electrochemistry to predict electron transfer rates and therefore as a method for screening possible candidates for a new sensor molecule. At the end of the chapter, preliminary results from *in vitro* fluorescence measurements of AB covalently linked to a polymer membrane will be presented and discussed.

5.1 9-Methylaminomethylanthracene (MAMA)

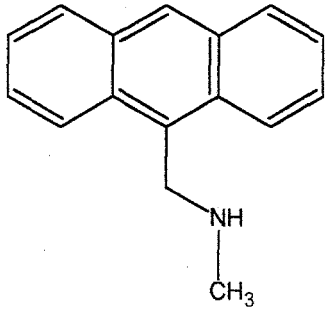

5.1.1 Relevance

MAMA is the parent compound for many fluorescent sensor molecules with the fluorphore-spacer-receptor architecture (Bissell, 1993). AB is just one example of a compound that uses MAMA as a building block. Specifically, AB is MAMA with an additional methylphenylboronic acid linked to the amine. The molecules built from MAMA are useful as sensors for many different analytes including sodium, potassium, pH, carboxylate, sulfate, and saccharides. (deSilva, 1986; Huston, 1989; deSilva, 1985) To understand anthracene boronate as a saccharide sensor, MAMA was studied to isolate the interaction between the amine and the anthracene without the influence of the phenyl ring or the boronic acid. Aqueous buffered solutions with pH values ranging from 2 to 13 were used to examine the acid-base equilibrium of the amine on MAMA. Different percentages of methanol in phosphate buffered saline (PBS) were also used to examine possible changes in fluorescence lifetime or electron transfer rate due to different solvent dielectric constants.

5.1.2 Steady State Measurements in Buffered Solutions

Fluorescence measurements were made in solutions of pH buffers ranging from 2 to 13. No methanol was used with these solutions to keep conditions close to physiological at pH values near 7. Excitation and emission spectra for MAMA in PBS (pH = 7.4) are shown below in Figure 5.1.

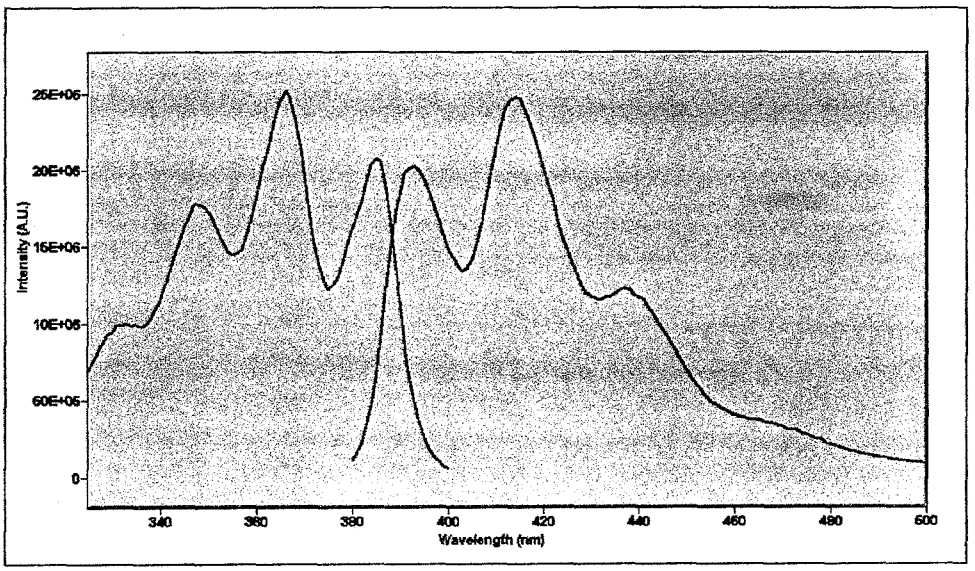

Figure 5.1 - Excitation and emission spectra of MAMA in PBS

The excitation maximum is at 366 nm and the emission maximum is 414 nm. The total fluorescence intensity is obtained by integrating over the emission spectra, as detailed in the previous chapter.

At low pH, binding occurs between protons in solution and the lone pair electrons of the amine on MAMA, creating MAMAH. The protonation of the amine prevents PET; therefore the maximum fluorescence intensity from MAMA occurs in solutions with low pH (Figure 5.2). When the amine is not protonated, its lone pair electrons are available to quench the anthracene fluorescence through PET (Figure 5.2).

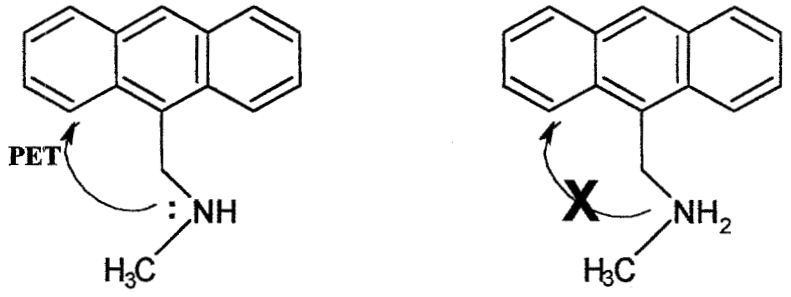

MAMA (pH >> pKa) **MAMAH (pH << pKa)**

Figure 5.2 - The amine of MAMA transfers an electron to quench the fluorescence of anthracene. In MAMAH these electrons participate in a bond with a hydrogen ion and are not available to quench the fluorescence of anthracene.

To examine the relative intensity (R) as a function of pH, intensities at pH values are compared to the maximum fluorescence intensity value at pH 2. The result can be seen in Figure 5.3 as a decrease in R with increasing pH.

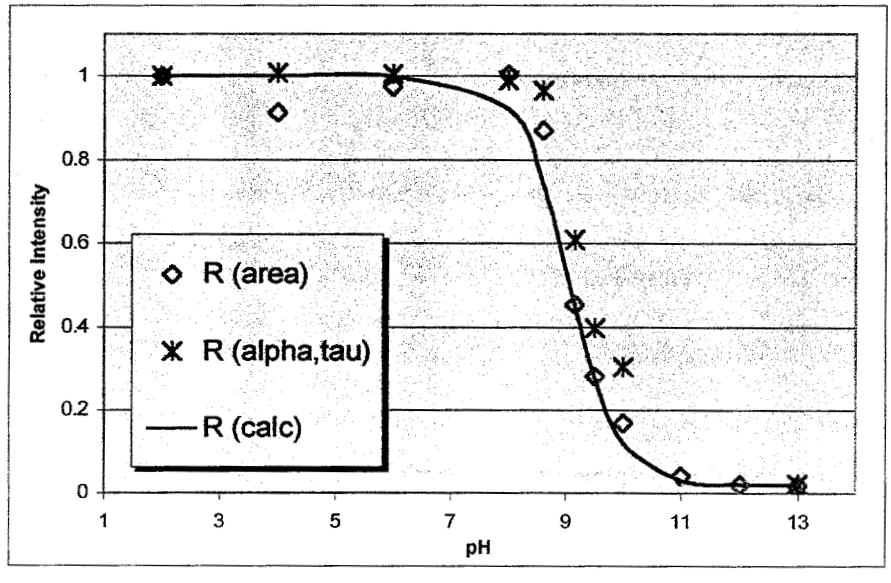

Figure 5.3 - Relative intensity of MAMA in 100% buffered solutions.

The relative intensity can also be calculated from the lifetime measurements (Equation 3.41). These data points, R(alpha, tau), show good agreement with the steady-state data.

A common method for measuring the pK_a from fluorescence data assumes that the pK_a is equal to the pH at the inflection point of the relative intensity curve. For a two component system this is approximately equivalent to the pH where the relative intensity has a value of 0.5. This method yields a pK_a of 8.96. The relative intensity can also be written as a function of the concentrations of MAMA and MAMAH, and their quantum yields.

$$R = \frac{1 + Q_R \dfrac{[MAMAH]}{[MAMA]}}{Q_R\left(1 + \dfrac{[MAMAH]}{[MAMA]}\right)} \qquad 5.1$$

The quantum yield ratio, $Q_R = Q_{MAMAH}/Q_{MAMA}$, can be determined by the ratio of measured lifetimes. Replacing [MAMAH]/[MAMA] in the equation above with Equation 3.8 yields an expression for R in terms of the pK_a.

$$R(calc) = \frac{1 + \tau_R\left(10^{pK_a - pH}\right)}{\tau_R\left[1 + \left(10^{pK_a - pH}\right)\right]} \qquad 5.2$$

Experimental R values, are compared with those calculated from the above equation using a least squares fit letting the pK_a value vary. This leads to a pK_a value of 9.06. For this method the lifetime values used are those measured when the concentrations of either MAMAH or MAMA are at a maximum. The lifetime values used are $\tau_{MAMAH} = 10.97$ nsec and $\tau_{MAMA} = 0.23$ nsec.

A problem with using only the relative fluorescence intensity values to determine pK_a is that the concentrations of the protonated and non-protonated species are not

considered. (Wehry, 1976) A more accurate method for calculating pK_a values from fluorescence uses the lifetime data to account for the different fluorescent intensity contributions of each species with a different lifetime. This will be discussed in the following section.

5.1.3 Lifetime Measurements in Buffered Solutions

Fluorescence lifetime data were also obtained using the same pH buffered solutions used in the steady state measurements. Typical phase and modulation curves for MAMA in pH 2 buffer, PBS (pH = 7.4), and pH 13 buffer are shown in Figure 5.4. Note that the data (Figure 5.4) for pH 2 and pH 7.4 look almost identical because most of the molecules are protonated (MAMAH) until the pH exceeds the pK_a value.

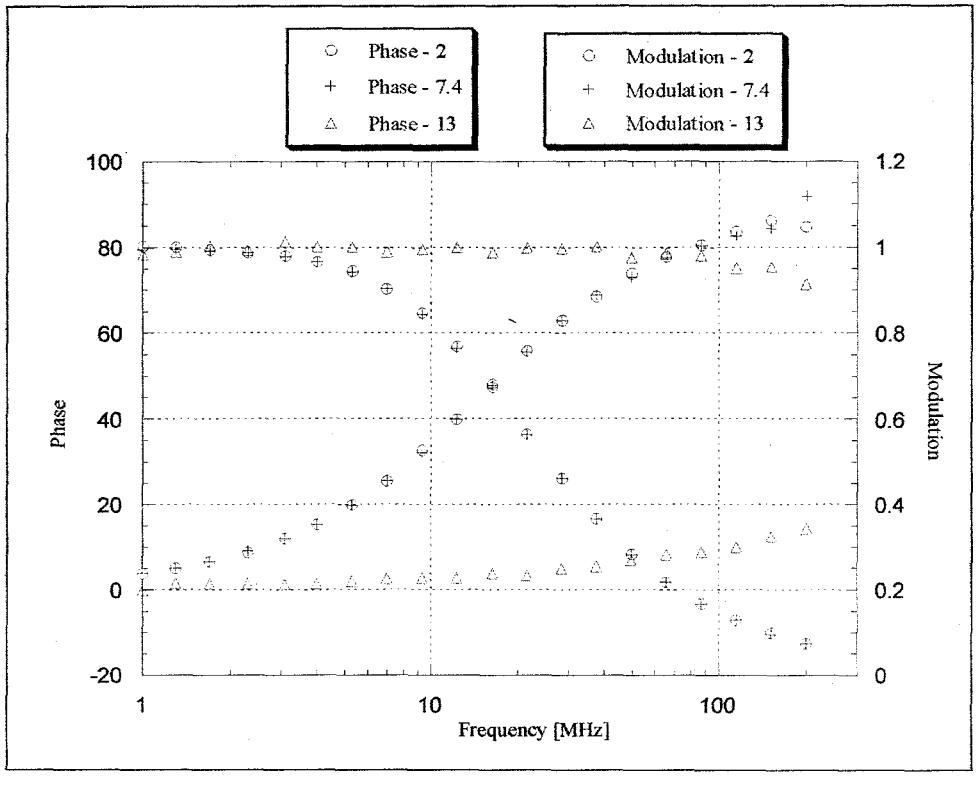

Figure 5.4 - Phase and Modulation data taken for MAMA in pH 2, 7.4 and 13.

Two lifetimes were found to exist in the measured pH range (Figure 5.5). The shorter lifetime ranges from 1.2 nsec to 0.23 nsec, while the longer lifetime is approximately 10.8 nsec.

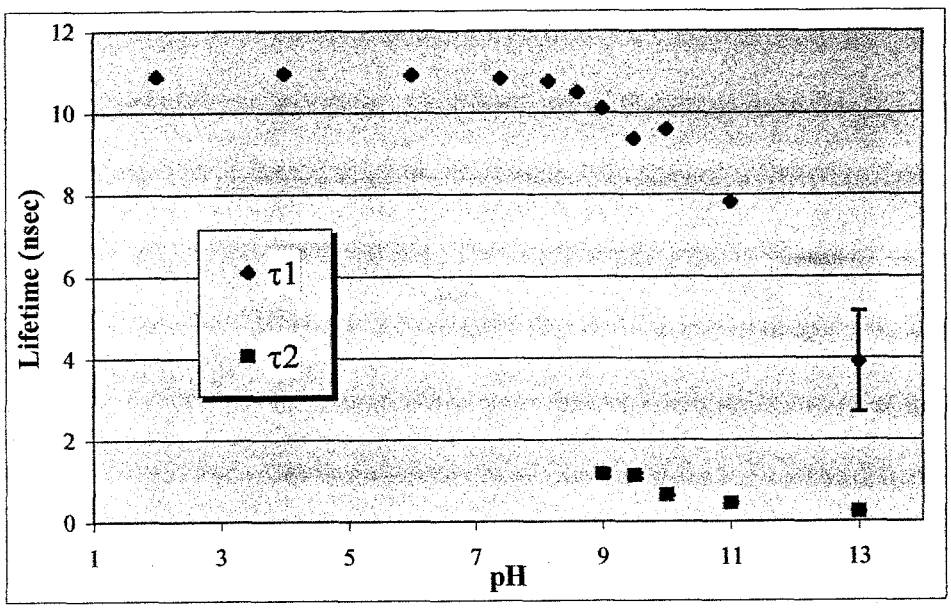

Figure 5.5 - Fluorescence lifetimes of MAMA in pH buffered aqueous solutions.

The shorter lifetime is associated with the unprotonated fluorescent species of MAMA quenched by PET. This lifetime is shorter due to the additional competitive excited state decay pathway. The longer lifetime is due to the fluorescence of MAMAH. Note that at pH 13 the longer lifetime (τ_1) is 3.9 nsec, significantly shorter than the 10.9 nsec lifetime at pH 2. The shorter lifetimes of τ_1 at high pH is most likely due to fluorescence quenching by the high concentration of OH^- ions in solution. (Wehry, 1976) As the OH^- concentration increases, the hydrogens that are bound to the amine on MAMA begin to interact with the OH- ions. Recall that the H bound to the amine allows anthracene to

fluoresce unquenched by PET. Therefore, if the N-H bond is affected by the OH^- ion, quenching may again occur.

The lifetime values for MAMA with and without PET are taken where the amounts of each species (α's) are at a maximum, as done with the pK_a calculations earlier. The lifetime values are $\tau_{MAMAH} = 10.97$ nsec and $\tau_{MAMA} = 0.23$ nsec. Using these values in Equation 3.30 yields an electron transfer rate of approximately 4.26×10^9 sec^{-1}. This is well within the common range of 10^6 to 10^{11} sec^{-1} found in the literature (Rehm, 1970; Bissell, 1993; Kavarnos,1993)

When analyzing the lifetime data it was found that in some cases both a triple exponential and a double exponential fit are possible. This possibility of three distinct lifetimes occurs at pH values from 9.5 to 10. The third lifetime is approximately 3 nsec when included, but consists of only a small fraction (less than 10%) of the total fluorescence (Figure 5.6). This component may possibly be attributed to OH^- quenching of the fluorescence previously described. However, analysis of the data suggests the two component system is more probable.

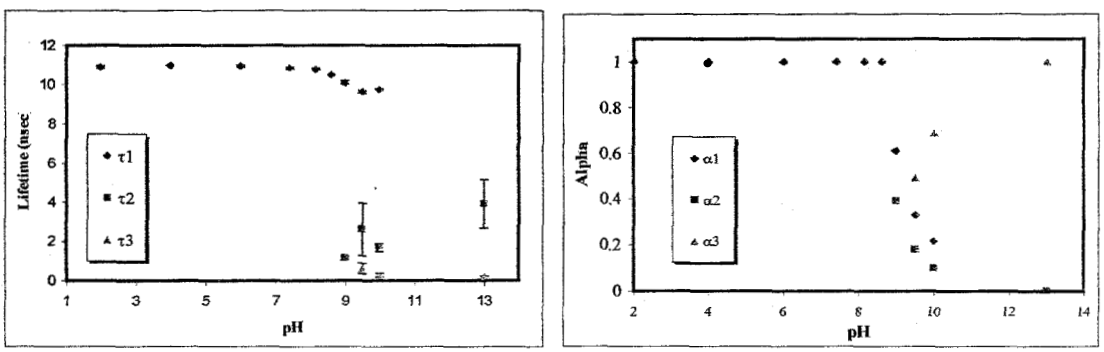

Figure 5.6 – Possible lifetime and pre-exponential components (α) for a triple exponential fit of MAMA data.

The χ^2 values (Equation 4.9), used to characterize the quality of the fit between the data and the time dependent equation (Equation 3.37), are lower when three lifetime components are used to fit the data. However, χ^2 is closer to unity with two components (Table 5.1). χ^2 values of unity indicate that the fit is consistant with the measured standard deviation of errors. Values of χ^2 much less than unity suggest that the errors used in fitting are larger than actual errors in the measurements.

pH	χ^2 - 2 comp	χ^2 - 3 comp
9.5	0.686	0.437
10.0	0.605	0.480

Table 5.1 - Comparison of the χ^2 values for a 2 component and a 3 component fit of MAMA data.

Another indication that the data were fit better with a two component exponential was the shape of the chi-confidence plots (see Appendix C). The chi-confidence plots produced by the software analysis package, Globals Unlimited, were similar or slightly worse for a three component fit. The possible explainations for a third component include OH^- quenching by the solvent and possible contamination. However, with the supporting data analyis, possible solvent effects and contaminations were neglected and the double exponential fit was chosen as the best representation of the fluorescence lifetimes of MAMA.

As the pH is increased, the amount of fluorescence associated with the shorter lifetime increases, while the amount due to the longer lifetime decreases. This is shown in the values of the pre-exponential coefficients, α_1 and α_2, in Figure 5.7.

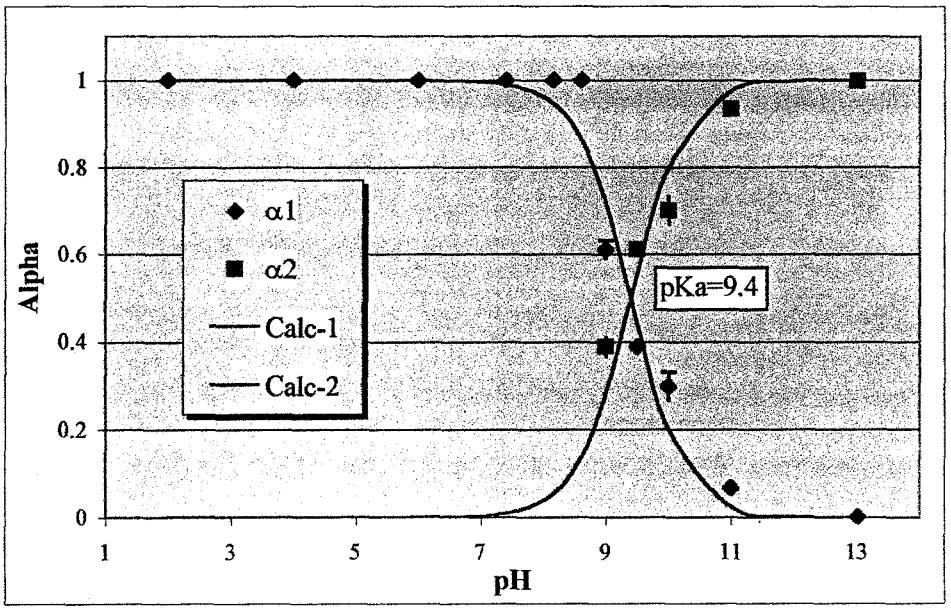

Figure 5.7 - Pre-exponential components, measured and calculated (Equation 3.43), for MAMA lifetimes in 100% aqueous buffered solutions.

This information can be used to calculate the pK_a because the ratio of alphas is equal to the ratio of concentrations (Equation 3.43).

$$pK_a = pH + \log\left(\frac{\alpha_1}{\alpha_2}\right) \qquad 5.3$$

Using lifetime data (α's) to measure the pK_a is more accurate than using relative fluorescence measurements due to the unequal intensity contribution to the steady state fluorescence by each species with a different fluorescence lifetime. The pK_a value obtained from Equation 5.3 is 9.4, only slightly higher than the value calculated (9.06) from the steady state fluorescence and fixed lifetime values (Equation 5.2), and somewhat higher than the value measured by the inflection point of the relative intensity curve (8.62).

5.1.4 Steady State Measurements in 50% Buffer:50% MeOH

Although MAMA is easily dissolved in buffered solutions, AB and boronic acids do not easily remain dissolved in these buffers without the addition of methanol. To make a direct comparison between MAMA and other molecules, measurements on MAMA were also done with fifty percent methanol and fifty percent pH buffer solutions. Adding methanol did not change the shape of the spectra, but it did reduce the fluorescence intensity by 67% (Figure 5.14).

The relative intensity as a function of pH was again found by dividing fluorescence intensity by the intensity at pH 2. The curve for fifty percent methanol (Figure 5.8) looks similar to the previous curve (Figure 5.3) for 100% buffered solutions.

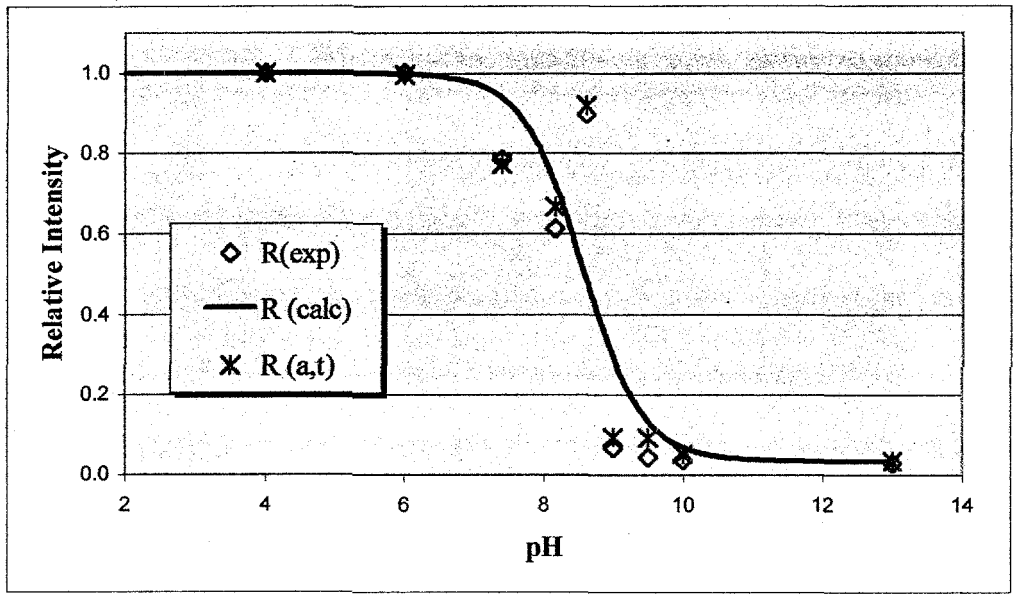

Figure 5.8 - Relative intensity of MAMA in buffered solutions with 50% MeOH.

Equation 5.2 yields a pK_a of 8.56 using measured lifetime values of τ_{MAMAH} = 9.87 nsec and τ_{MAMA} = 0.34 nsec. The pK_a of MAMA (in buffered solutions with fifty percent methanol) measured from the inflection point (R = 0.5) is 8.62. In 100% buffered solution pK_a values were measured as 9.06 and 8.96 using lifetime values (Equation 5.2) and the inflection point, respectively. From this we see that the addition of methanol to the pH buffers slightly lowers the pK_a of MAMA. Although the pK_a of MAMA is too high (>7.4) to be used as a sensor in a physiological environment, this trend may be useful in predicting how the pK_a of AB will shift from an environment with some percentage of methanol to a physiological one without methanol.

5.1.5 Lifetime Measurements in 50% Buffer:50% MeOH

Lifetime data was also taken for samples with fifty percent methanol (Figure 5.9). Phase and modulation curves are similar to those taken in 100% buffer solutions.

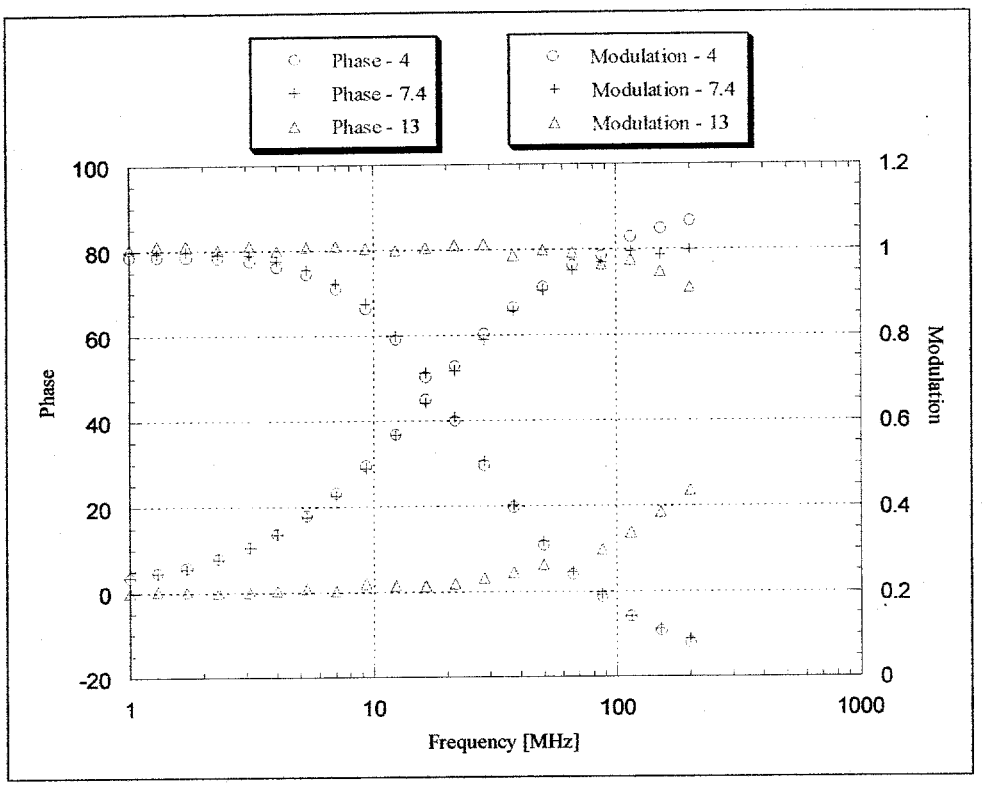

Figure 5.9- Phase and modulation data for MAMA in 50% MeOH:50% buffer. pH = 4, 7.4 and 13.

The lifetime data (Figure 5.10) shows a long lifetime of approximately 9.8 nsec and a short lifetime of approximately 0.54 nsec. However, at pH 9 the long lifetime changes abruptly to a much shorter lifetime of approximately 2.5 nsec. This change coincides with the pK_a of MAMA in solutions with fifty percent methanol (8.6).

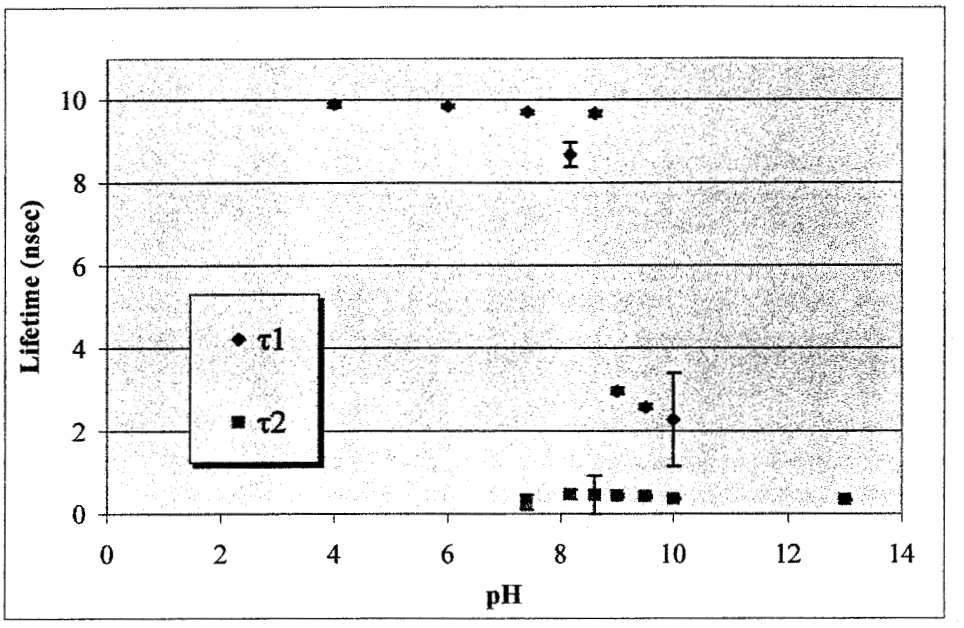

Figure 5.10 - Fluorescence lifetimes for MAMA in MeOH and aqueous buffered solutions (1:1 by volume).

As with MAMA in 100% buffer, the drop in the values of τ_1 at high pH (>9) is most likely due to OH^- quenching of the fluorescence. (Wehry, 1976)

The pre-exponential components shown in Figure 5.11 estimate the pK_a to be 8.86.

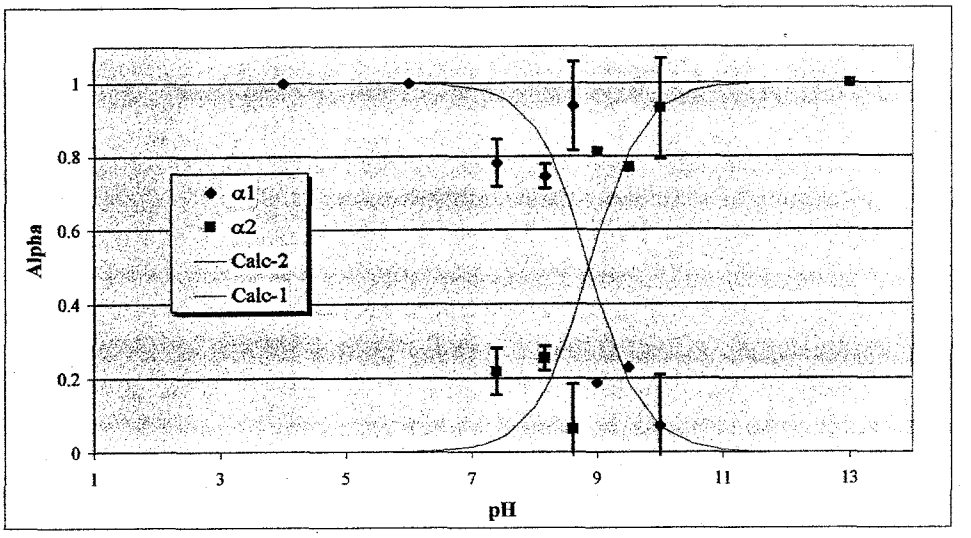

Figure 5.11 - Pre-exponential factors in MAMA lifetimes measured in MeOH and aqueous buffered solutions (1:1 by volume) and calculated by Equation 3.43.

The longer lifetimes (from molecules not undergoing PET) measured in fifty percent methanol are shorter than those measured in buffered solutions. However, the lifetimes for molecules undergoing PET are shorter for MAMA in 100% buffer.

MAMA	100% Buffer	50% Buffer 50% MeOH
Long lifetime at low pH (nsec)	10.97	9.87
Long lifetime at high pH (nsec)	3.9	2.5
Short lifetime (nsec)	0.23	0.34

Table 5.2 - Summary of lifetime data for MAMA in 100% buffer and 50% buffer:50% MeOH.

The short lifetime is directly related to the rate of electron transfer. The relationship between this rate and the amount of methanol in solution will be examined later.

5.1.6 Lifetime Measurements in Acetonitrile

Fluorescence lifetime data were also obtained using solutions of MAMA in acetonitrile (ACN) with 0.1M tetrabutylammonium perchlorate (TBAP) to measure the electron transfer rates and directly compare those values with the rates calculated from electrochemical measurements which were made in ACN/0.1M TBAP (Section 5.1.8). Electrochemical measurements were not made in PBS and MeOH because the hydrogen donating ability of PBS interferes with the measurement. It should also be noted that degassing of the solution by N_2 did not effect the measurements.

Two lifetimes were found for MAMA in ACN/0.1M TBAP (Table 5.3), similar to the lifetimes found previously for MAMA at high pH.

	Component 1	**Component 2**
Lifetime (nsec)	4.63	0.16
Fractional contribution to the fluorescence intensity	0.43	0.57
Pre-exponential (alpha)	0.03	0.97

Table 5.3 - Lifetime data for MAMA in ACN/0.1M TBAP.

Using Equation 3.30, the value of the electron transfer rate in ACN/0.1M TBAP is 5.92 x 10^9 sec^{-1}. This value is slightly higher than any rate calculated for MAMA from

experimental data in 100% or 50% buffered solvents. A more complete discussion of electron transfer rates follows.

5.1.7 Solvent Effects

To examine the effect of a change in energy barrier due to solvent changes, varying amounts of methanol were added to PBS. This changed the dielectric constant of the solvent. The values of relevant solvent properties for methanol, water and acetonitrile are as follows.

Property	MeOH	Water	ACN
Index of refraction, n (Weast, 1976)	1.326	1.333	1.342
Dielectric Constant (at 25°C), ε_s (Weast, 1976)	32.63	78.36	37.5
Polarity (Kavarnos, 1993)	6.6	10.2	6.2
Outer-sphere Reorganizational Energy, λ_o (kcal/mol)	44.38	45.86	46.9

Table 5.4 - Properties of solvents used in measurements.

Recalling Marcus' electron transfer theory, the activation energy of electron transfer is a function of the inner (λ_i) and outer (λ_o) sphere reorganizational energies.

$$\Delta G_{ET}^{\neq} \approx \frac{(\lambda_i + \lambda_o)}{4}\left(1 + \frac{\Delta G_{ET}}{4}\right)^2 \qquad 5.4$$

where λ_o is dependent on both the index of refraction and the dielectric constant of the solvent. An increase in the dielectric constant of the solvent will cause an increase in the

energy barrier height for electron transfer. The reader is referred to Figure 3.2 for a diagram of barrier height.

The inner sphere reorganizational energy is not dependent upon solvent, and thus will be taken as constant in our treatment of the solvent dependence on the rate of electron transfer. In the case of MAMA, λ_i can be estimated from Equation 5.4 using the free energy (ΔG_{ET}) measured in electrochemical measurements and λ_o with varying amounts of methanol in the solvent. The barrier height is calculated from Rehm and Weller's empirical equation (Equation 3.54), and ranges from 1.35 kcal/mol to 1.32 kcal/mol with increasing amounts of methanol. Using this technique, λ_i is estimated to be 19.36 kcal/mol for MAMA.

The ΔG_{ET} value measured for MAMA (-2.85 kcal/mol) is small enough to easily classify it in the normal (rather than the inverted) region where $-\Delta G_{ET} < \lambda$. As the dielectric constant of the solution increases, or the percentage of methanol decreases, λ increases. This results in an increased energy barrier for electron transfer. The increased $\Delta G_{ET}^{\neq}$ accounts for the smaller percentage of molecules undergoing PET in solutions with less methanol. This trend is seen in the lifetime measurements (Figures 5.12 and 5.13).

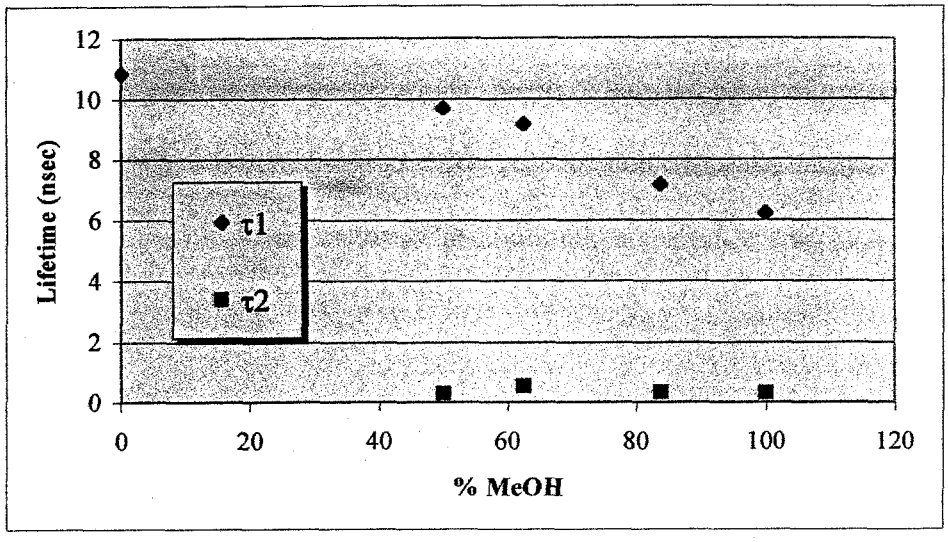

Figure 5.12 - Fluorescence lifetimes of MAMA in solutions with varying amounts of MeOH and PBS (pH=7.4).

The value of α_2 (corresponding to the lifetime quenched by PET) decreases with increasing dielectric constant as the energy barrier for PET increases (Figure 5.13).

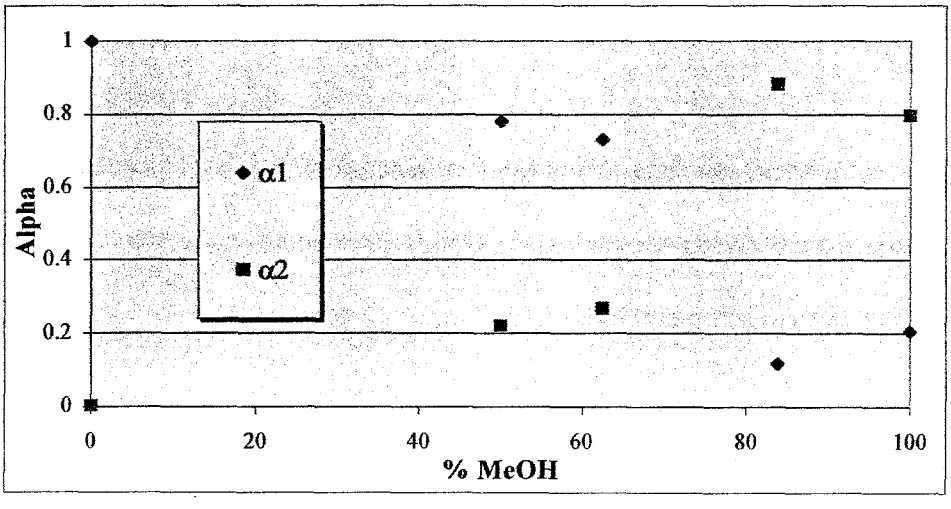

Figure 5.13 - Pre-exponential factors for MAMA in solutions with varying amounts of MeOH and PBS.

As the percentage of methanol increases, more molecules are quenched by electron transfer, which should reduce the total fluorescence intensity. This is supported by steady state fluorescence intensity data, shown in Figure 5.14 as a function of the percent of methanol in solution.

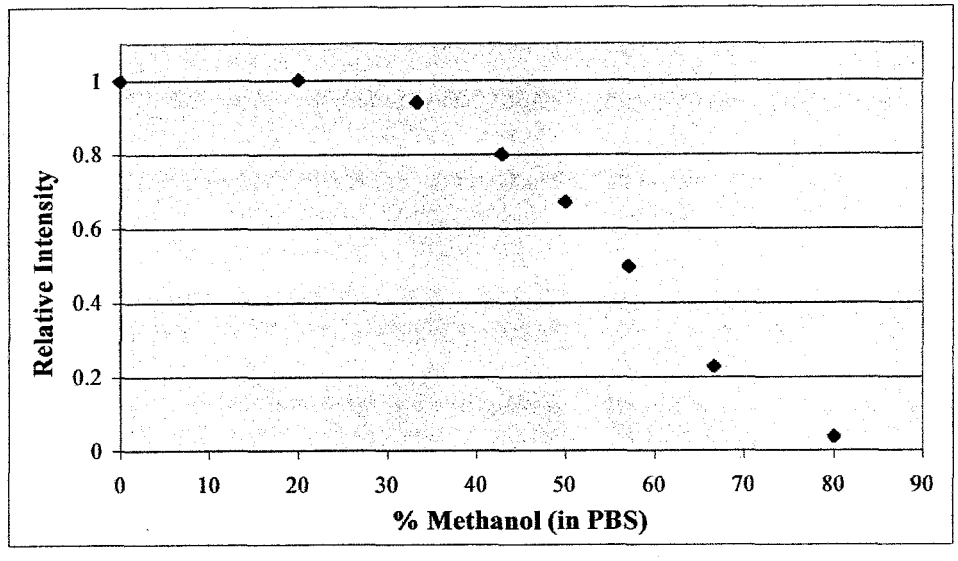

Figure 5.14 - Relative fluorescence intensity of MAMA in solutions with varying amounts of MeOH and PBS.

The increasing amount of molecules being quenched by PET with increasing methanol concentration suggests that the energy barrier to electron transfer is decreasing. A smaller energy barrier results in a faster PET rate, increasing as the percent of methanol in solution increases.

$$k_{ET} \propto \exp(-\Delta G_{ET}^{\neq} / RT) \qquad 5.5$$

This prediction will be examined in the next section.

5.1.8 Electron Transfer Rates

To calculate electron transfer rates, electrochemistry measurements were made on MAMA in ACN/0.1M TBAP. The reduction potential of the amine was measured to be 0.67 V and the oxidation potential of anthracene was –2.4 V. The zero level wavelength difference, λ_{00}, was measured in ACN/TBAP to be 388.5 nm (defined in Equation 3.59 as the average of the peak excitation and emission wavelengths). Putting these values into the Rehm-Weller equation (Equation 3.58) yields a change in free energy with electron transfer, ΔG_{ET}, of –2.85 kcal/mol. The free energy value is negative, therefore the electron transfer is thermodynamically feasible.

In the previous section the inner-sphere reorganizational energy, λ_i, was estimated to be 19.36 kcal/mol. Using this and the values for the free energy barriers calculated from Equation 3.54, the electron transfer rates are calculated for MAMA. In solutions of 100% buffer, the rate of electron transfer is found to be 2.75×10^9 sec^{-1}. For solutions with 50% methanol, the electron transfer rate is 2.79×10^9 sec^{-1}. Assuming that λ_i is constant in different solvents, the rate of electron transfer is not predicted to change significantly.

Using the lifetime values taken at the maximum α, the experimental values for k_{ET} (using Equation 3.30) are 4.29×10^9 sec^{-1} in aqueous buffered solutions and 2.87×10^9 sec^{-1} in solutions containing fifty percent methanol. If the value of k_{ET} is calculated using the measured lifetimes at each pH value, rather than with the lifetime values at the maximum α, the rate varies (Figure 5.15).

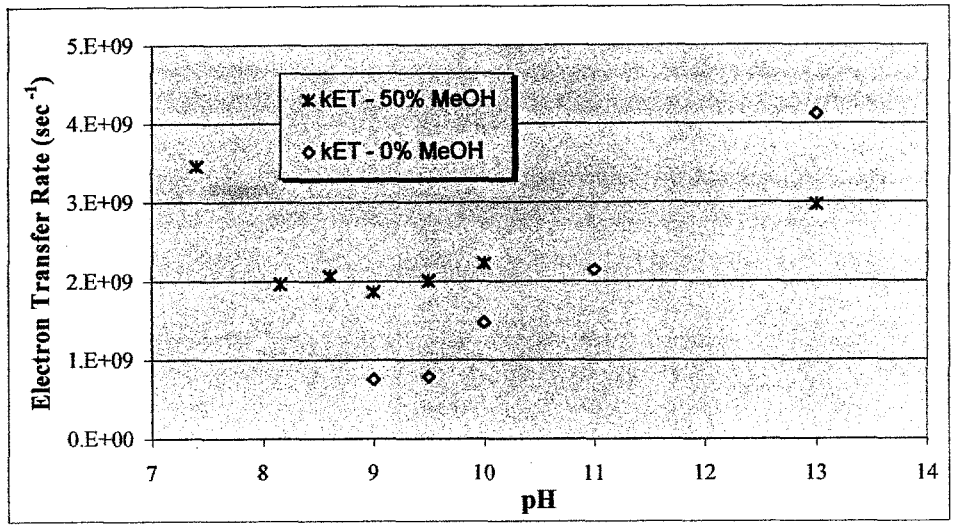

Figure 5.15 - Rates of electron transfer in 0% and 50% MeOH solutions, calculated from the measured lifetime values.

Many rates for electron transfer in MAMA have been suggested in the previous sections. Although the rates vary, almost all of them are on the order of 10^9 sec^{-1}. In Section 5.1.7 it was predicted that with an increased dielectric constant (or a decrease in methanol concentration) the rate of electron transfer would decrease due to the increased energy barrier. Slower rates of electron transfer are seen in 100% PBS for calculations based on the average rate over the pH range, as well as the minimum rate found by lifetime measurements. Typically (Figure 5.15), the electron transfer rate is slower in solutions with increased dielectric constant, supporting the prediction made in the previous section based on Marcus theory.

5.2 N-benzyl-N-methyl-N-methyl anthracene (AB-B)

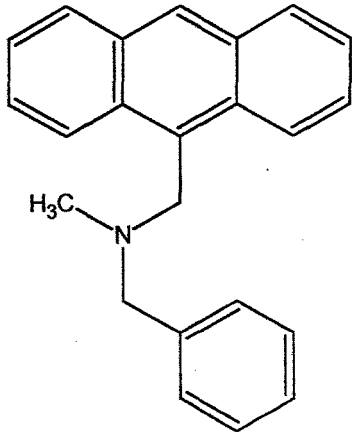

5.2.1 Relevance

AB-B is an intermediate step between MAMA and anthracene boronate (AB). By studying AB-B the effects of the phenyl ring can be isolated from the effects of the boronic acid. This molecule, like MAMA, is not sensitive to glucose and therefore the electron transfer was studied by varying the pH of the solvent. Solutions of methanol and pH buffer (1:1 by volume) were used with pH values ranging from 2 to 13. Also, solutions with different concentrations of methanol in PBS (pH 7.4) were used to study the fluorescence properties of AB-B in solvents with different dielectric constants.

5.2.2 Steady State Measurements

The excitation and emission spectra of AB-B are red shifted slightly from that of MAMA. Excitation and emission spectra for AB-B in pH 7.4 buffer and methanol (1:1 by volume) are shown below (Figure 5.16) along with spectra from MAMA in the same solvent. Excitation and emission peaks for MAMA are at 367 nm and 413 nm, respectively, while peaks for AB-B are at 369 nm and 418 nm.

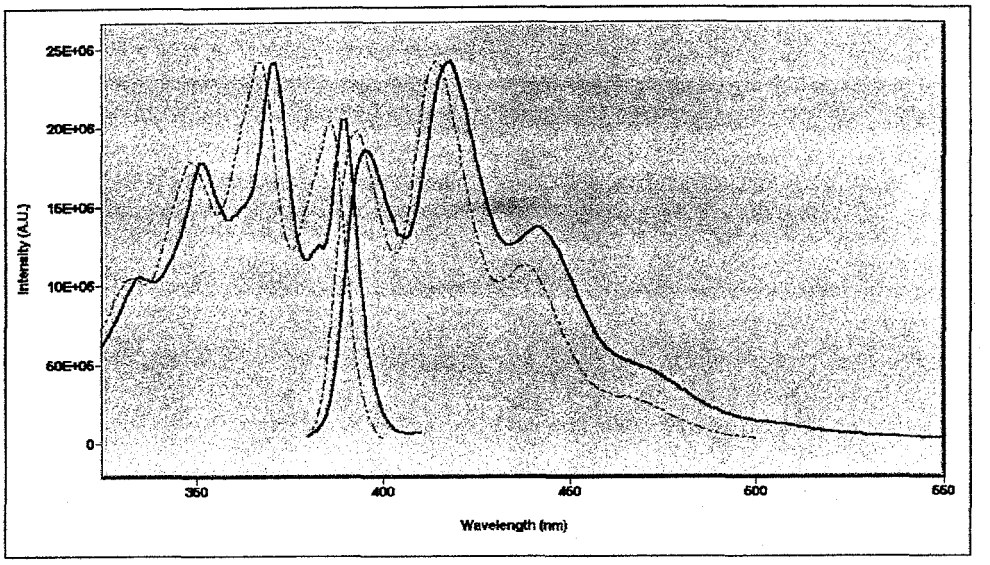

Figure 5.16- Excitation and emission spectra of AB-B (solid) are red shifted compared to the spectra of MAMA(dashed).

As with MAMA, the protonation of the amine on AB-B prohibits PET, thus increasing the fluorescence yield. The relative fluorescence intensities for measured solutions of 50% pH buffer and 50% methanol show this increase in intensity with decreasing pH (Figure 5.17).

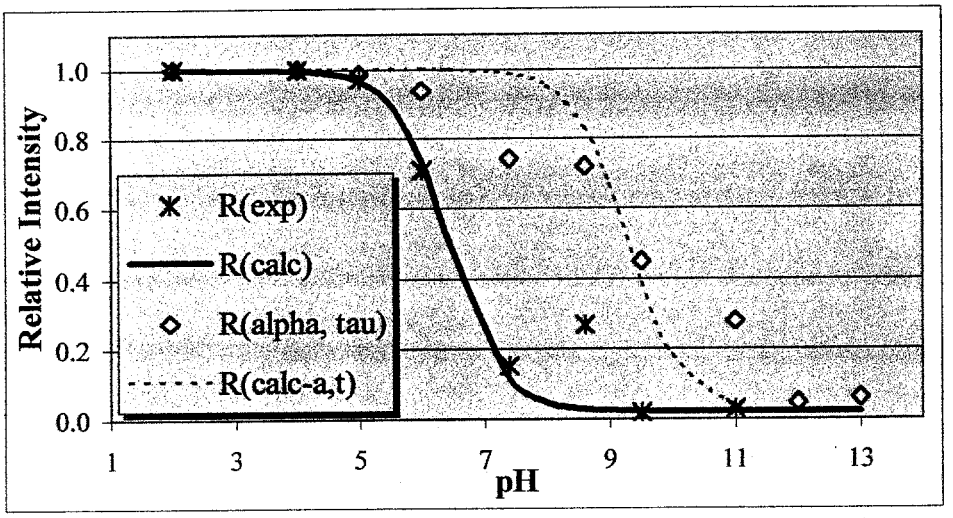

Figure 5.17 - Relative fluorescence intensity of AB-B as a function of pH.

The experimental values for relative intensity, R(exp), were measured by integrating the emission spectra. The calculated curve, R(calc), was determined using Equation 5.2. The ratio of measured lifetimes ($\tau_{AB\text{-}BH}/\tau_{AB\text{-}B}$) used to approximate the ratio of the quantum yields ($Q_{AB\text{-}BH}/Q_{AB\text{-}B}$) was calculated from the lifetime values where $\alpha_{AB\text{-}BH}$ or $\alpha_{AB\text{-}B}$ is at a maximum. By choosing one lifetime value characteristic to each species, a curve of relative intensity may be extrapolated over the entire pH range. These values are $\tau_{AB\text{-}BH}$ = 11.73 nsec and $\tau_{AB\text{-}B}$ = 0.26 nsec, and the resulting pK_a is found to be 6.42. The pK_a determined from the inflection point of this curve is 6.44; in very nice agreement with the previous value calculated from the ratio of lifetimes. However, the second calculated curve, R(calc-a,t) in Figure 5.17 uses the same equation as R(calc), but is fit to the relative intensity data calculated (Equation 3.41) from lifetime measurements, R(alpha, tau). The pK_a calculated from this curve, fitted to the lifetime data, is a much higher 9.28. This suggests that a possible excited state reaction is occurring, and it is

possible that the higher pK_a is actually the excited state pK_a, or pK_a^*. This possibility is left as a question for future research.

5.2.3 Lifetime Measurements in 50% Buffer:50% MeOH

Fluorescence lifetime data was also taken with the pH buffered solutions used in the steady state measurements. Typical phase and modulation curves for AB-B in pH 2, 7.4 and 13 shown below (Figure 5.18).

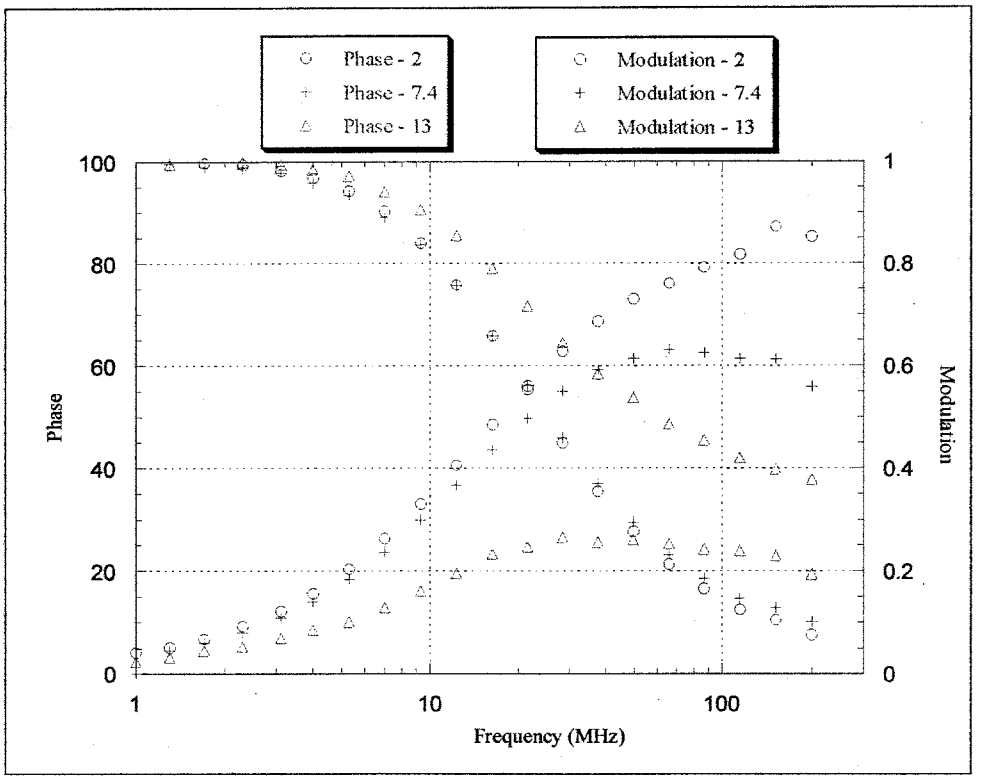

Figure 5.18 - Lifetime data for AB-B in 50% MeOH:50% pH buffer. pH values of 2, 7.4 and 13 are shown with curves shifting to the right with increasing pH.

The downward curvature at high modulation frequencies displayed by the phase data at pH 7.4 and 13 is mainly due to scattering. As the amount of fluorescence decreases, the amount of excitation light must be increased to allow the fluorescence to be detected. It is common for some of the excitation light to penetrate the emission detector filter. Since scattered light has an effective lifetime of zero, its contributions become more apparent at higher modulation frequencies. The scattered light in the measurements is easily seen in the analysis, and therefore taken out of resulting lifetime data summary.

Unlike the lifetimes measured for MAMA, AB-B always has two measurable and distinct fluorescence lifetimes over the pH range from 2 to 13 (Figure 5.19).

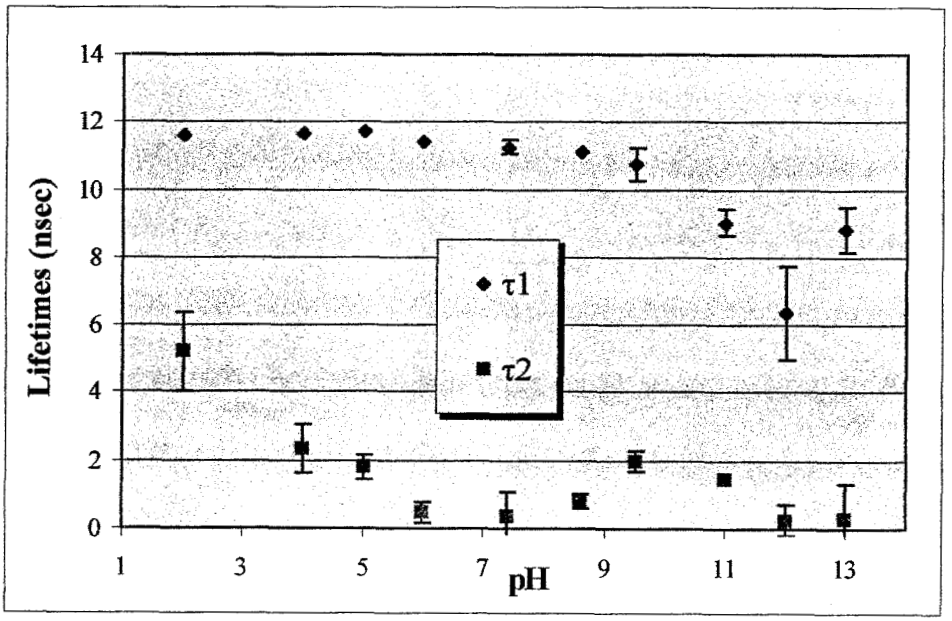

Figure 5.19 - Fluorescence lifetimes of AB-B in MeOH and aqueous buffered solutions (1:1 by volume).

Although two lifetimes are always present, their relative amounts still vary as a function of pH. The curves of the pre-exponential factors (Figure 5.20) as a function of pH are

similar to expected from a two component system, yet the fit between the data and the model is not as good. This suggests that AB-B is more complex than the simple two component system seen with MAMA.

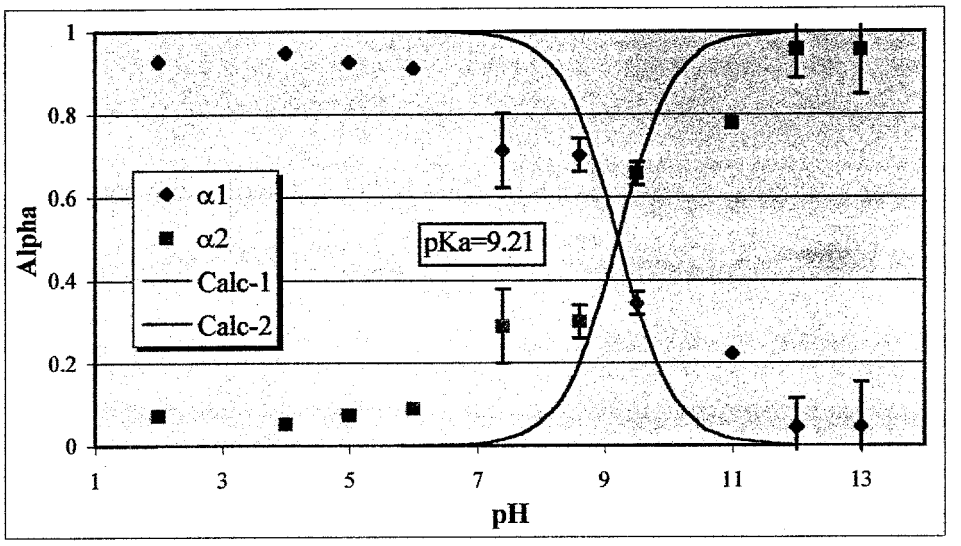

Figure 5.20 - Pre-exponential factors of AB-B lifetimes.

With increasing pH, the PET fluorescence quenching increases and the shorter lifetime component (α_2) dominates the fluorescence at high pH. The transition from low pH, where α_1 dominates the fluorescence, to high pH, where α_2 becomes the dominant component is more gradual than observed with MAMA. The pK_a, determined by the crossing of the two pre-exponential factors, when $\alpha_1 = \alpha_2 = 0.5$, is 9.21. This is much higher than the pK_a calculated from the relative intensity data (6.4). There also seems to be two transitions in the pre-exponential components. The first transition is approximately where the steady state pK_a was measured (~6.4), while the second is closer to pH 9.

5.2.4 Solvent Effects

Different amounts of methanol were added to PBS (pH 7.4) to examine the effect of changing the electron transfer barrier height on the fluorescence of AB-B. Methanol decreases the dielectric constant, thereby decreasing the outer-sphere solvent reorganizational energy, λ_0. Equation 3.55 shows that a decreased λ_0 causes a decrease in the energy barrier to electron transfer, $\Delta G_{ET}^{\neq}$, assuming that ΔG_{ET} remains the same. When adding small amounts of methanol (10% and 33%) to PBS, the solution became cloudy indicating that AB-B was precipitating out of solution. This resulted in a reduced relative intensity for small percentages of methanol. At fifty percent methanol and higher, the AB-B remains in solution and the relative intensity curve decreases in the same manner as MAMA (Figure 5.21).

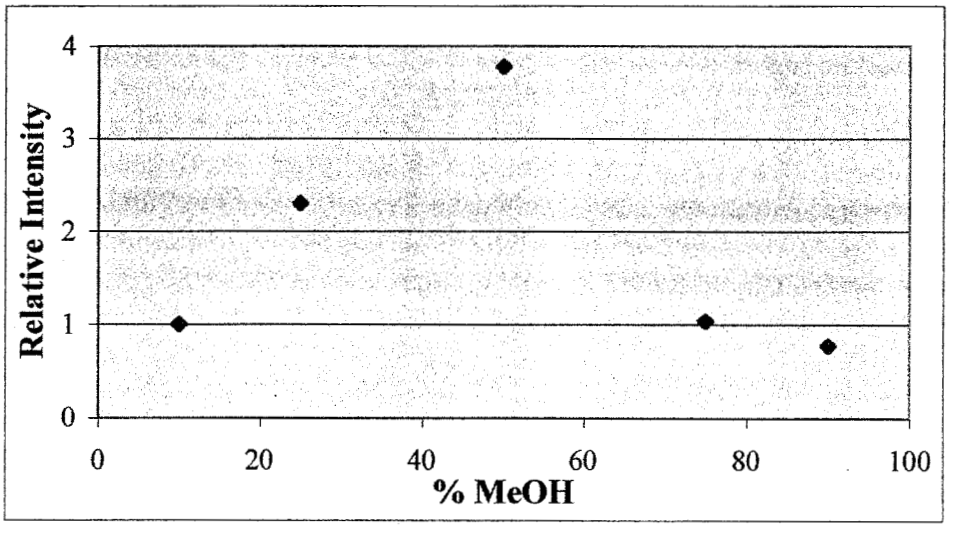

Figure 5.21 - Relative intensity of AB-B in PBS with different amounts of MeOH. At 15% and 33% MeOH, the solubility of AB-B is limited.

Fluorescence lifetime measurements were also made on AB-B in solutions with different amounts of methanol. Again, two lifetimes are always present (Figure 5.22).

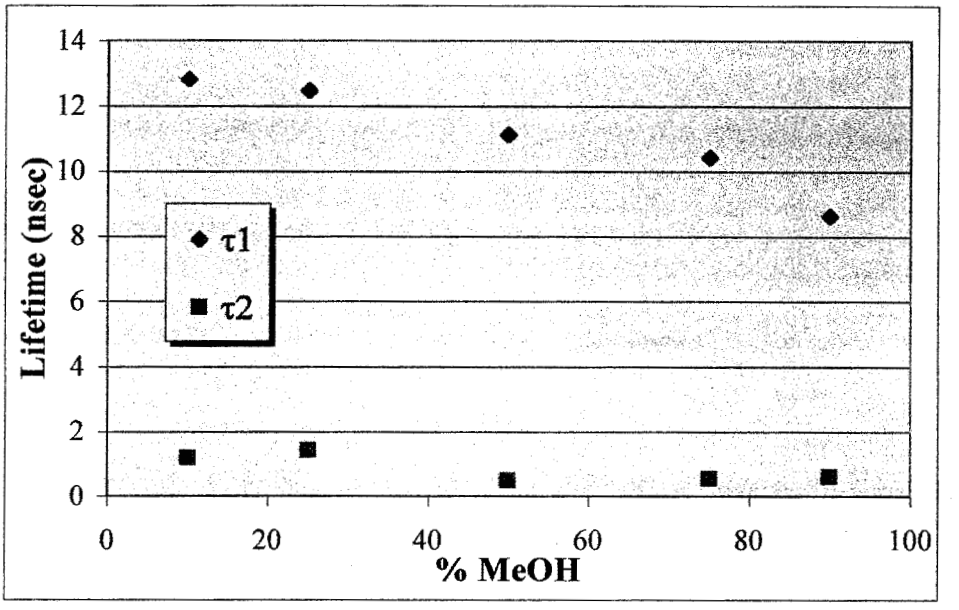

Figure 5.22 - Fluorescence lifetime measurements of AB-B in PBS with different amounts of MeOH.

As with MAMA the longer lifetime decreases with increasing methanol. However, the pre-exponential components (Figure 5.23) differ from what was seen with MAMA.

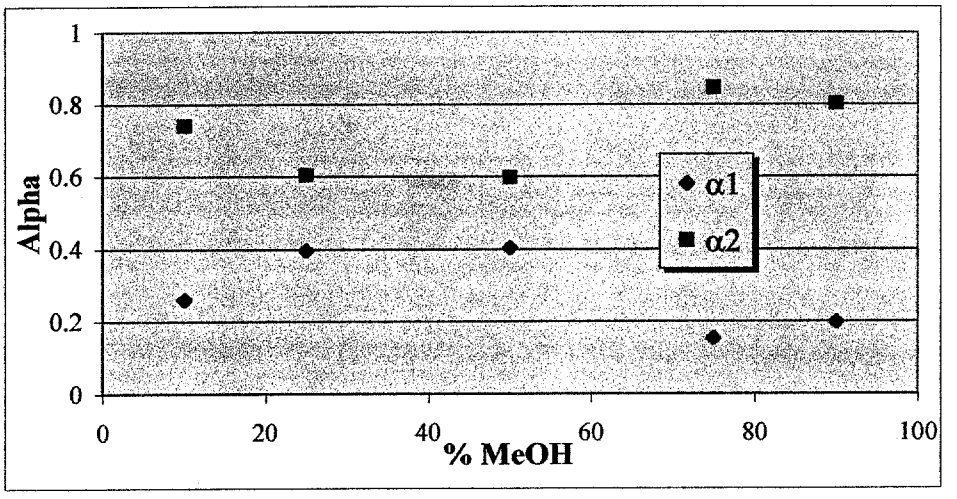

Figure 5.23 - Alpha values for AB-B in different MeOH/PBS solutions.

The short lifetime component, α_2, is due to the unprotonated species, AB-B, and is the main contributor to the fluorescence regardless of the amount of MeOH in PBS. This component has a shorter lifetime due to electron transfer. Instead of the curves crossing at 20% MeOH, the curves come together and reverse direction. The reason for this is unknown, but perhaps the ability for an electron to be transferred in AB-B is effected by the low solubility with small percentages of methanol. The electron transfer rate (Figure 5.24), calculated from the lifetime data above ranges from 6.2×10^8 sec^{-1} at 33% MeOH to 1.96×10^9 sec^{-1} at 50% MeOH. Note the slower electron transfer rates occur for solutions of 15% and 33% MeOH, where solubility of AB-B is a problem.

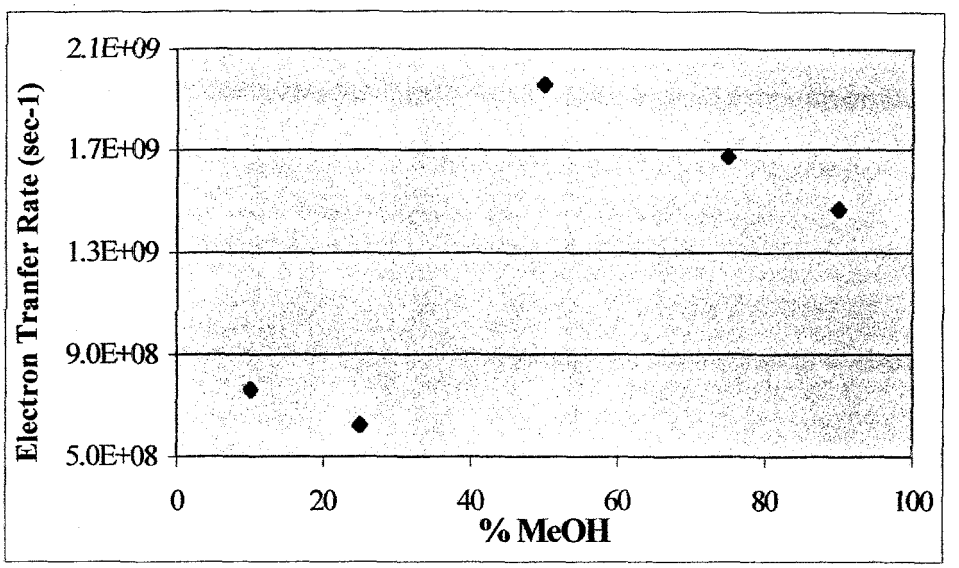

Figure 5.24 - Electron transfer rates calculated from lifetime data on AB-B in PBS and MeOH.

Due to the lack of uniform trend as a function of dielectric constant, and the relatively small effect it has on the rate of electron transfer, little can be learned from AB-B in different amounts of methanol. Perhaps methanol has little effect on the electron transfer, or perhaps a reaction is occurring in the excited state of AB-B. This question is left to future research. However, solubility is clearly a factor with this molecule and should be considered in future studies.

5.2.5 Lifetime Measurements in Acetonitrile

Fluorescence lifetime measurements of AB-B in ACN/TBAP were performed so that the measured electron transfer rates could be directly compared to the free energy value measured by electrochemistry. It was found that degassing the solutions with N_2 changed the lifetime values. This suggests that the fluorescence of AB-B in ACN/TBAP is quenched by oxygen. Without degassing, the lifetimes were 6.8 nsec and 0.7 nsec.

After degassing the solution, lifetime measurements (Table 5.5) were made while the sample compartment was supplied a constant flow of N_2.

	Component 1	Component 2
Lifetime (nsec)	14.21	1.06
Fractional Fluorescence Contribution	0.61	0.39
Pre-exponential (alpha)	0.10	0.90

Table 5.5 – Lifetime values of AB-B in ACN/TBAP, degassed with N_2.

The value of electron transfer calculated from these lifetime measurements is 8.73×10^8 sec^{-1}. This will be compared to other rates of electron transfer in the next section.

5.2.6 Electron Transfer Rates

Electrochemistry measurements made on AB-B were done in ACN/TBAP. The reduction potential of the amine was found to be 0.73 V and the oxidation potential of anthracene was –2.3 V. The excitation and emission peak wavelengths in ACN/TBAP are 370 nm and 417 nm, resulting in a λ_{00} value of 393.5 nm. Using these values, the Rehm-Weller equation (Equation 3.58) yields a ΔG_{ET}, of -2.80 kcal/mol. This is slightly more positive than the value for MAMA (-2.85 kcal/mol), but the difference is within the margin of error ($\pm$ 0.1 kcal/mol for errors in wavelength measurements ($\pm$ 1 nm) alone). This suggests that the addition of a phenyl ring onto MAMA has little or no effect on the free energy change involved in electron transfer. The barrier height, $\Delta G_{ET}^{\neq}$, depends upon ΔG_{ET}, λ_i, and λ_0 according to Marcus (Equation 3.54). The outer-sphere solvent reorganizational energy, λ_0, depends only on the solvent and the distance between the

acceptor and donor sites, and should be similar for MAMA and AB-B in the same solution assuming the electron transfer mechanism remains constant. The free energy, ΔG_{ET}, was measured to be similar for MAMA and AB-B, and λ_i should not change significantly because it involves vibrations characteristic to the bonds involved in electron transfer. However, the electron transfer rate calculated for AB-B in ACN/TBAP is almost an order of magnitude slower than the value measured for MAMA in the same solvent: 8.73×10^8 sec^{-1} for AB-B and 5.92×10^9 sec^{-1} for MAMA.

For AB-B in solutions of fifty percent methanol and fifty percent pH buffer, the electron transfer rates fluctuate by more than one order of magnitude.

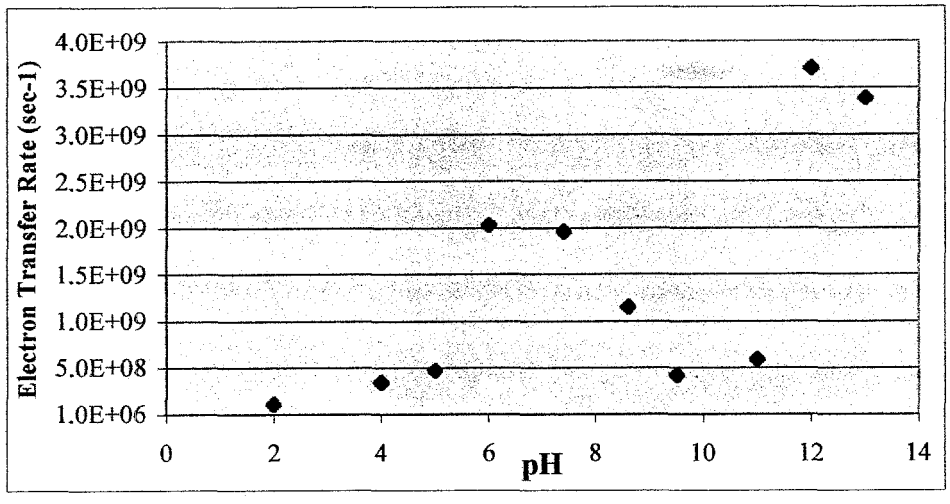

Figure 5.25 - Electron tranfer rates for AB-B as a function of pH.

At pH 2 the rate of electron transfer is 1.06×10^8 sec^{-1}, while at pH 12 the rate is 3.70×10^9 sec^{-1}. Comparing the electron transfer rates of AB-B to those of MAMA in 50% MeOH and 50% PBS shows that the rates for AB-B are usually a little bit lower than the electron transfer rates of MAMA (Figure 5.26).

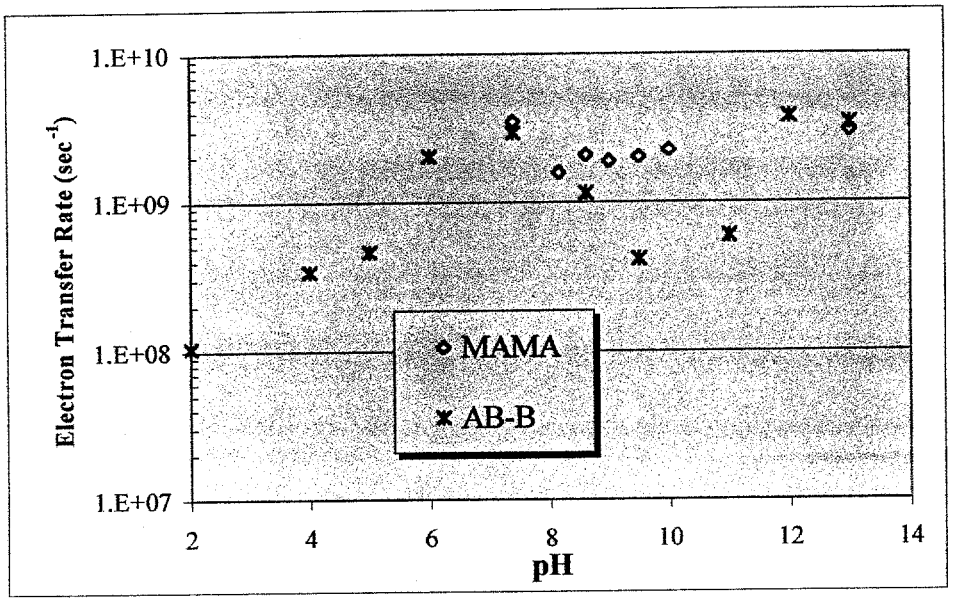

Figure 5.26 - Comparison of electron transfer rates for MAMA and AB-B in PBS and MeOH (1:1 by volume).

The electron transfer rates above (Figure 5.26) were calculated using measured lifetime values in Equation 3.30. At pH values below 7 electron transfer does not occur in MAMA because all of the molecules are protonated (MAMAH).

5.3 N-methyl-N-(9-methylene anthryl)-2-methylenephenylboronic acid (AB)

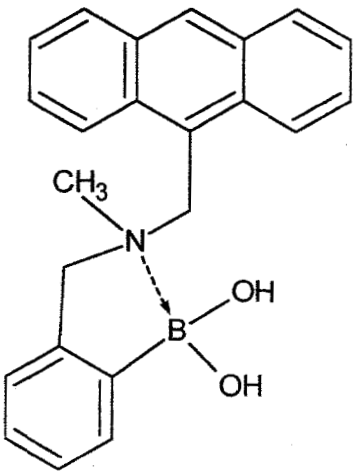

5.3.1 Relevance

Anthracene boronate (AB) is the starting molecule against which all other potential glucose sensor molecules have been compared. It is known to have increased fluorescence intensity with the addition of glucose, or with an increase in hydrogen ions. (James, 1994) The addition of the boronic acid to the previous molecule, AB-B, creates another mechanism by which PET can be prevented. The dative bond between the amine and the boron may prohibit the lone pair electrons from quenching the anthracene fluorescence. The nature of this dative, or coordination, bond was examined in chapter two. In this section the N→B interaction will be studied using fluorescence measurements. Our experiments will measure the fluorescence lifetimes of AB in solutions of pH buffers and methanol, similar to the previous measurements of MAMA and AB-B. Additionally, the fluorescence of AB will be characterized as a function of the glucose concentration. An examination of AB's potential as a glucose sensor molecule will be presented. By obtaining a thorough understanding of the fluorescence

and electron transfer characteristics of AB, the next generation of sensor molecules with a fluorophore other than anthracene may be better evaluated for use in a glucose sensor.

5.3.2 Steady State Measurements vs. pH

Solutions of AB (μM) in buffered aqueous solutions and methanol (1:1 by volume) were examined. The emission spectra is similar to that of MAMA in the same solution at pH 7.4, and blue shifted by approximately 6 nm from the peak of AB-B (Figure 5.27). The peak excitation wavelength is 367 nm and the peak emission wavelength is 412 nm.

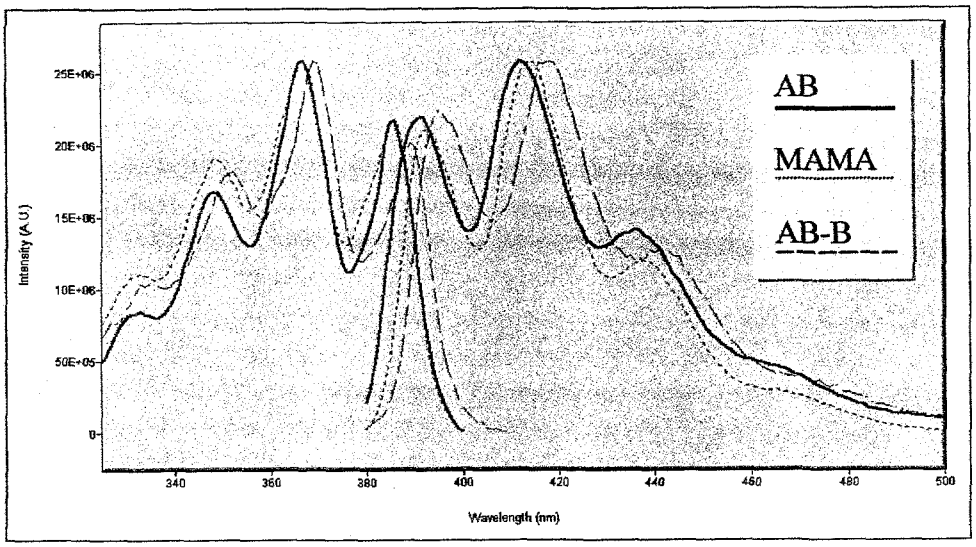

Figure 5.27- Fluorescence excitation and emission spectra of AB (solid) in PBS (pH=7.4) and MeOH (1:1 by volume), compared to spectra from MAMA (dotted) and AB-B (dashed) in similar solution.

In AB the amine is always involved in a dative bond with the boron (N→B) as described in Chapter two (Figure 5.28). This bond involves the lone pair on the amine, thereby restricting the ability of the amine to transfer an electron in PET.

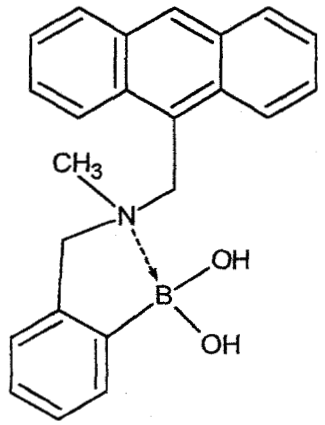

Figure 5.28 - AB with N→B dative bond, PET may or may not occur.

At low pH the amine on AB can bind to a hydrogen ion (Figure 5.29). This prevents PET completely by involving the lone pair on the amine in a covalent bond with the hydrogen.

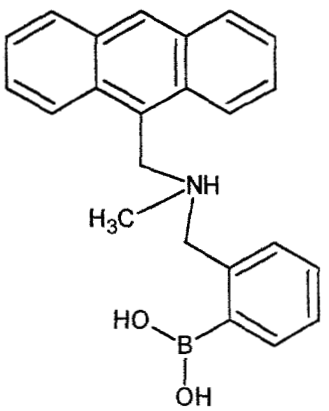

Figure 5.29 - ABH, no PET occurs.

When the amine is not protonated, the lone pair of electrons on the amine has a probability of participating in PET, which quenches the fluorescence. This probability is directly related to the orbital overlap between the amine and the boron, which can be characterized by the tetrahedral character (THC) of the boron atom as mentioned in Chapter two (Equation 2.1).

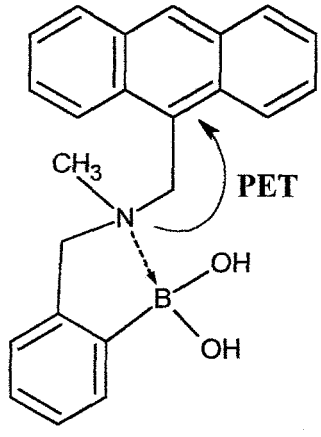

Figure 5.30 - AB, PET quenches fluorescence.

At high pH the boron can bind to three hydroxyl groups. The bond with the third OH^- group involves the molecular orbital previously engaged in the dative bond with the amine. Thus the N→B bond cannot exist simultaneously with $B(OH)_3$, permitting the electrons on the amine to quench the fluorescence through PET (Figure 5.31).

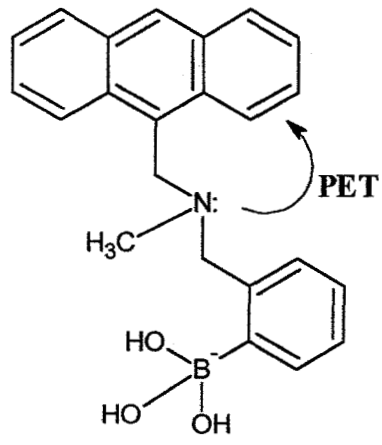

Figure 5.31 - ABOH, PET quenches fluorescence.

Solutions of AB in fifty percent methanol and fifty percent pH buffers were used to measure the both the pK_a and pK_b. Fluorescence measurements were made on samples with and without glucose, and although both are shown here and used in the pK_a and pK_b measurements, the effects of glucose binding will be discussed later in this chapter. As before, a theoretical model of the relative intensity was fitted to the values measured from the fluorescence emission spectra. With increased fluorescence due to protonation of AB and quenched fluorescence due to hydroxylation, the relative fluorescence intensity decreases with increasing pH (Figure 5.32).

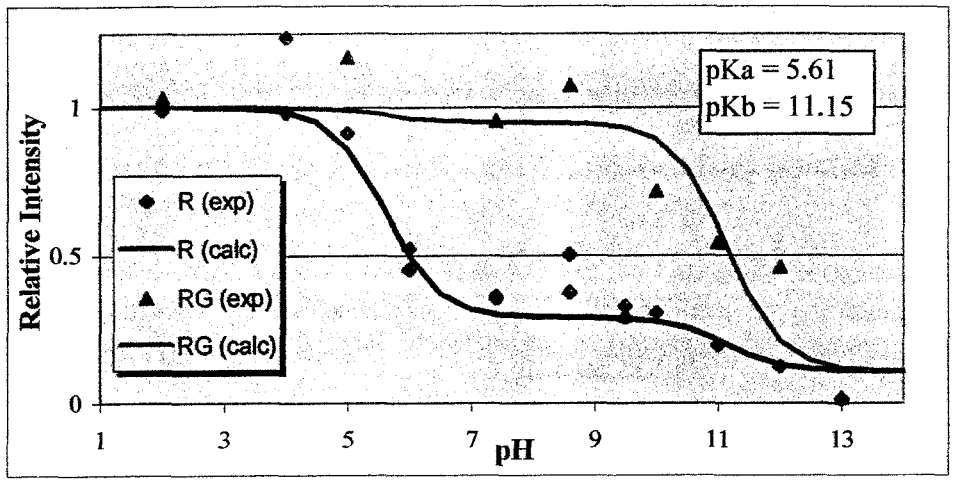

Figure 5.32 - Relative fluorescence intensity, with and without glucose (0.21 M), as a function of pH.

Using the data from AB solutions without glucose (R(exp)), the pK_a was found to be 5.77 and the pK_b was found to be 11.05. The pK_b was difficult to determine because the signal to noise is low at higher pH due to the increased quenching of the fluorescence. The relative intensity curve of AB with glucose should be more accurate in predicting the pK_b value due to the more dramatic decrease in intensity at high pH. Data from solutions with glucose (RG(exp)) yielded a pK_b of 11.17, while the pK_a was 5.71. Using data from both the relative intensity without glucose (R(exp)) and the relative intensity with glucose (RG(exp)), the values for the pK_a and pK_b were 5.79 and 11.16, respectively. The values for pK_a and pK_b do not vary considerably, however, the latter (pK_a = 5.79 and pK_b = 11.16) are more accurate because all of the data was used in the curve fit. One important note is that the pK_a found here is higher than the value reported previously. James, et al. measured the relative fluorescence of AB in 0.05 M NaCl as a function of pH and found the pK_a to be 2.9. (James, 1994) Therefore it is presumed that the addition of fifty

percent methanol increases the pK_a from 2.9 to 5.8. However, with MAMA the pK_a decreased by approximately 0.5 when methanol was added to the solvent, so this trend may not be relevant to other molecules.

5.3.3 Lifetime Measurements vs. pH

Fluorescence lifetimes of AB were measured in solutions of fifty percent pH buffer and fifty percent methanol. As the pH increases, the average lifetime of AB decreases causing the phase and modulation curves to shift to the right (Figure 5.33).

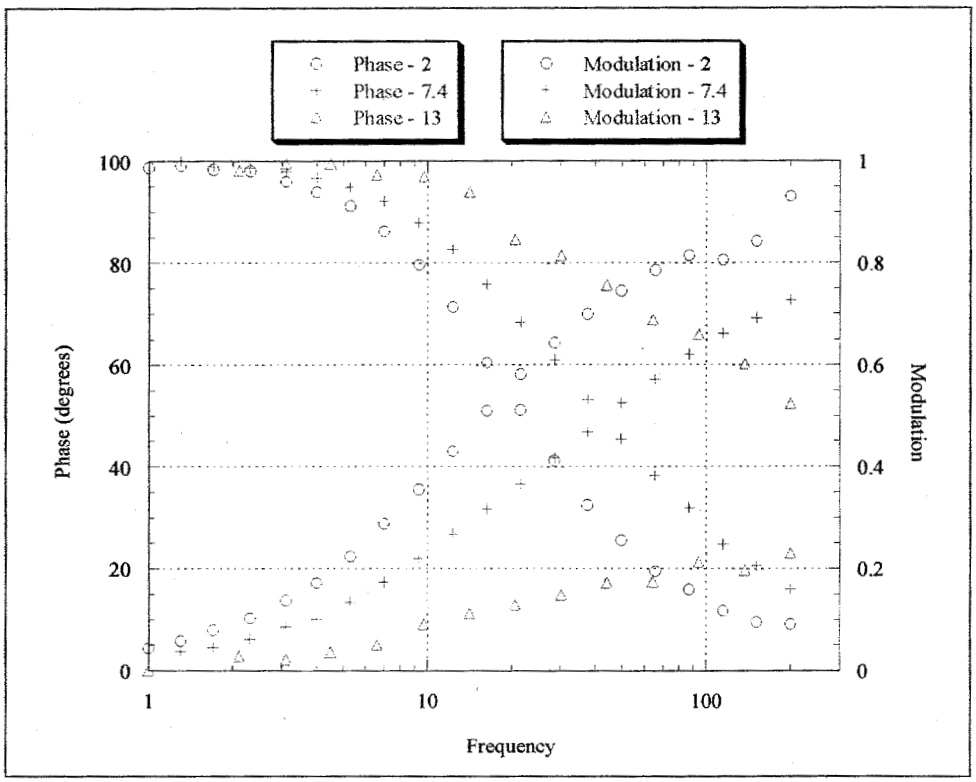

Figure 5.33 - Lifetime measurements of AB in MeOH and pH buffers (1:1 by volume). The curves shift to the right with increasing pH, indicating that the average lifetime is decreasing.

AB has three exponential lifetime components over the pH range (Figure 5.34). The first component (11.1 nsec) is due to the protonation of AB (ABH), as well as some AB molecules where the N→B dative bond prevents PET. Unfortunately, these two forms are indistinguishable with fluorescence. The second lifetime component is associated with AB quenched by PET, resulting in a lifetime value of 3.2 nsec. The last component is approximately 0.34 nsec and was not expected in the two component model of AB.

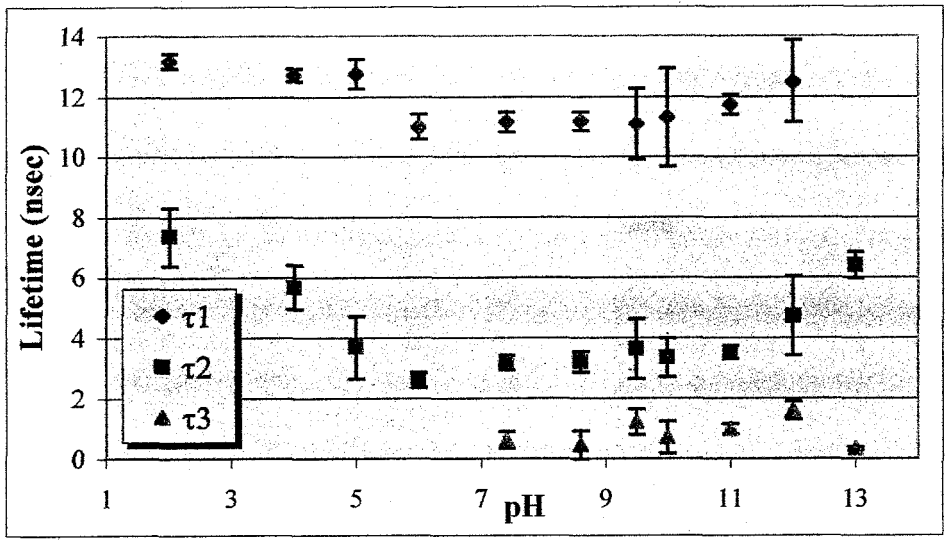

Figure 5.34 - Fluorescence lifetimes as a function of pH. Solvent is aqueous buffered solution with methanol (1:1 by volume).

Unlike measurements on MAMA, where the third lifetime was attributed to contamination due to the relatively small amount of fluorescence, the third lifetime measured for AB contributes significantly—especially at high pH. Therefore, the pre-exponential factors (Figure 5.35) for the lifetimes above deviate from the expected two component curves.

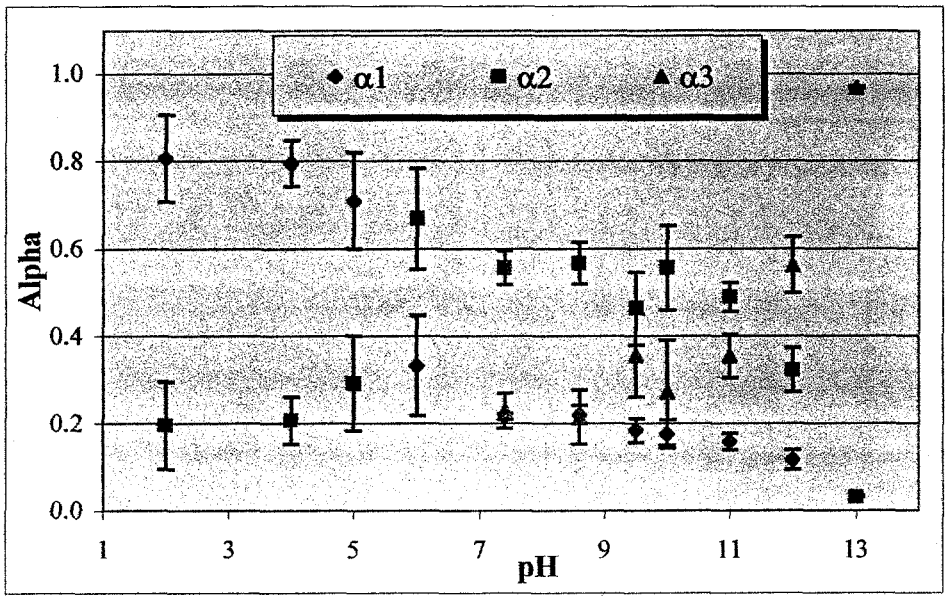

Figure 5.35 - Pre-exponential factors for fluorescence lifetimes of AB as a function of pH. Lifetime values are τ_1~11.1, τ_2~3.2, τ_3~0.34 nsec.

Below pH 7, α_1 and α_2 resemble curves from a two component model, however, α_1 never reaches unity and α_2 never has a value of less than 0.2. ABH and AB without PET are the species associated with α_1. At pH 4 the maximum value of α_1 is only 0.8, meaning that 20% of the molecules have their fluorescence quenched by PET. However, with a pKa of 5.8, all AB molecules should be protonated at pH values at and below 4. Recall that for AB-B two lifetime components also exist at low pH (Figure 5.20), while MAMA has only one lifetime (Figure 5.11). The reason for the two components is unclear, but perhaps the phenyl ring effects the geometry at low pH, allowing the fluorescence to be quenched.

At pH values above 7 the third component, α_3, appears. The increasing value of α_3 as a function of increasing pH suggests that this component could be due to the

fluorescence of ABOH. It was previously assumed that ABOH had similar fluorescence properties to AB; both molecules have electrons available to quench the fluorescence through PET. However, it is possible that the extra OH group on the boron changes the geometry in such a way as to increase the efficiency of electron transfer. A molecule with a higher rate of PET would have a shorter fluorescence lifetime. However, because the pKa was determined to be approximately 11.16, the concentration of ABOH from pH 7.4 to 9 should be close to zero. Perhaps the conformational change due to the additional OH group occurs naturally in a small fraction of the molecules in this pH range. The possibility of ABOH has not yet been proven, but will be assumed for the sake of argument in the following analysis.

Because three lifetime components exist in combinations of no less than two components, we do not have enough information to use the simple relationship between α and concentration that was used in the two component model. We can, however, look at each pair of components separately to find the approximate pK value (Figure 5.36). For the first pair, α_1 and α_2, the pK_a is found to be 5.55. This is only slightly lower than the value found using steady state data (5.79).

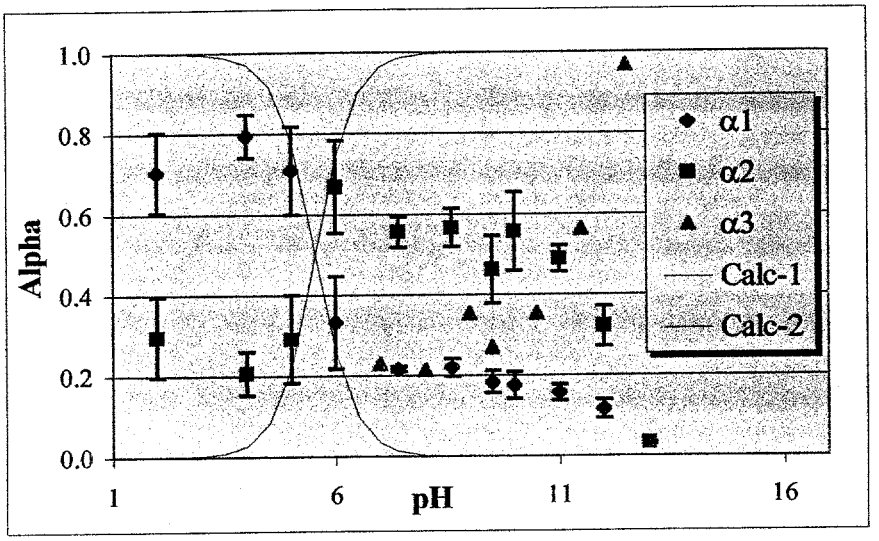

Figure 5.36 - Calculation of the pK_a of AB from α_1 and α_2.

For the second pair of alphas, α_2 and α_3, because we are assuming that α_3 is due to ABOH, the crossing point for the curves will be the approximate pK_b (Figure 5.37). In this case, the pK_b is 11.57, close to the value measured with steady state data (11.16).

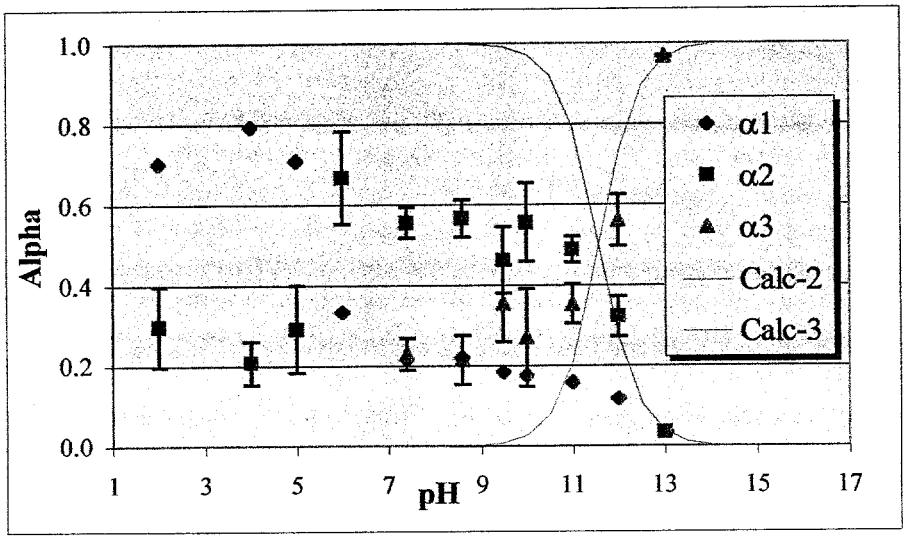

Figure 5.37 - Calculation of the pK_b of AB from α_2 and α_3.

The values for α_2 and α_1 between pH 7 and 11 deviate from the two component model. The amount of fluorescence with a long lifetime is higher than expected due to hydrogen bonding alone. This is partially due to the N→B interaction. With this dative bond some of the unprotonated molecules are not quenched by PET and thus fluoresce with a long lifetime and contribute to the population of α_1. This increase in α_1, decreases the amount of molecules (α_2) fluorescing with a shorter lifetime (τ_2). Without the dative bond, the value of α_1 above the pK_a (5.8) would be expected to fall to zero. If the contribution from α_3 is neglected at pH 7.4 when it first appears and is most likely to be small, the amounts of α_1 and α_2 are 0.28 and 0.72, respectively. This suggests that the enhanced N→B interaction takes place in approximately 28% of AB molecules that are not involved in amine protonation or boron hydroxylation. This translates into a tetrahedral character (THC), first discussed in Section 2.2.4, of approximately 28%. In other words, AB molecules have a seventy-two percent chance of an electron escaping the dative N→B bond and quenching the anthracene fluorescence via PET. This is a direct result of the orbital overlap between the N and the B atoms, and translates into a reduced sensitivity to glucose. Almost one-third of all AB molecules are fluorescing with a lifetime identical to AB when glucose is bound, and fluorescence measurements are unable to distinguish between the two. The other two-thirds of AB molecules show a change in fluorescence lifetime upon binding to glucose although all AB molecules are equally available to bind to a glucose molecule. As discussed earlier, the N→B dative bond is present in all of the AB molecules. The THC is simply a way of characterizing the possibility of electron transfer. If the THC were lower than 28%, the possibility of PET in a neutral AB molecule would be increased and the values of α_1 above the pK_a would decrease

compared to those seen in Figure 5.37. This would yield a larger switching fraction and increased sensitivity to glucose by reducing the fluorescence at neutral pH. However, the pK_a would also shift with a change in THC because it is also a measure of the amine's ability to become protonated. A lower THC would not only allow for more PET, it would increase the ability of the amine to become protonated causing the pK_a to increase. Too much of an increase in pK_a, and it would be above the physiological pH of 7.4, rendering AB useless as a biological sensor molecule.

5.3.4 Lifetime Measurements in Acetonitrile

Fluorescence lifetime measurements in 0.1M TBAP/ACN were made on AB. It was determined that degassing of the solution with N_2 has a significant effect on the lifetime values (Tables 5.6 and 5.7). The change in fluorescence lifetimes after bubbling N_2 indicates that without degassing the fluorescence of AB in TBAP/ACN is most likely quenched by oxygen (Section 4.1).

AB in ACN/TBAP, no N_2	**Component 1**	**Component 2**
Lifetime (nsec)	2.92	1.50
Fractional Fluorescence Contribution	0.29	0.71
Pre-exponential (alpha)	0.17	0.83

Table 5.6 - Lifetime measurements of AB in ACN (0.1M TBAP), no degassing.

AB in ACN/TBAP, with N_2	**Component 1**	**Component 2**
Lifetime (nsec)	6.34	1.76
Fractional Fluorescence Contribution	0.18	0.82
Pre-exponential (alpha)	0.06	0.94

Table 5.7 - Lifetime measurements of AB in ACN (0.1M TBAP), degassing with N_2.

By degassing the solution, the lifetimes become longer indicating that the amount of oxygen quenching is reduced (Table 5.7). After degassing the solution, lifetime measurements detected only 6% of molecules fluorescing with a lifetime of 6.34 nsec. In the current solvent, TBAP/ACN, there are not any free hydrogen ions (except from contaminants) able to bind with AB and prevent PET. Therefore, we can deduce that this small percentage of molecules not quenched by PET have enhanced N→B dative bonds, or have possibly found a contaminant hydrogen ion to bind with the amine. Measurements made previously on MAMA in the same solvent show only 3% of the longer lifetime fluorescence (not quenched by PET). Because MAMA does not have a boron atom, the percentage of long lifetime fluorescence is most likely due to contaminants. The rate of electron transfer calculated from the lifetimes measured in degassed ACN/TBAP is 4.1×10^8 sec^{-1}. This will be discussed in the following section.

5.3.5 Electron Transfer Rates

Measurements of AB in 0.1M TBAP/ACN yielded values of 0.86 V for the reduction potential of the amine and –2.3 V for the oxidation potential of anthracene. The value of λ_{00} (Equation 3.59) for AB, taken from the average of the excitation and

emission peaks, is 388nm. Using the Rehm-Weller equation (Equation 3.58), ΔG_{ET} equals -0.83 kcal/mol.

The experimental value for the rate of electron transfer varies greatly with pH due to the variation in lifetime values. The shortest lifetime ($\tau_3 = \tau_{ABOH}$) is ignored and the rate of PET is calculated from the intermediate lifetime of the AB ($\tau_2 = \tau_{AB}$), so that the rate of electron transfer can be written as

$$k_{ET} = \frac{1}{\tau_{AB}} - \frac{1}{\tau_{ABH}} \qquad 5.6$$

This leads to a variation of electron transfer rates ranging from 4.3 x 10^7 sec^{-1} at pH 2, to 2.3 x 10^8 sec^{-1} at pH 7.4, and 1.6 x 10^8 sec^{-1} at pH 13 (Figure 5.38).

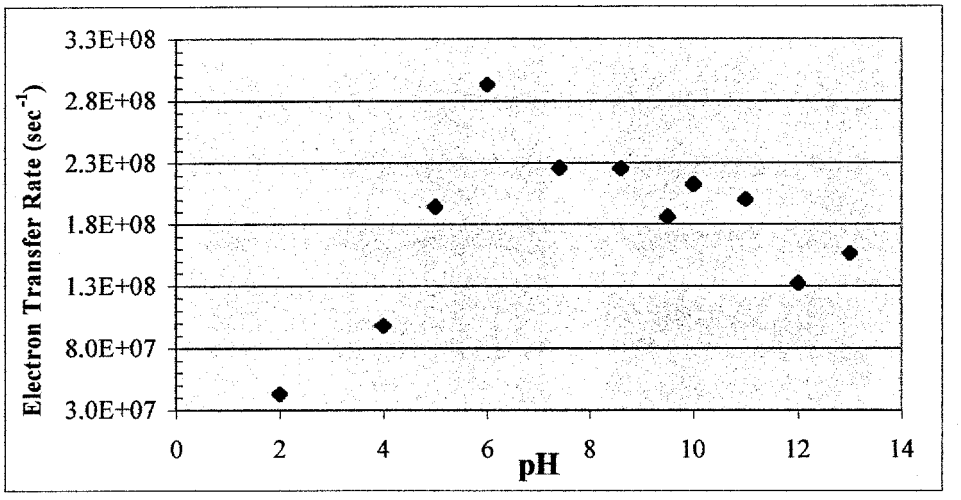

Figure 5.38 - Rates of electron transfer, calculated with two measured lifetime values (τ_1~11.1 nsec and τ_2~3.2 nsec, varying with pH).

The average value of the electron transfer rate in buffer and methanol is 1.8 x 10^8 sec^{-1}. The experimental value calculated in ACN/TBAP is 4.1 x 10^8 sec^{-1}. The electron transfer

rate found in ACN/TBAP is only slightly faster than the values in buffer and methanol. This difference is most likely due to solvent effects such as dielectric constant and polarity which might change the conformation of the molecule and the energy difference between the excited state ($D\text{-}A^*$) and charge transfer species ($D^+\text{-}A^-$). Equation 5.4 shows the dependence of the barrier height to electron transfer with the outer-sphere reorganizational energy (varying with solvent properties) put forth by Marcus theory. This relationship on solvent properties predicts the rate of electron transfer to be faster in 50% MeOH and 50% buffer than in ACN/TBAP, contrary to what was measured. However, if the third (0.34 nsec) lifetime is included, the electron transfer rate changes at pH values above 7 (Figure 5.39). The average rate of electron transfer is 1.1×10^9 sec^{-1} and the rate at pH 7.4 is 1.9×10^9 sec^{-1}, both values are an order of magnitude faster than previously calculated without the third lifetime.

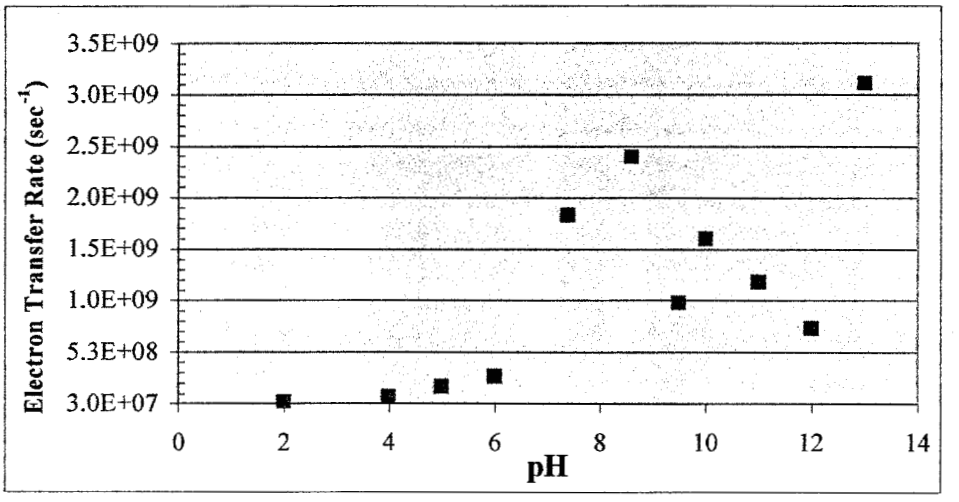

Figure 5.39 - Rates of electron transfer, calculated with all measured lifetime values.

The short lifetime was proposed to be a consequence of through-space electron transfer, rather than through-bond. This suggests that electron transfer of AB in ACN/TBAP is also through-space due to the conformation of AB in this solvent.

5.3.6 Steady State Measurements vs. Glucose

The fluorescence intensity was measured as a function of glucose concentration. When glucose (>500 mg/dL) is added to AB at pH 7.4, the emission spectra red shifts causing the peak emission value to increase from 412 nm to 415 nm (Figure 5.40).

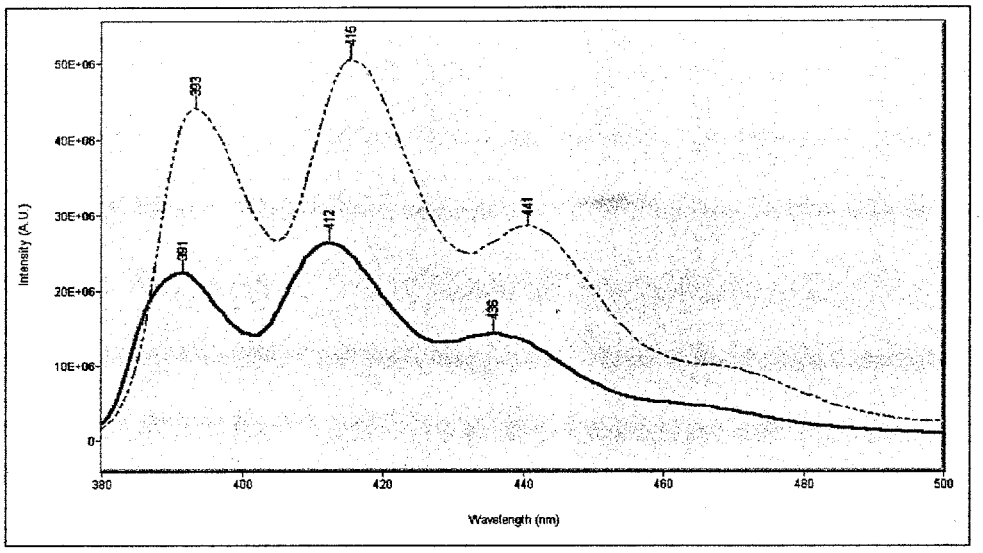

Figure 5.40 - Fluorescence emission increases with glucose in a solution of AB in 50% PBS and 50% MeOH.

This red shift can also be seen with increased acidity of the solvent, demonstrating the similarity of the fluorescence of the protonated (ABH) species, and the AB complex attached to glucose (ABG). The attached glucose molecule creates a more electronegative boron atom, strengthening the N→B bond. As the concentration of

glucose is increased, the relative intensity of AB fluorescence increases to more than double the original amount of fluorescence (Figure 5.41).

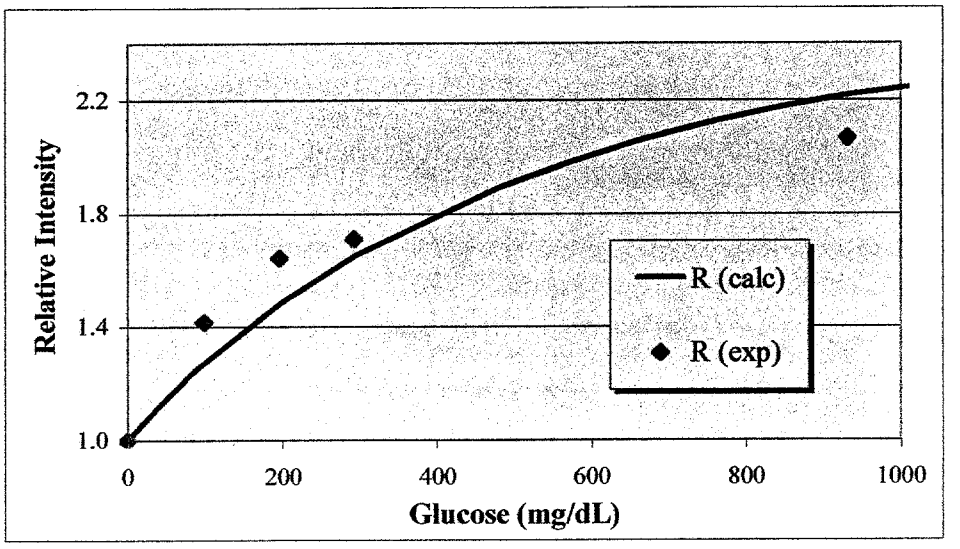

Figure 5.41 - Relative intensity of fluorescence with additions of glucose.

The total switching fraction (Equation 3.36) of AB in a solution of fifty percent PBS and fifty percent methanol with 1000 mg/dL glucose is 1.1.

5.3.7 Lifetime Measurements vs. Glucose

Average fluorescence lifetime values measured at pH 7.4 (with fifty percent methanol) increase with glucose concentration. This is seen in the shift toward lower modulation frequency by the phase and modulation curves (Figure 5.42).

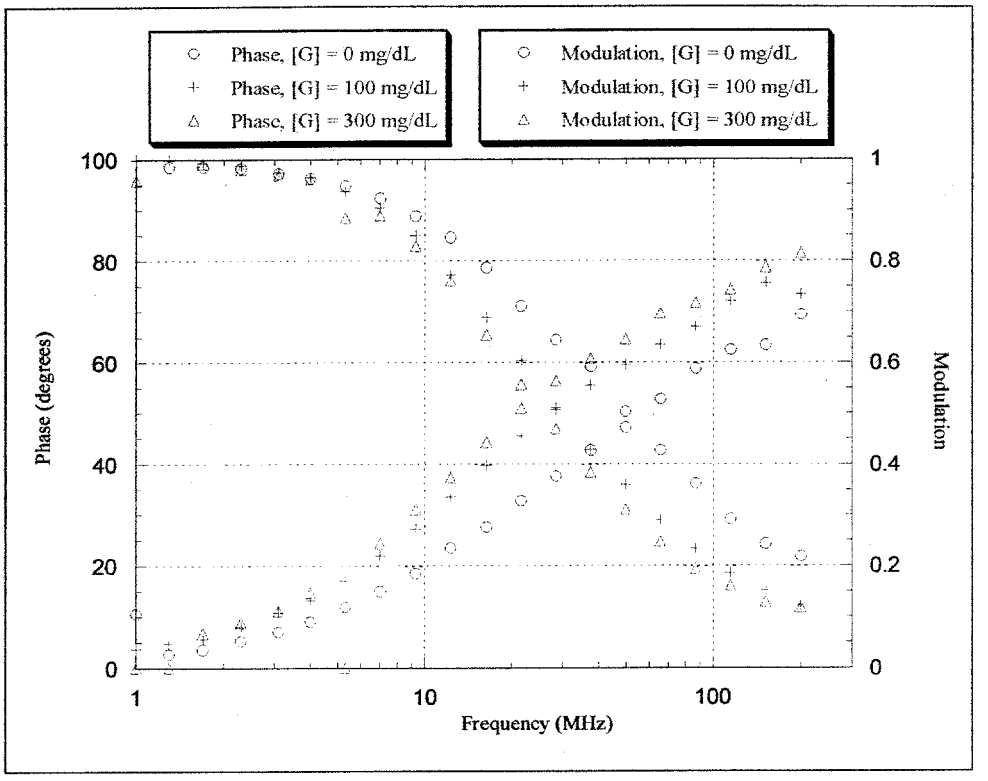

Figure 5.42 - Lifetime data for AB in PBS:MeOH (1:1 by volume). The addition of glucose shifts the curves to the left.

Although the difference between the lifetime data curves as a function of glucose is not as significant as when the pH is varied (Figure 5.33), the change in phase and modulation values is large enough to measure physiological concentrations of glucose. This will be made clear later in this chapter.

As expected from the pH measurements, three lifetimes are seen at low glucose concentration. However, the shortest lifetime, attributed to ABOH earlier, disappears at glucose concentrations above 300 mg/dL (Figure 5.43). Glucose should not effect the amount of ABOH present in solution, thus supporting the theory that the short lifetime results from conformations of AB existing at pH 7.4.

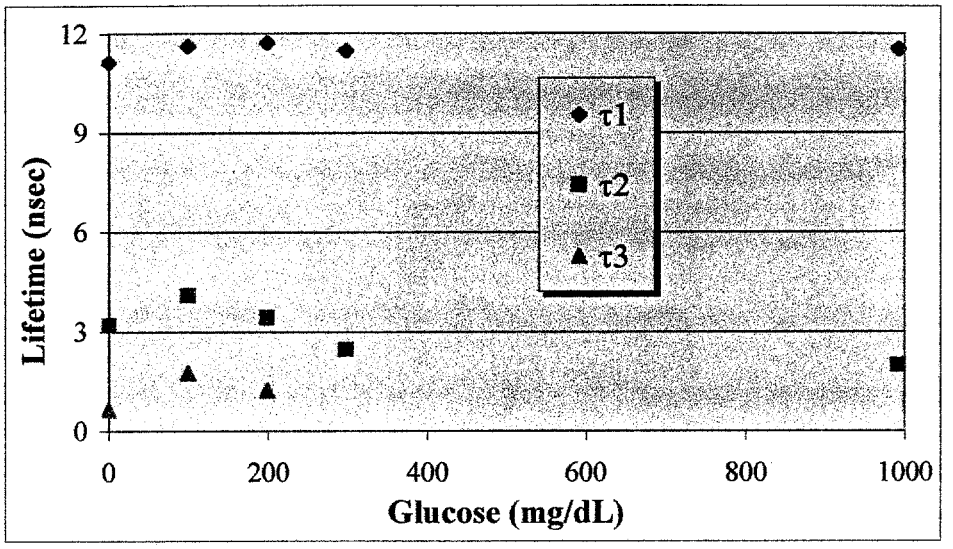

Figure 5.43 - Fluorescence lifetimes of AB with glucose.

The longer, approximately 11.6 nsec, lifetime is characteristic of both the protonated AB (ABH) and the AB with glucose (ABG) due to the enhanced N→B bond when glucose is bound. The intermediate lifetime due to the AB species is approximately 3.0 nsec in duration. The third lifetime from the AB species with a conformation favoring through-space electron transfer is roughly 1.2 nsec. The existence of this lifetime does not effect the ability of AB to measure glucose. The lifetime measurements are based upon a change in average lifetime with glucose (Section 5.3.9). Recall Equation 3.46 describing the relationship between the average lifetime and the pre-exponential components.

$$\langle \tau \rangle = \frac{\sum_i \alpha_i \tau_i^2}{\sum_i \alpha_i \tau_i} \qquad 3.46$$

The presence of a short lifetime at zero glucose concentration helps to shorten the average lifetime, creating a larger difference in the lifetime of a sample with glucose

present. However, in the normal physiological range (80mg/dL – 120mg/dL), the third lifetime exists in approximately the same amount (Figure 5.44), therefore the effect of the third lifetime on a glucose sensor is minimal.

The pre-exponential component, α_2, for the PET quenched lifetime shows a sharp drop between 0 and 100mg/dL. This is accompanied by a rise in α_1, the component for the long lifetime due to ABH and ABG (Figure 5.44). The reason for this is not clear, and requires further studies.

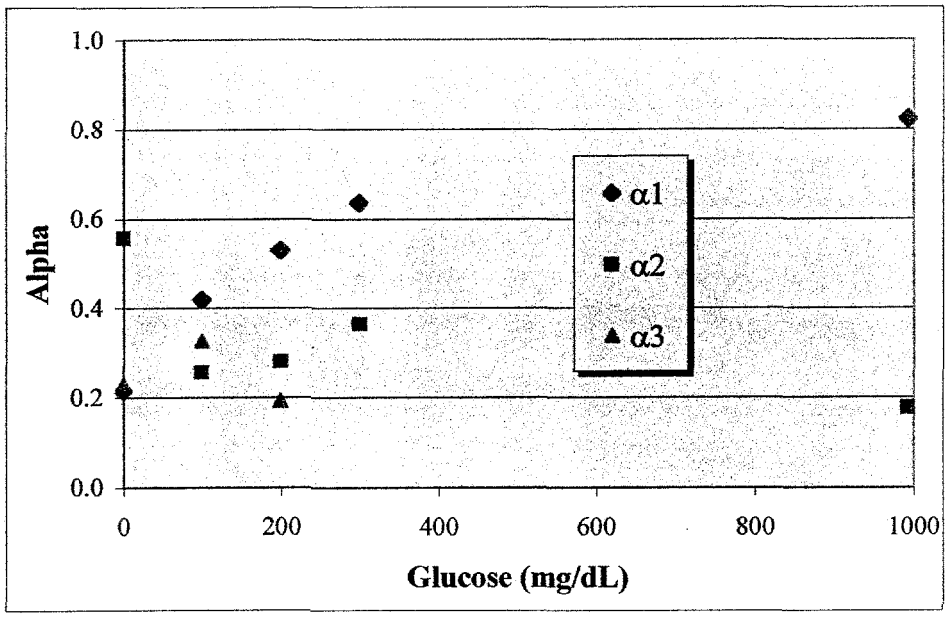

Figure 5.44 - Pre-exponential components of the lifetime of AB with glucose.

It is interesting to note that with 1000 mg/dL glucose (or 5000 mg/dL, not shown) two lifetime components, α_1 and α_2 exist. With an abundance of glucose in solution one might expect every AB molecule to be bound to a glucose molecule. However, twenty percent of molecules are exhibiting PET, which does not occur in ABH, ABG, or ABGH.

Therefore, it is suggested that twenty percent of AB molecules are fixed in a position allowing PET. This was seen previously in Figure 5.35 where at low pH values twenty percent of AB molecules had a short lifetime characteristic of fluorescence quenching by PET.

Fluorescence lifetimes were also examined with glucose (>4000 mg/dL) over pH values ranging from 5 to 11 (Figure 5.45). Steady state fluorescence measurements on the addition of glucose in solutions at pH 2 and 4 did not show an increase in intensity. This is consistent with the lifetimes remaining constant as well.

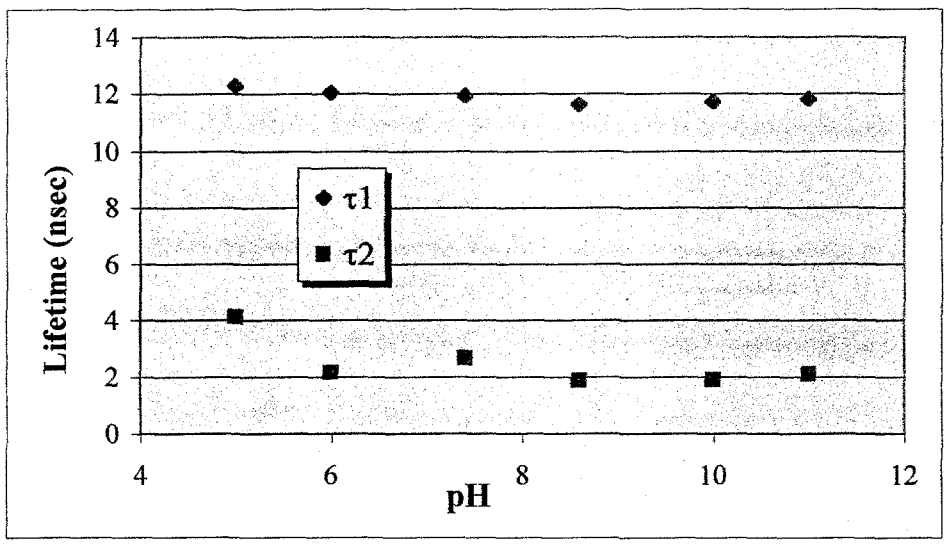

Figure 5.45 - Lifetimes of AB, with over 4000 mg/dL glucose, as a function of pH.

Two lifetime components exist, one at approximately 12 nsec, and one at approximately 2 nsec. This is approximately constant over the entire pH range studied. The uniformity

in the lifetimes of AB with glucose is reflected in the pre-exponential components (Figure 5.46).

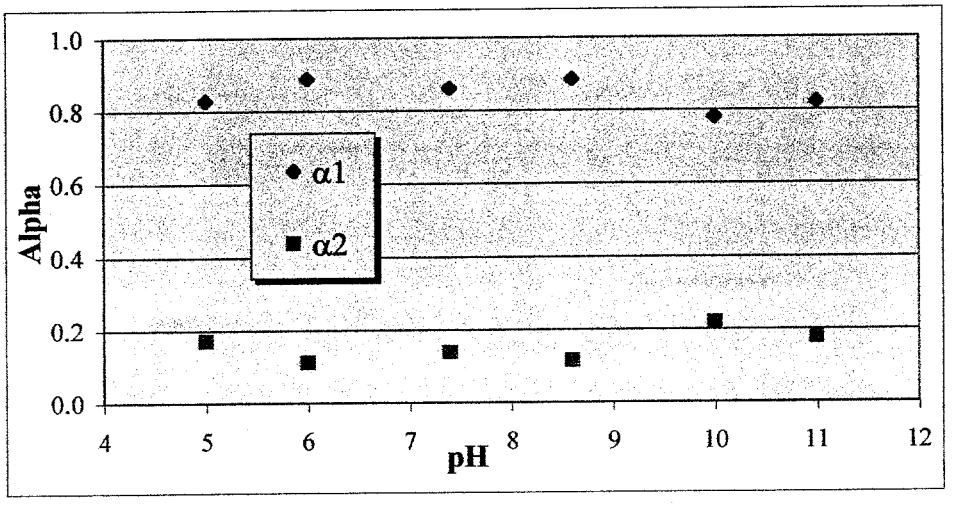

Figure 5.46 - Alphas of AB, with over 4000 mg/dL glucose, as a function of pH.

The alpha values indicate that regardless of pH and in spite of a large amount of glucose, roughly twenty percent of AB molecules are quenched by PET.

5.3.8 Solvent Effects

The percentage of methanol in solution changed the relative intensity of AB with and without glucose (Figure 5.47). The values are relative to the maximum intensity measured for all data sets.

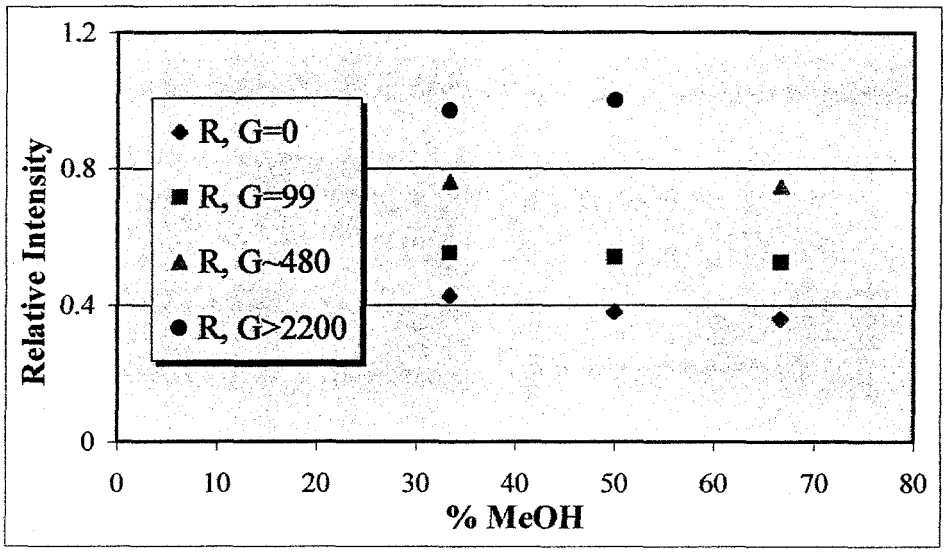

Figure 5.47 - Relative intensity of AB in PBS solutions with 33, 50, and 67% MeOH. Glucose was added to see if the fractional intensity increase changed.

From the data of AB without glucose we can see that more methanol in solution will decrease the fluorescence intensity slightly. As glucose is added the increase in intensity is slightly greater for the solution with more methanol. The switching fraction for a solution with one-third methanol is approximately 0.78 at 485 mg/dL. For the solution with two-thirds methanol, the switching fraction is 1.06 with 473 mg/dL of glucose. Therefore, methanol increases the possible switching fraction of AB in PBS.

5.3.9 Sensor Potential

For AB to be a candidate for a glucose sensor we must be able to accurately measure the phase shift or amplitude modulation (defined in Equations 4.5 and 4.6) as a function of glucose at the modulation frequency of the incident light. The maximum phase shift with glucose is detected at 17 MHz. Using light modulated at 17 MHz, the

phase difference between the incident light and the fluorescence is a simple function of glucose (Figure 5.48).

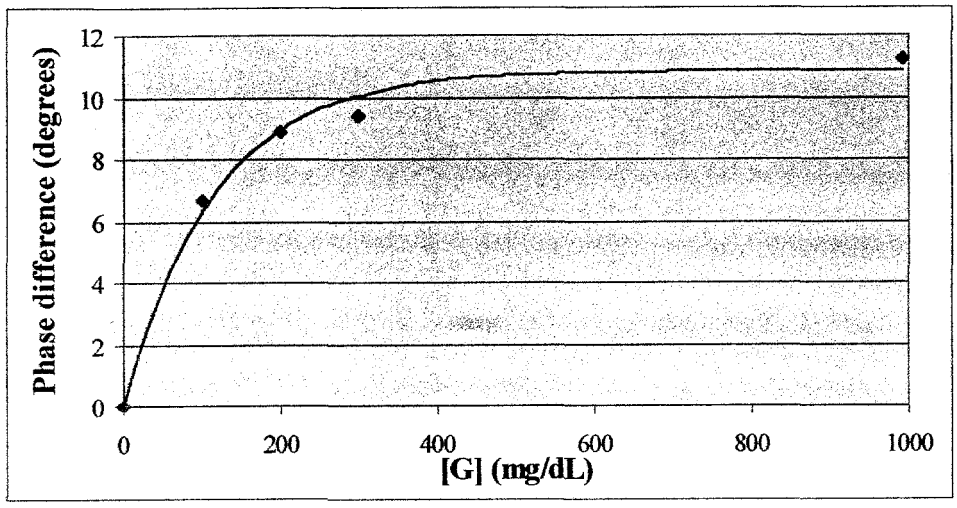

Figure 5.48 - Phase lag between the fluorescence and excitation as a function of glucose.

The phase difference in Figure 5.48 was determined by first calculating the average lifetime from the two or three lifetime values measured (Equation 3.46), and then using the simple relationship between phase and lifetime given in Equation 4.3.

$$\phi = \tan^{-1}\left(\frac{1}{\omega}\sum_i f_i\tau_i\right) \qquad 5.1$$

In Equation 5.1, ω is the frequency of modulation, f_i is the fractional contribution of species i to the fluorescence, and τ_i is the lifetime of species i. For AB this becomes

$$\Delta\phi = \tan^{-1}\left[\frac{1}{\omega}\left(f_{ABG}\tau_{ABG} + f_{AB}\tau_{AB}\right)\right] - \tan^{-1}\left[\frac{1}{\omega}\left(f_{AB}\tau_{AB}\right)\right] \qquad 5.2$$

where lifetime components due to ABH and ABOH have been neglected because they do not change with glucose concentration. From this equation it is apparent that phase difference can be increased by increasing the lifetime of ABG, decreasing the lifetime of AB, or uniformly increasing both lifetimes. A technique of introducing a long lifetime component (~ μsec), independent of glucose concentration, is under investigation at the University of Maryland (Tolosa, 1999). In theory, the long lifetime should increase the phase difference, and may even allow for greater accuracy of glucose measurement at lower modulation frequencies.

An equation for the curve (Equation 5.3) in Figure 5.48 was found using a least squares fit of the data, letting the constant (10.85) and the exponential factor (0.0087) vary.

$$\Delta\phi = 10.85\left(1 - e^{-[G]0.0087}\right) \qquad 5.3$$

Looking at the glucose range of physiological interest, it is noticeable that the largest change in phase is at the lower end of the range (Figure 5.49). This is advantageous for accurate measurements in the hypoglycemic range.

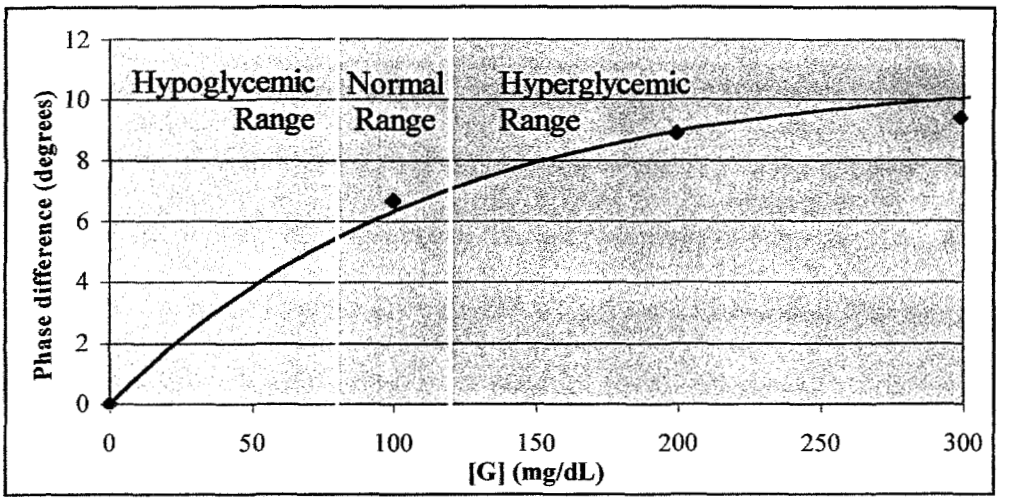

Figure 5.49 - A close up of the physiological glucose range and the phase difference expected at 17MHz.

Small (120 x 60 x 30 mm), portable fluorescence lifetime sensors have been built using only one frequency of modulation. (Trettnak, 1996) The typical accuracy of the phase measurements is 0.2 degrees, with 0.1 degree possible. To obtain measurements within 5% of the actual glucose value, the required phase accuracy varies with glucose concentration (Figure 5.50). Phase difference was determined using Equation 5.3 to predict the change in phase with glucose concentrations ranging ± 5% of the true values.

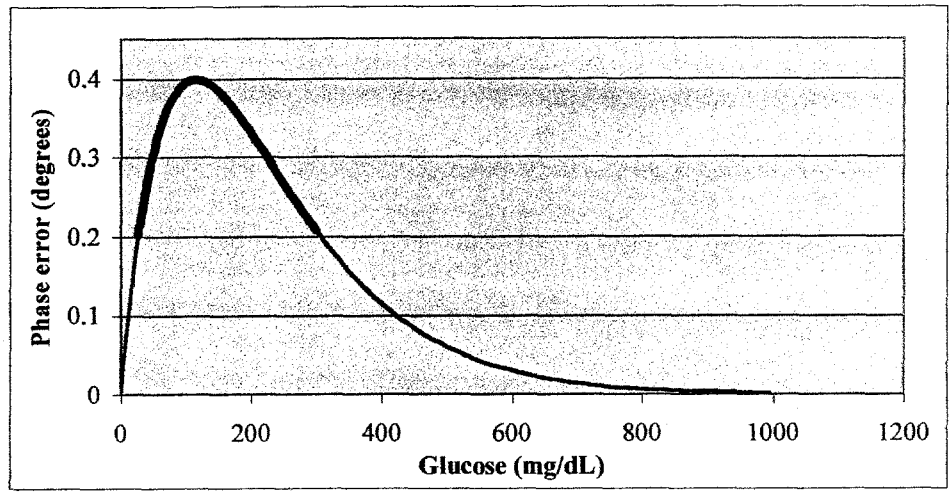

Figure 5.50 - Phase accuracy needed to obtain accurate glucose measurements to within 5%.

Figure 5.50 shows a 0.4 degree error is needed to accurately measure a glucose concentration of 110 mg/dl. With an error of 0.2 degrees, 95% accuracy can be achieved for glucose concentrations ranging from approximately 27 mg/dL to 300mg/dL. This covers the range of interest for a diabetic: the hypoglycemic range below 80 mg/dL, as well as the hyperglycemic range above 120 mg/dL. This is easily obtained for a glucose sensor using a solution of AB in PBS and methanol. However, the ability of AB to measure glucose *in vivo* is only beginning to be demonstrated. Preliminary work with AB incorporated into a membrane will be discussed in the next section.

5.4 Membrane Development

Using a carbon chain attached to both the methyl group of the amine and a monomer before polymerization, AB has been successfully incorporated into a PHEMA (poly hydroxy ethyl methacrylate) membrane. PHEMA is a biocompatible hydrogel that

is non-toxic and does not solicit an immune response *in vivo*, thereby discouraging encapsulation when implanted. Because it is a hydrogel, it has a high water content to support efficient diffusion of interstitial fluid, including glucose, through the membrane. Typical diffusion coefficients for glucose across the PHEMA membrane are 1~5 x 10^{-6} cm^2/sec (for sucrose in H_2O, D=5.23 x 10^{-6} cm^2/sec). The pore size in the PHEMA can be determined by the number of cross-linkers (ethylene glycol dimethacrylate) added during synthesis. The cross-linkers act like rungs in a ladder, connecting the hydrogel monomers together. (Grant, 1996)

5.4.1 Preliminary Results

Although AB has been successfully incorporated into a membrane, its ability to measure glucose is significantly lower than AB in solution. Steady state measurements show a maximum switching fraction of approximately 0.25 (Figure 7.1). This is very low compared to a switching fraction of 1.1 measured on AB in solution (Figure 5.42).

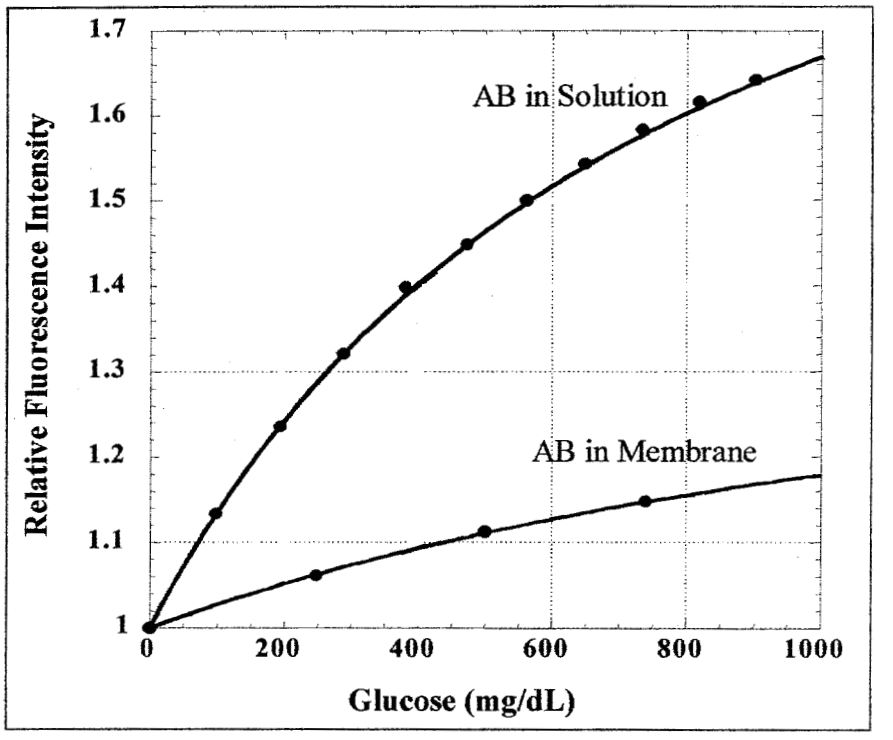

Figure 5.51 - Relative intensity of AB in solution and covalently bound to a polymer membrane.

Two lifetimes were measured on AB in a polymer membrane. Without glucose, the two lifetimes are approximately 14.2 nsec and 1.4 nsec. With 1000 mg/dL glucose the lifetimes increase slightly to 17.3 nsec and 3.1 nsec. Alpha values for the longer lifetime increase from 0.43 nsec to 0.46 nsec with the addition of 1000 mg/dL glucose. Although this change is small, it translates into a switching fraction of approximately 0.38 with 1000 mg/dL glucose. This is less than one-third of the switching fraction of AB in solution and is not enough for a physiological glucose sensor. This work is just beginning, and these preliminary results are very promising.

5.4.2 Future Work

AB has been successfully incorporated into a polymer membrane. A carbon chain attached to the polymer structure covalently links each AB molecule. Although the average lifetime changes with glucose concentration, the switching fraction (0.38 with 1000mg/dL glucose) should be much higher for an *in vivo* glucose sensor with accuracy comparable to currently available devices. Investigations into optimizing the polymer membrane must be performed. This should include studies incorporating AB into PHEMA membranes with various pore sizes as well as incorporating AB into different types of membranes to learn how the polymer environment affects the ability of AB to change fluorescence with glucose.

REFERENCES

Bissell, R.A. et al. Fluorescent PET (Photoinduced Electron Transfer) Sensors. *Topics in Current Chemistry* 168: 223-264. Springer-Verlag, Berlin, 1993.

James, T.D., et al. Novel Photoinduced Electron-transfer Sensor for Saccharides based on the Interaction of Boronic Acid and Amine. *J. Chem. Soc., Chem. Commun.*: 477-478, 1994.

Kavarnos, G.J. Fundamentals of Photoinduced Electron Transfer. VCH Publishers, Inc., New York, 1993.

Rehm, D., and A. Weller. Kinetics of Fluorescence Quenching by Electron and H-Atom Transfer. *Israel Journal of Chemistry* 8: 259-271, 1970.

Tolusa, L., et al. Glucose Sensor for Low-Cost Lifetime-Based Sensing Using a Genetically Engineered Protein. *Analytical Biochemistry* 267: 114-120, 1999.

Trettnak, W., et al. Miniaturized luminescence lifetime-based oxygen sensor instrumentation utilizing a phase modulation technique. Sixth International Meeting on Chemical Sensors, Gaithersburg, MD, USA. Elsevier, 1996.

Weast, R.C., ed. Handbook of Chemistry and Physics, 57th edition. CRC Press, Cleveland, Ohio, 1976.

Wehry, E.L., ed. Modern Fluorescence Spectroscopy 2. Plenum Press, New York, 1976.

Chapter VI

RESULTS – Long Wavelength Fluorophores

The fluorescence of AB responds very well to changes in glucose concentration. However, it is not possible to use AB as the sensor molecule in an implanted membrane with transdermal illumination (Figure 2.2) because the wavelengths needed for excitation (367 nm) and emission (412 nm) do not propagate far enough through the skin. To overcome this problem, novel molecules have been synthesized with the same functional (glucose sensing) part of AB, but with a fluorophore that emits at a wavelength longer than anthracene.

6.1 6-Chloro-10methyl-5Hbenzo[a]phenoxazin-5-one (COB)

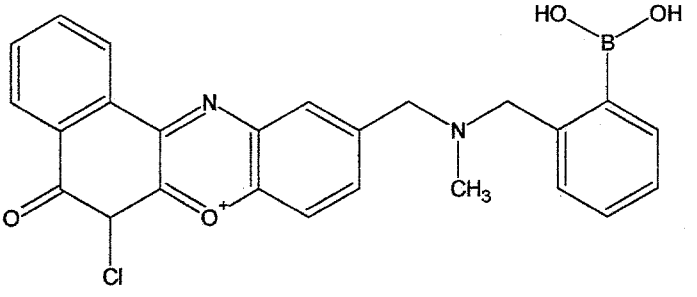

6.1.1 Relevance

The first successful synthesis of a sensor molecule with a longer wavelength fluorophore was chloro-oxazone boronate (COB). COB was chosen as a potential sensor molecule based on electrochemical and steady state fluorescence measurements of oxazine 170, which is a cationic dye with a structure similar to COB. The reduction potential of oxazine 170 is -0.55 V in 0.1M TBAP/ACN, the excitation wavelength is 625

nm, and the emission wavelength is 649 nm. A figure of merit (ΔE) was created based on a comparison of these values with measurements of anthracene. (Gray, 1999)

$$\Delta E = (E_{\lambda O} - E_{\lambda A}) - (ER_A - ER_O) \qquad 6.1$$

The reduction potential of anthracene (A) and oxazine 170 (O) are given by ER_A and ER_O, respectively, while $E_{\lambda A}$ and $E_{\lambda O}$ represent the energy difference between the ground state and the excited state (approximated by the average of the excitation and emission peak wavelengths). For oxazine 170, ΔE was found to be 0.69 kcal/mol. A ΔE of zero is desirable because it means the energy levels for oxazine 170 are similar to those of anthracene. Addition of the amine and the boronic acid to oxazine 170 (or similar fluorophores) should, in theory, create a sensor molecule similar to AB.

6.1.2 Steady State Fluorescence

The COB measurements were done in a mixture of 67% MeOH and 33% PBS. This solution was chosen instead of the 50% MeOH and 50% PBS used with AB because AB demonstrated an increased switching fraction with a higher percentage of methanol in solution. Steady state fluorescence measurements (Figure 6.1) show excitation peaks at 366 nm and 450 nm and a single emission peak at 565 nm.

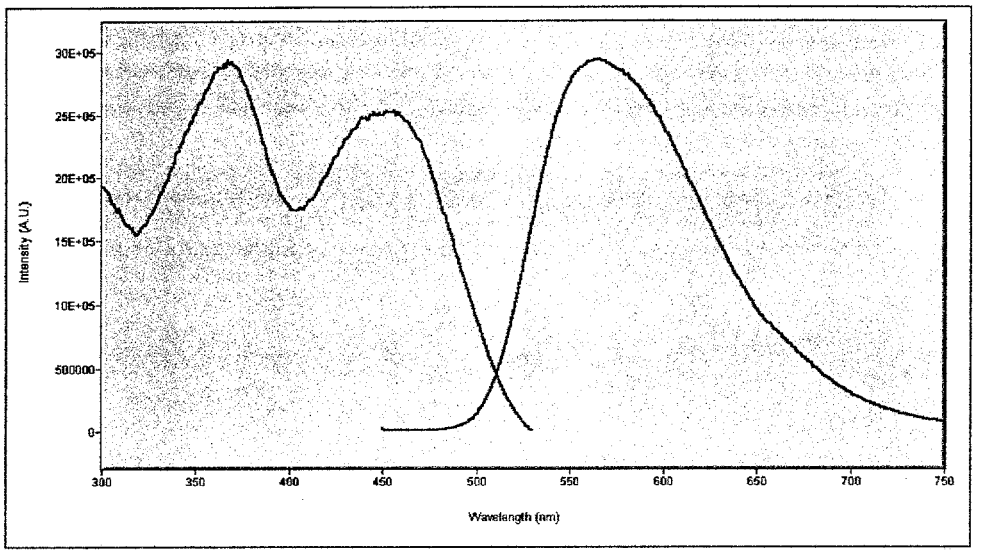

Figure 6.1 - Excitation and emission spectra of COB in 67% MeOH and 33% PBS.

Excitation at 450 nm was used, even though it is not the most intense peak, because the purpose of COB is to be able to excite the sensor molecule at a wavelength longer than 367nm (the excitation peak of AB). Excitation at 366 nm did not change the shape of the emission curve. The relative intensity was measured with glucose concentrations of 0 mg/dL, 958 mg/dL, and 1858 mg/dL (Figure 6.2).

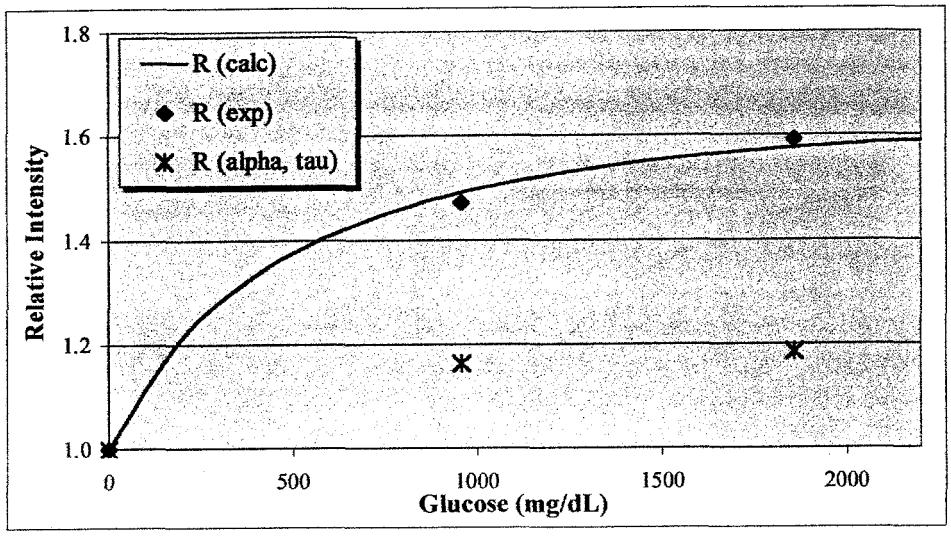

Figure 6.2 - Relative intensity of COB as a function of glucose concentration.

The maximum switching fraction for COB is 0.6, which is about half of the maximum switching fraction for AB (1.1). Note that the relative intensity values calculated from the lifetime data, R (alpha, tau), are much lower than measurements of R from steady state fluorescence. This will be discussed in the following section.

6.1.3 Lifetime Measurements

Lifetime measurements were done with excitation at 450 nm, and emission above 500 nm using a high pass filter. POPOP could not be used as a reference fluorophore because it cannot be excited at 450 nm, so glycogen was used as a reference. Data shown in Figure 6.3 are for COB with glucose concentrations of 0 mg/dL and 1858 mg/dL.

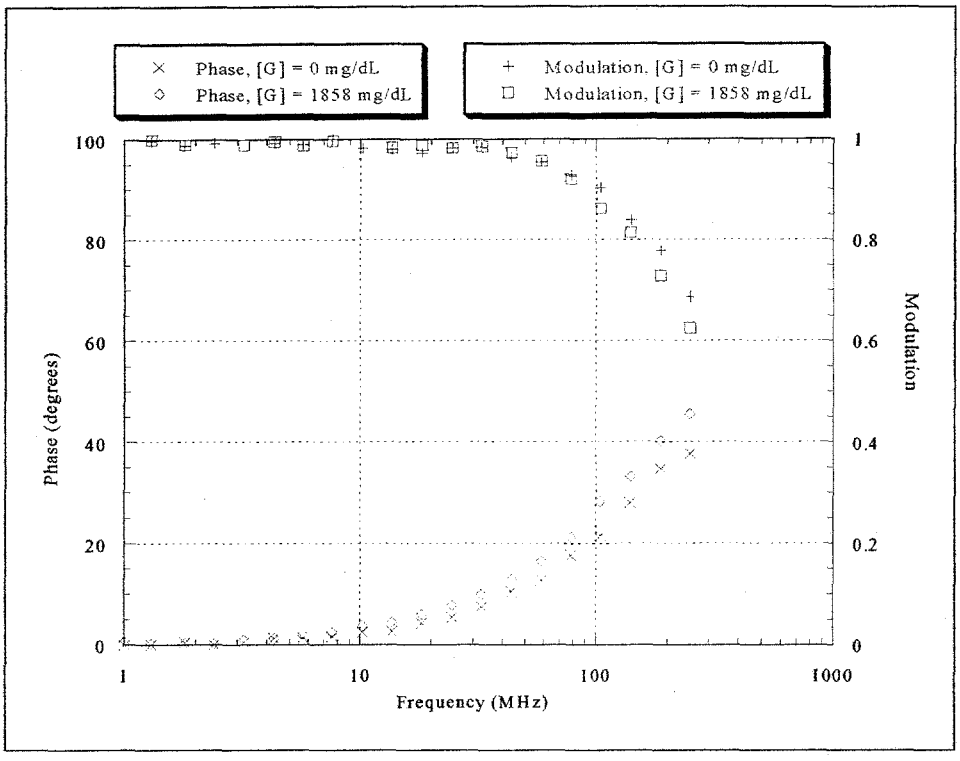

Figure 6.3 - Lifetime data for COB in 67% MeOH and 33% PBS. Phase and modulation curves with glucose are shifted slightly to the left.

Lifetimes for all glucose concentrations were linked together, forcing the values to remain constant while the amount of fluorescence due to each component varied. Data that were not linked together, but allowed the lifetime values to vary with glucose concentration had χ^2 values similar to or worse than in the linked case. For AB as a function of glucose, the lifetime values did not vary significantly (Figure 5.44). Thus linking the lifetime values together was deemed acceptable in this case.

A triple exponential decay was measured with lifetime values of $\tau_1 = 1.1$ nsec, $\tau_2 = 0.57$ nsec, and $\tau_3 = 22$ nsec. The pre-exponential factors, α_1, α_2, varied slightly with glucose concentration, while the third component, α_3, did not (Figure 6.4). The third

component contributes less than 2% of the fluorescence, and was deemed to be a contaminant.

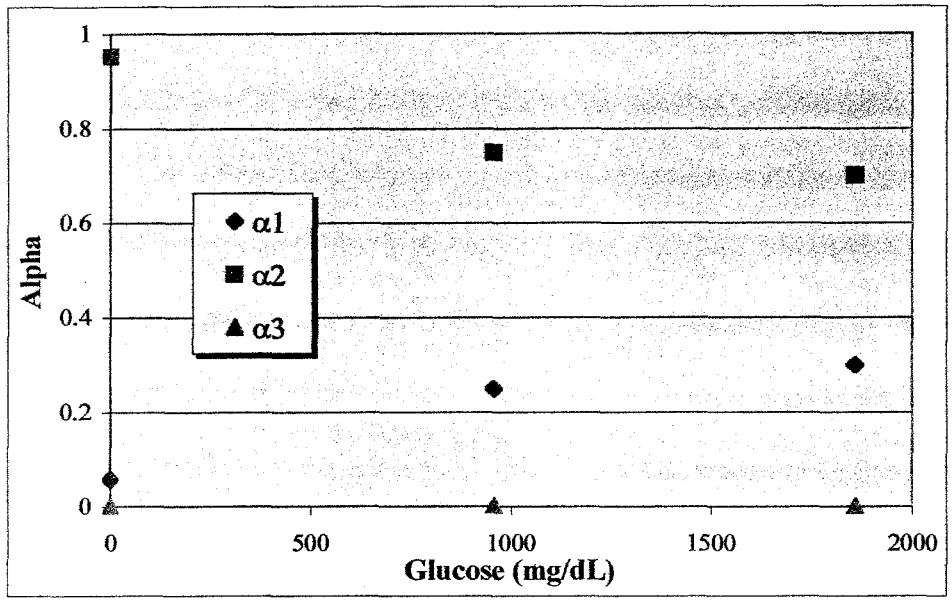

Figure 6.4 - Pre-exponential components for COB with glucose. Lifetime values are τ_1 = 1.1 nsec, τ_2 = 0.57 nsec, and τ_3 = 22 nsec.

Recall that in a two component exponential decay the alpha values are proportional to the concentrations of each species (Equation 3.44). Figure 6.4 shows that most of the fluorescence is coming from molecules with the shorter lifetime, τ_2 =0.57 nsec. The amount of these molecules, which are being quenched through PET, slightly decreases with glucose concentration. The longer lifetime species, with a correspondingly higher quantum yield, rises from 6% of the total molecules without glucose to only 30% at [G] = 1858 mg/dL. The small change in alpha values would not be desirable for a glucose sensor.

6.1.4 Electrochemistry and Electron Transfer Rates

Electrochemical measurements made on COB in 0.1M TBAP/ACN resulted in a fluorophore reduction potential of 0.88V and an amine oxidation potential of -1.1V. The wavelength of the zero-zero transition is 492.5, resulting in a free energy change, ΔG_{ET}, of -12.4 kcal/mol. This is significantly higher than the value for AB (-0.83 kcal/mol). Using the method of Rehm and Weller to calculate the electron transfer rate from (Equation 3.58), $k_{ET} = 1.3 \times 10^{10}$ sec^{-1}. This same equation predicted the electron transfer rate to be 2.31×10^{9} sec^{-1} for AB. This equation uses empirical data from intermolecular electron transfer, and is therefore not ideal for our intramolecular case. However, the Marcus equation for electron transfer (Equation 3.54) requires a value for the inner-sphere reorganizational energy as well as the frequency factor to calculate an electron transfer rate. Use of the Rehm Weller equation may not be able to provide exact values, but it may likely show trends in electron transfer rates with only the prior knowledge of electrochemical data.

The rate of electron transfer calculated from the measured fluorescence lifetimes of COB is 8.54×10^{8} sec^{-1}. This is on the order of the transfer rate measured for AB in 67% MeOH and 33% PBS (2.95×10^{8} sec^{-1}), although slightly higher.

6.1.5 Summary

Although the relative intensity shows a switching fraction of 0.6 with approximately 2000 mg/dL glucose, the lifetime data falls short with a switching fraction of 0.2. The lifetime values are short (1.1 nsec and 0.57 nsec) requiring higher modulation frequencies to be used when measuring a change in phase as a function of glucose. The electron transfer rate does not offer any insight into why the lifetime data does not agree

with the steady state. However, perhaps the large difference in ΔG_{ET} for COB and AB is the reason for the difference in the behavior of these two molecules. Although preliminary measurements of COB do not display the same magnitude of lifetime changes as seen with AB, a change due to glucose concentration was measured. This is a good step toward the creation of a longer wavelength sensor molecule.

6.2 Naphthylimide Boronate (NIB-2T)

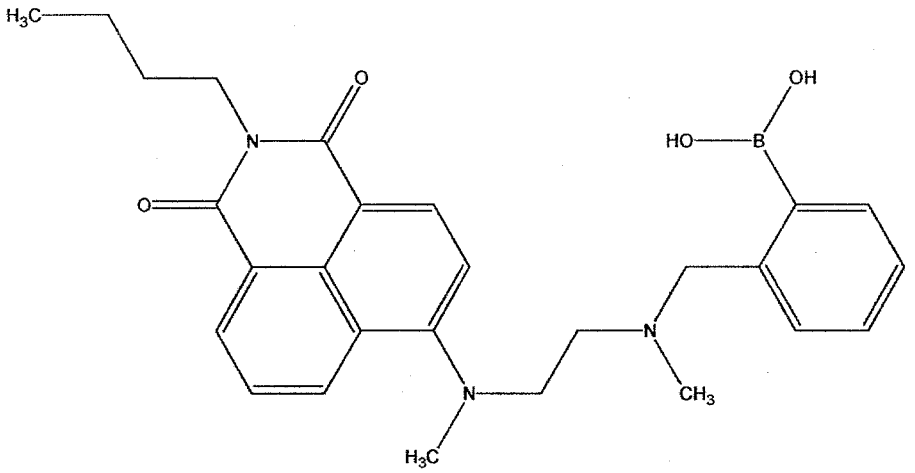

6.2.1 Relevance

NIB-2T, was chosen as a potential sensor candidate from previous electrochemical and fluorescence studies of napthylimides in the literature. (Borzenko, 1995; Borzendo, 1993; Pardo, 1990) Napthylimides were shown to be soluble in water and to have their fluorescence quenched by PET, making it a good candidate for our sensor design. (Biczók, 1999; Martin, 1998; Martin, 1996).

6.2.2 Steady State Measurements

The measurements of NIB-2T were done with a solvent of 100% PBS. However, 30uL of methanol was present from the stock solution of NIB-2T. Steady state data show the excitation peak at 425 nm, and the emission peak at 538 nm (Figure 6.5).

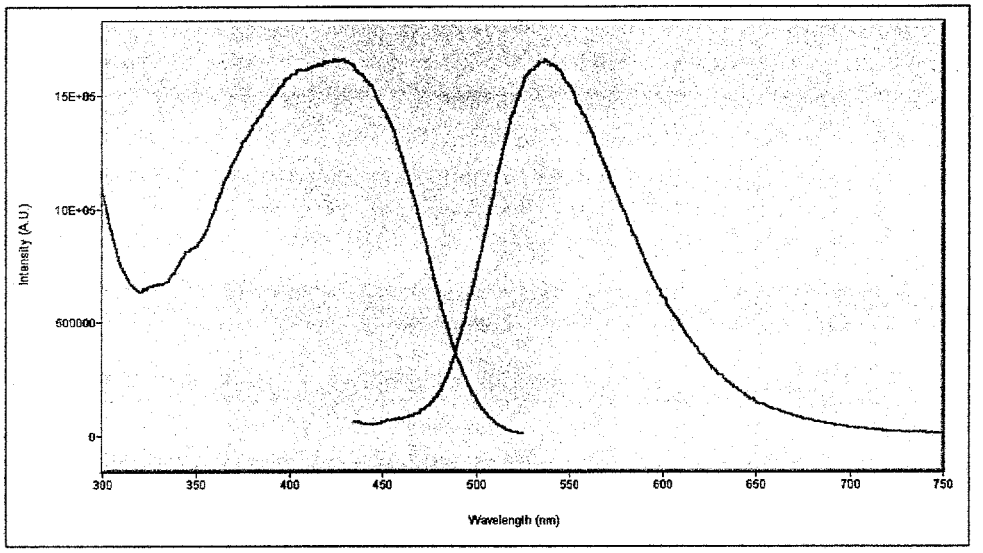

Figure 6.5- Excitation and emission spectra of NIB-2T in 100% PBS.

Measurements were made at glucose concentrations of 0 mg/dL and 1858 mg/dL. The switching fraction is 0.41 with the addition of 1858 mg/dL glucose.

6.2.3 Lifetime Measurements

Fluorescence lifetime measurements (Figure 6.6) were made with an excitation wavelength of 425 nm. The fluorescence was collected with a 500 nm high pass filter (Schott KV500).

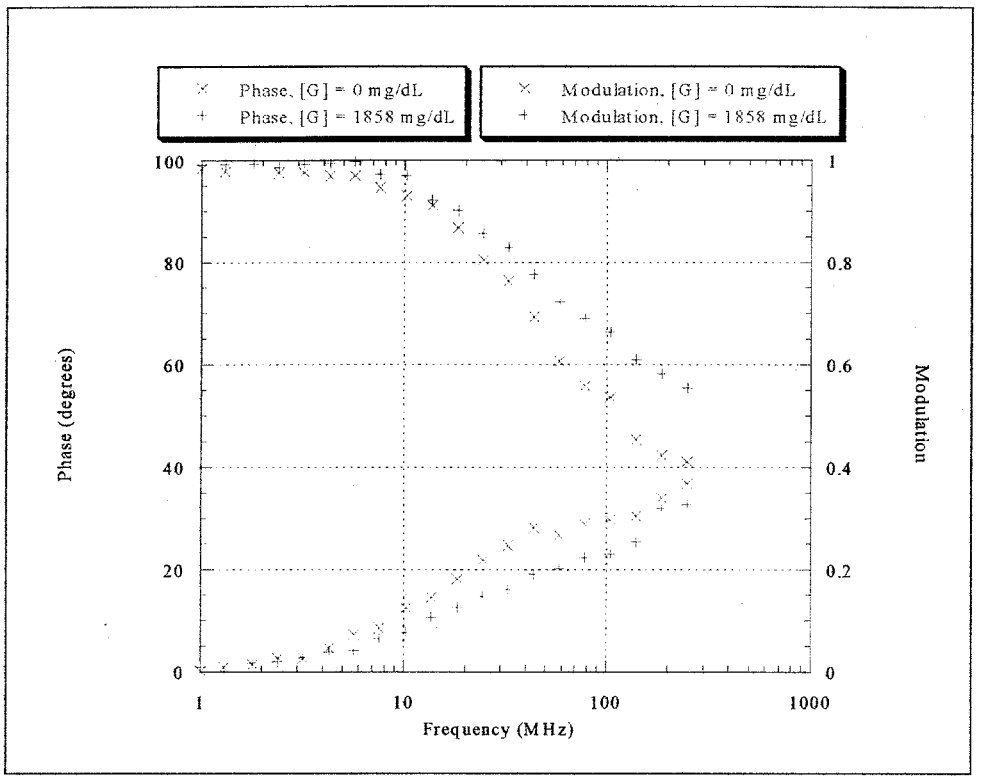

Figure 6.6 - Phase and modulation curves for NIB-2T. The addition of 1858 mg/dL of glucose pushes the curves to the outside.

As with COB, the data sets were linked together so that the lifetime values did not change with glucose while the pre-exponential factors varied. A double exponential fit was found for NIB-2T. The lifetimes values are $\tau_1 = 5.6$ nsec, and $\tau_2 = 0.43$ nsec. The pre-exponential factors (Figure 6.7) change slightly with glucose concentration.

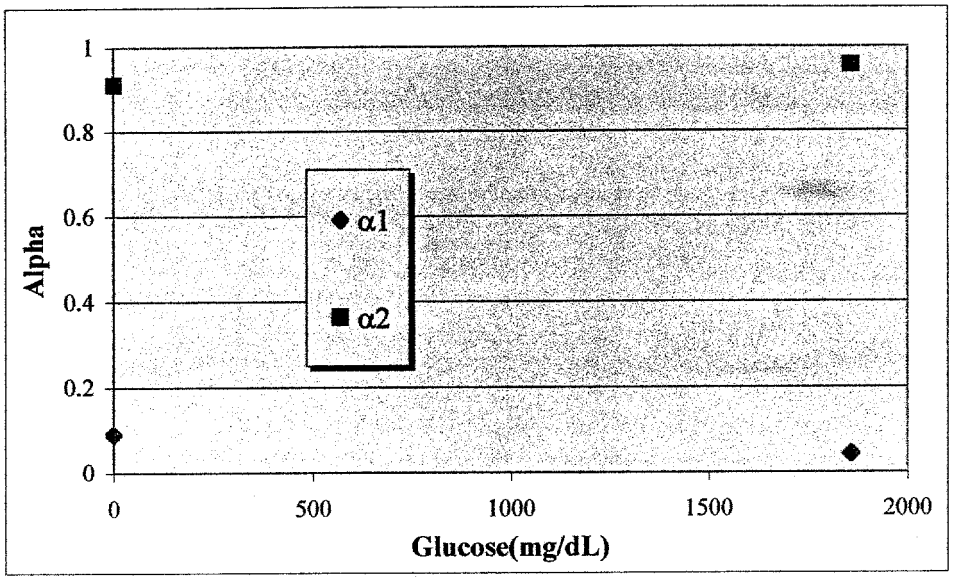

Figure 6.7 - Pre-exponential components for NIB-2T, with and without glucose.

The amount of the long lifetime component (α_1) decreases with glucose, while the short lifetime increases. This results in the average lifetime decreasing from 3.34 nsec without glucose to 2.34 nsec with glucose. Therefore, the lifetime values predict a decrease in relative fluorescence intensity with increasing glucose concentration (SF = -0.27). However, steady state fluorescence measurements show an increase of fluorescence intensity with glucose (SF = 0.41).

6.2.4 Summary

The reason behind the discrepancy between the steady state data and lifetime data is unclear. It could not be the result of something such as energy transfer or solubility because both steady state and lifetime would be effected. In the following section a

molecule similar to NIB-2T is examined and an explaination for the discrepancy is suggested.

6.3 NIB-B-2S

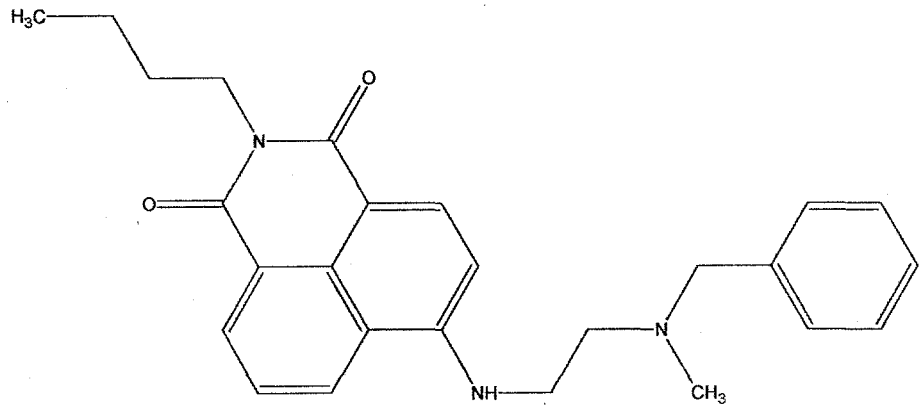

6.3.1 Relevance

After discovering that lifetime data for NIB disagreed with the steady state results, a new molecule without the boronic acid was synthesized. NIB-B-2S is similar to NIB-2T, but with a secondary (rather than tertiary) amine, and no boronic acid. The fluorescence excitation and emission spectra (Figure 6.8) of NIB-B-2S is similar to that of NIB-2T. The fluorescence excitation wavelength is 434 nm and the emission wavelength is 524 nm for NIB-B-2S.

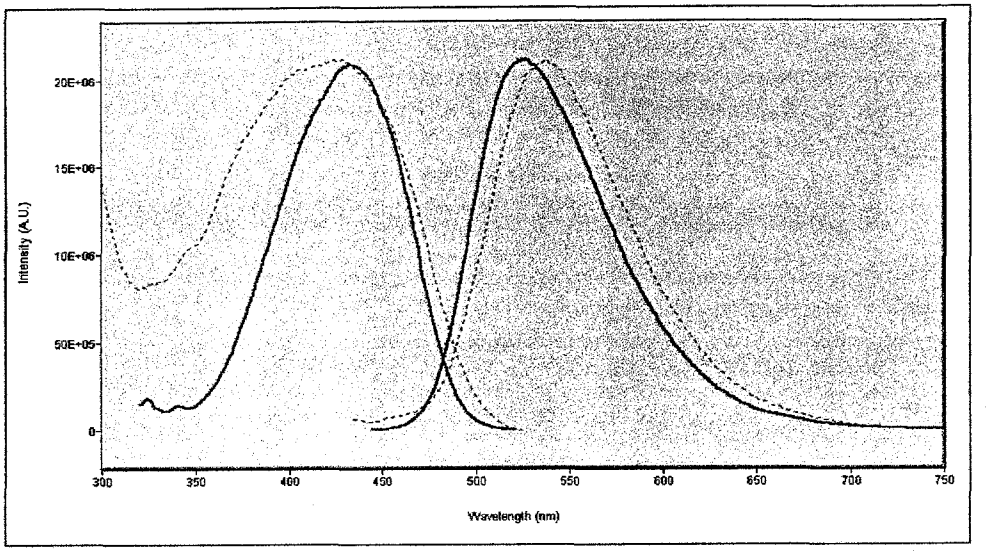

Figure 6.8 - Excitation and emission spectra of NIB-B-2S (solid) and NIB-2T (dashed) in PBS. Intensities have been normalized.

Because NIB-B-2S lacks the boronic acid necessary for binding with glucose, its fluorescence properties were examined by varying the pH.

6.3.2 Steady State Measurements

NIB-B-2S was tested in aqueous solutions at pH 2, 7.4 and 12.5. First NIB-B-2S was added to a solution PBS, then HCl was added to decrease the pH and NaOH was added to increase it. Litmus paper was used to measure the pH values.

Spectra of NIB-B-2S at pH 2 look similar to that of pH 7.4, however the excitation and emission spectra red shifts at pH 12.5. The excitation peak shifts from 434 nm at pH 7.4 to 450 nm at pH 12.5, while the emission peak shifts from 524 nm to 546 nm. (Figure 6.9)

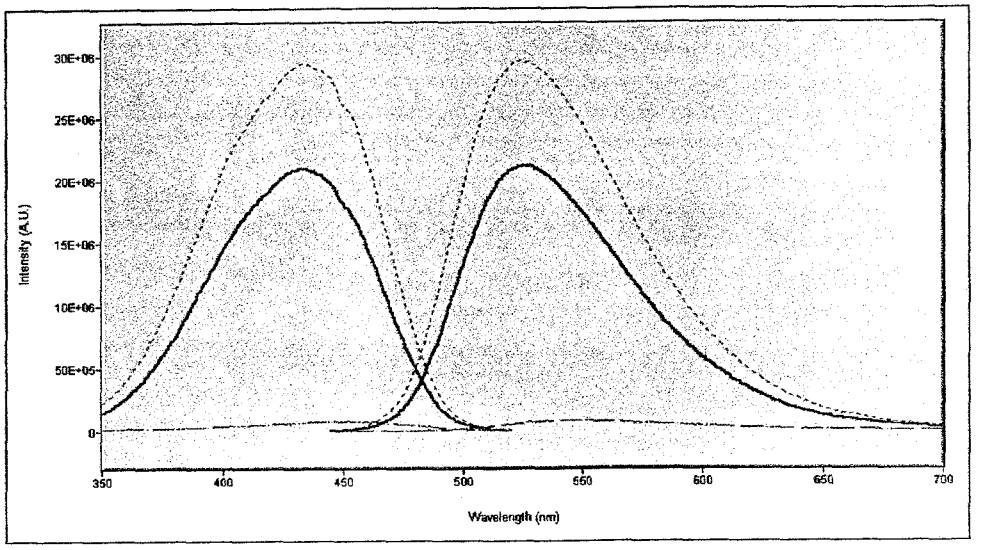

Figure 6.9 - Excitation and emission spectra for NIB-B-2S in aqueous solutions at pH 2 (dashed), pH 7.4 (solid), and pH 12.5 (dotted).

The relative intensity increased from unity at pH 12.5 to approximately 25 at pH 7.4 and then to approximately 36 at pH 2. This translates into a switching fraction of 35 over the pH range measured.

6.3.3 Lifetime Measurements

The fluorescence lifetimes were measured (Figure 6.10) in aqueous solutions at pH 2, 7.4 and 12.

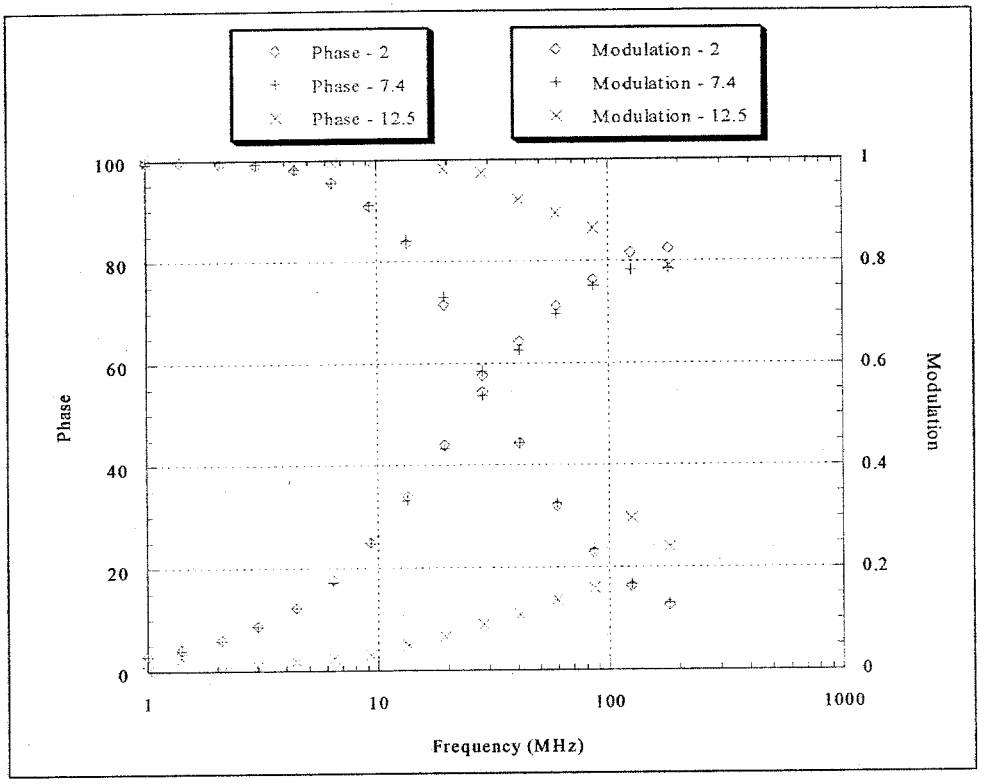

Figure 6.10 – Phase and modulation curves for NIB-B-2S at pH 2, 7.4, and 12.5. Curves at pH 2 and 7.4 are almost identical, while curves at pH 12.5 never cross.

Measurements of the lifetime values confirm an increase in the relative intensity, rather than a decrease as seen with NIB-2T. However, the increase calculated from lifetime measurements is less than measured with steady state fluorescence. Also, the lifetimes (Figure 6.11) are longer (8 nsec, and ~1 nsec) than those measured for NIB-2T (5.6 nsec, and 0.43 nsec).

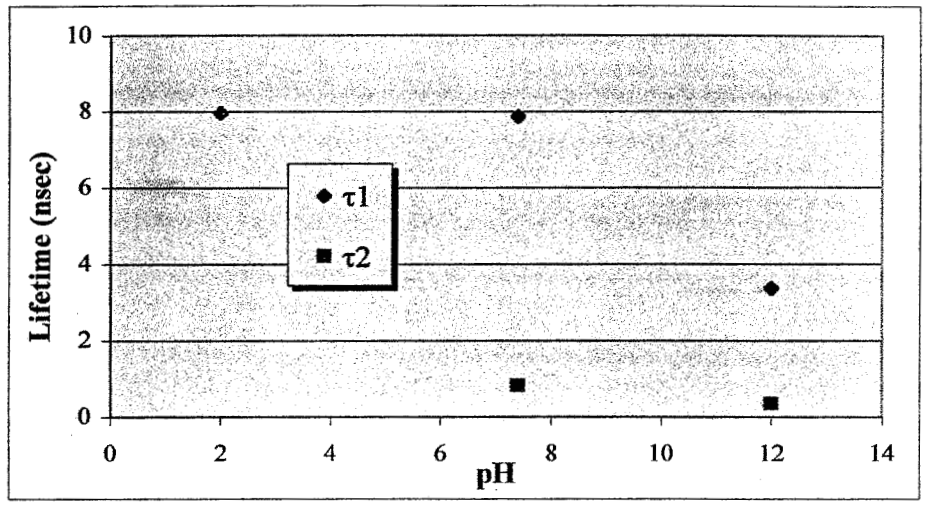

Figure 6.11 - Lifetimes of NIB-B-2S for pH 2, 7.4 and 12.5 (aqueous solutions).

The pre-exponential components (Figure 6.12) vary in a manner consistant with a two component model similar to MAMA.

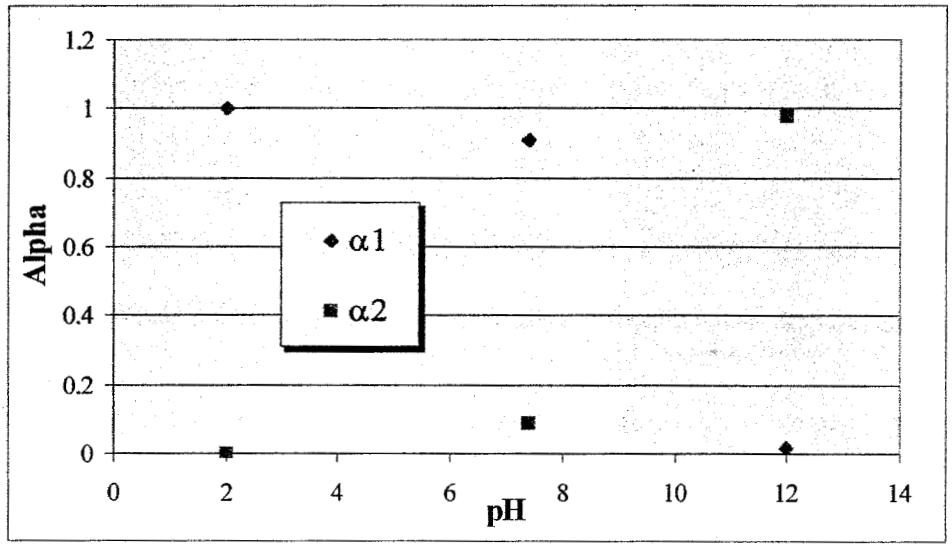

Figure 6.12 - Alpha values for NIB-B-2S in aqueous solutions at pH 2, 7.4 and 12.5.

The switching fraction calculated from lifetime data is 17 from pH 12.5 to pH 2, while the switching fraction from steady state fluorescence is 35.

6.3.4 Interconversion

One possible explanation for the inconsistency between the measured lifetimes of NIB-B (2105) and the relative intensity is based on the interconversion between two fluorescing states. The two fluorescing states are protonated NIB-B (NIB-BP) and unprotonated NIB-B. The diagram in Figure 6.13 describes this system.

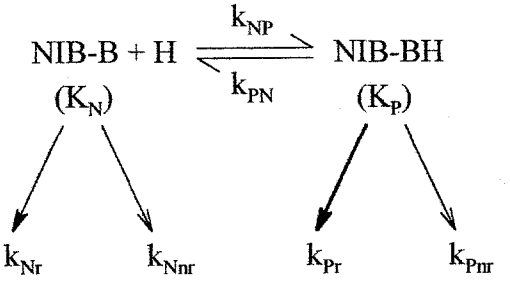

Figure 6.13 - Scheme depicting two interconverting states, both with fluorescent decay.

where $K_{N,P}$ are the decay rates of the two states, k_{Nr} and k_{Pr} are the radiative decay rates, and k_{Nnr} and k_{Pnr} are the non-radiative decay rates. The populations of each state can be described by

$$\frac{dN_N}{dt} = -\Gamma_N N_N + k_{PN} N_P \qquad 6.2$$

and

$$\frac{dN_P}{dt} = -\Gamma_P N_P + k_{NP} N_N \qquad 6.3$$

where N_N and N_P are the populations of NIB-B and NIB-BH, respectively. Γ_N and Γ_P are defined as the sum of the decay rate and the rate of converstion out of that state.

$$\Gamma_N = k_{NP} + K_N \qquad 6.4$$

$$\Gamma_P = k_{PN} + K_P \qquad 6.5$$

The solutions to these equations are:

$$N_N(t) = a_1 e^{-m_1 t} - a_2 e^{-m_2 t} \qquad 6.6$$

and

$$N_P(t) = b_1 e^{-m_1 t} - b_2 e^{-m_2 t} \qquad 6.7$$

where

$$m_{1,2} = \tfrac{1}{2}\left\{\Gamma_N + \Gamma_P \pm \left[\left(\Gamma_N - \Gamma_P\right)^2 + 4k_{NP}k_{PN}\right]^{1/2}\right\} \qquad 6.8$$

$$a_{1,2} = \left[a_0\left(\Gamma_N - m_{2,1}\right) - b_0 k_{PN}\right] / \left(m_1 - m_2\right) \qquad 6.9$$

$$b_{1,2} = \left[b_0\left(\Gamma_P - m_{2,1}\right) - a_0 k_{NP}\right] / \left(m_1 - m_2\right) \qquad 6.10$$

The initial fraction of excited NIB-B molecules is given by a_0 and the initial fraction of excited NIB-BH molecules is b_0. The fluorescence intensity is given by

$$I(t) = AN_N(t) + BN_P(t) \qquad 6.11$$

where A and B are constants dependant upon the wavelength. (Alcala, 1987) For our purposes we will assume that the wavelengths of emission are equal for NIB-B and NIB-BH. *Therefore, A and B will be set equal to one.*

These equations were set up to simulate the measured lifetimes and intensities of NIB-B-2S. Values of interconversion rates, m_1, m_2, a_0, and b_0 were varied and the difference between the resulting α and τ values and experimental values was minimized. The interconversion rate from NIB-B to NIB-BH, k_{NP}, was found to be 31.4 nsec, while the rate of k_{PN} was 8.16 nsec. The ratio of k_{NP} to k_{PN}, defined as K_{eq}, equals 3.85. The values of α (corresponding to a_0) and τ (corresponding to $1/m_1$ and $1/m_2$) in the limit of a slow interconversion (where steady state measurements agree with lifetime measurements) are

τ_1	0.67 nsec
τ_2	27.14 nsec
α_1 (pH 2)	0.1
α_1 (pH 7.4)	0.2
α_1 (pH 12.5)	1.0

Table 6.1 - Values of α and τ in the limit of slow interconversion.

Using these values in Equations 6.2 through 6.11, the apparent, or measured, values for α and τ are calculated.

	pH 2	pH 7.4	pH 12.5
α_1	0.97 (0.98)	0.09 (0.09)	0 (0)
τ_1 (nsec)	0.66 (0.35)	0.66 (0.82)	0.66 (N/A)
τ_2 (nsec)	6.39 (3.36)	6.39 (7.86)	6.39 (7.95)

Table 6.2 - Apparent α and τ values calculated with interconversion between two states. Experimental values are in parentheses.

The calculated apparent lifetime values are constant, and thus do not follow the trend seen in experiment. However, the values predicted for the pre-exponential components are in very good agreement with experiment. Relative intensity values can also be found from the calculated lifetime values.

	R (exp)	R (calc)
pH 12.5	1.0	1.0
pH 7.4	25.4	33.9
pH 2	35.6	37.1

Table 6.3 - Relative intensity values measured from steady state experiments, R (exp), and calculated R (calc).

6.3.5 Summary

The increase in the relative fluorescence intensity of NIB-2T with glucose contradicts the lifetime measurements. This phenomenon was not seen in NIB-B-2S, suggesting that it is a result of the N→B interaction. The disagreement between the relative intensity increase from steady state and lifetime measurements of NIB-B-2S may be due to the protonation and deprotonation occurring on the time scale of the radiative

lifetimes. The theory of interconverting states may also be applied to COB, with a rapid interconversion between COB and COBG (COB with glucose) causing a similar discrepancy in measurements. Future experiments are needed to confirm or reject this theory for both COB and NIB-B-2S. However, if the lifetimes shown in Table 6.1 (27.14 nsec and 0.67 nsec) are the approximate lifetimes of NIB with and without glucose bound, then it potentially has a very high sensitivity to glucose. If the interconversion can be stabilized, then it may be possible to use NIB as the sensor molecule in a transdermally illuminated glucose sensor.

REFERENCES

Alcala, J.R., E.Gratton, and F.G. Prendergast. Fluorescence Lifetime Distributions in Proteins. *Biophys. J.* 51: 597-604, 1987.

Biczók, L., P. Valat, and V. Wintgens. Effect of molecular structure and hydrogen bonding on the fluorescence of hydroxy-substituted naphthalimides. *PCCP (Incorporating Faraday Transactions)* 20: 4759-4766, 1999.

Borzenko, O.V., et al. Electrochemical and Electrochemiluminescence Properties of Naphthalimide Derivatives. *Kharkov Radio and Electronic Engineering Institute, Ministry of Education of the Ukraine*. Translated from *Elektrokhimiya* 29(2): 253-260, 1993.

Borzeko, O.V., A.I. Bykh, and N.N. Rozhitskii. Energetics and Kinetics of Homogeneous Electrochemiluminescent Electron Transfer Reactions in Naphthalimide Solutions. *Russian Journal of Electrochemistry* 32(11): 1273-1278, 1996.

Gray, K. Personal communications, 1999.

Martin, E., R. Weigand, and A. Pardo. Solvent dependence of the inhibition of intramolecular charge-transfer in N-substituted 1,8-naphthalimide derivatives as dye lasers. *J. of Luminescence* 68L 157-164, 1996.

Martin, E. and R. Weigand. A correlation between redox potentials and photophysical behavior of compounds with intramolecular charge transfer: application to N-substituted 1,8-naphthalimide derivatives. *Chemical Physics Letters* 288: 52-58, 1998.

Pardo, A., et al. Double Exponential Fluorescence Decay in the Protonation Equilibrium of 4-Methoxy-N-[2-(1-Pyrrolidin)ethyl]-1,8-Napthalimide]. *J. of Luminescence* 46: 381-385, 1990.

Chapter VII

SUMMARY AND DISCUSSION

Extensive measurements of the fluorescence lifetimes of anthracene boronate have (AB) demonstrated its ability to measure physiological glucose concentrations in solution. For the first time the fluorescence properties and PET mechanism of AB have been characterized as functions of pH, percent methanol in the solvent, and glucose concentration. Based on this new understanding of AB, novel sensor molecules with longer wavelength fluorophores have been synthesized and have demonstrated changes in fluorescence properties with glucose concentration. Research has just begun in the development of a sensor molecule able to measure glucose with sensitivity comparable to AB, yet with the longer fluorescence wavelength desired for *in vivo* use. In the following sections a summary of the measurements made on AB, AB-B and MAMA will be presented along with a discussion of the information learned and suggestions for future research in this area.

7.1 Summary of Measurements – Anthracene Derivatives

In the following section a summary of the measurements made on MAMA, AB-B, and AB will be presented along with discussions on what was learned. Then a correlation between fluorescence and electrochemistry measurements as well as a comparison to Marcus theory (Section 3.4) will be shown. From the understanding of these molecules, suggestions will be made on the direction of further research on glucose sensor molecules.

7.1.1 Summary of pK_a Measurements

Three calculations of pK_a were done for each molecule: 1) using the inflection point of the relative intensity curve, 2) using the Equation 3.35 and the ratio of lifetimes to approximate the quantum yield ratio, and 3) using the pre-exponential components measured with fluorescence lifetime techniques. A comparison of the results is shown in Table 7.1.

	pK_a (Steady State)	**pK_a (Lifetime)**
MAMA (100% Buffer)	8.96, 9.06	9.4
MAMA (50% MeOH)	8.62, 8.56	8.86
AB-B (50% MeOH)	6.44, 6.42	9.21*
AB (50% MeOH)	5.79, 5.55	5.55

Table 7.1 - Summary of pK_a values measured for MAMA, AB-B, and AB. (Inflection point method, and R(calc) using tau ratio) *Should not be considered as the pK_a value due to lack of agreement with steady state data.

The pK_a values of MAMA calculated from steady state fluorescence measurements were lower than the pK_a values found from the pre-exponential factors of the lifetime measurements. This is attributed to the error caused by the small red shift in excitation spectra with pH. As the pH is increased near the pK_a value, the excitation (and emission) peaks shift due to the sharp decrease in the number of protonated (unquenched) molecules with slight differences in spectra. The wavelength of excitation remains constant, causing a small artificial decrease in measured fluorescence intensity.

The pK_a value of MAMA decreases approximately 6% from a solution with 100% PBS to a solution with 50% PBS and 50% MeOH. This is important when extrapolating values from AB (or another sensor molecule) in 50% PBS and 50% MeOH to predict values in 100% PBS. Recall that if the pK_a of a sensor molecule is much greater than 7.4, the sensitivity at pH 7.4 will be zero. The pK_a also decreases as more pieces of AB are added to MAMA (i.e. the phenyl ring and the boronic acid). The pK_a value of AB-B is 28% lower than the pK_a for MAMA, while the pK_a value for AB is 13% lower than the value for AB-B. The decrease in the acidity constant reveals that additional substituents make the amine more basic, causing it to have stronger bonds with protons in solution as well as an increased electron transfer rate as described in the following sections.

In the case of AB-B, the relative intensity as a function of pH measured from steady state fluorescence did not agree with the relative intensity calculated from fluorescence lifetime measurements (Figure 5.17). The exact cause of this is unknown, but it suggests that the phenyl ring causes the molecule to become unstable, rapidly interconverting between two different geometries while in the excited state similar to the phenomenon seen with NIB (Section 6.3.4), but not as pronounced. This "interconversion" would account for the difference in pK_a values measured with fluorescence steady state and lifetime techniques. Measurements of AB, and the agreement between steady state and lifetime pK_a values, suggest the N→B dative bond effectively stabilizes the excited state and eliminates interconversion proposed for AB-B. More experiments need to be performed to confirm or deny this theory. Lifetime measurements at low temperatures could slow the rate of interconversion and possibly shed light on the discrepancy.

7.1.2 Summary of Fluorescence Measurements

Fluorescence lifetime measurements for MAMA, AB-B and AB in PBS and methanol (1:1 by volume) are summarized in Table 7.2.

	Solvent	τ (nsec)	τ_{avg} (nsec)	k_{ET} (10^9 sec^{-1})
MAMA	PBS	10.85	10.85	--
	PBS:MeOH (1:1)	9.69, 0.28	9.61	3.47
	0.1M TBAP/ACN	4.63, 0.16	2.10	5.92
AB-B	PBS:MeOH (1:1)	11.27, 0.33	10.52	2.91
	0.1M TBAP/ACN	14.21,1.06	9.08	0.87
AB	PBS:MeOH (1:1)	11.15, 3.17, 0.61	7.54	0.23
	0.1M TBAP/ACN	6.34,1.76	2.56	0.41

Table 7.2 - Summary of lifetime measurements at pH 7.4 in PBS:MeOH (1:1 by volume).

Due to the aprotic nature of TBAP/ACN, or its inability to donate protons, lifetime values in this solvent are similar to lifetime values in a solution with pH 14. Therefore, the average lifetime values in TBAP/ACN are shorter than in PBS:MeOH (pH 7.4) due to the large number of molecules with the fluorescence being quenched by PET. The overall trend in electron transfer rates is similar in both PBS:MeOH and TBAP/ACN: $k_{ET}(MAMA) < k_{ET}(AB\text{-}B) < k_{ET}(AB)$. This supports the previous statement linking the trend in pK_a to the trend in electron transfer rate due to the acidity of the amine. An increased PET rate would be caused by an increase in the electron orbital overlap along the path of electron transfer. A larger electron orbital from the lone pair on the amine translates into a decreased acidity, or pK_a. Therefore, from a measurement of the pK_a

trend in a group (with a progression similar to MAMA, AB-B and AB) of potential longer wavelength sensor fluorophores correlates to the changes in electron transfer rates.

A measurement that did not match the expected theory was the fluorescence lifetime measurement of AB. AB was expected to have two lifetime components, one from the fluorescence quenched by PET and one from the fluorescence with no PET. However, a third fluorescence lifetime component was measured to be approximately 0.34 nsec. The short lifetime value indicates a fast, efficient quenching of the fluorescence through PET possibly due to ABOH and AB in a similar geometry where the N→B bond has been broken. However, the amount of this component is less than half of any other fluorescent component, except at pH values greater than 10, and does not change significantly with glucose concentration. Additionally, the small value of the lifetime indicates that its contribution to the average lifetime value is negligible in the measurement of glucose. In the future, NMR measurements made in high (>10) pH solutions, where the pre-exponential factor of the third lifetime component increases, might confirm the third component and suggest possible geometric configurations.

7.1.3 Summary of Electrochemical Measurements

Electrochemical measurements were made to provide insight into the energetics of the electron transfer process.

	$E^0(D/D^+)$ (±0.5)	$E^0(A^-/A)$ (±0.5)	E_{00} (±1 nm)	ΔG_{ET} (±1.0)
MAMA	15.5	-55.3	73.6	-2.8
AB-B	16.8	-53.0	72.7	-2.8
AB	19.8	-53.0	73.7	-0.8

Table 7.3 - Summary of electrochemical measurements.

All values in kcal/mol, solutions are 0.1 TBAP/ACN.

The most apparent trend in Table 7.3 is the increase in the oxidation potential of the amine ($E^0(D/D^+)$) from MAMA to AB-B to AB while the reduction potential of anthracene ($E^0(A^-/A)$) remains relatively constant. This suggests the electron transfer rate (shown in the previous section) is faster in MAMA than in AB because it takes less applied voltage to remove an electron, which follows logic. In the next section the correlation between $E^0(D/D^+)$ and k_{ET}, calculated from fluorescence lifetime measurements, will be investigated.

7.1.4 Correlation between Electrochemistry and Fluorescence Lifetimes

Measurements of intramolecular quenching rates of nucleic acids and coumarin 120 conjugates were shown to correlate with free energy values as predicted in Marcus theory. (Seidel,1991) MAMA, AB-B and AB also show a correlation between electron transfer rate and free energy, as well as agreement with Marcus theory (Figure 7.1). Recall from Chapter Three, the rate of electron transfer (k_{ET}) is related to the energy barrier ($\Delta G_{ET}^{\neq}$) as $k_{ET} \propto Exp(-\Delta G_{ET}^{\neq} / RT)$ where $-\Delta G_{ET}^{\neq}$ is given by Equation 3.54.

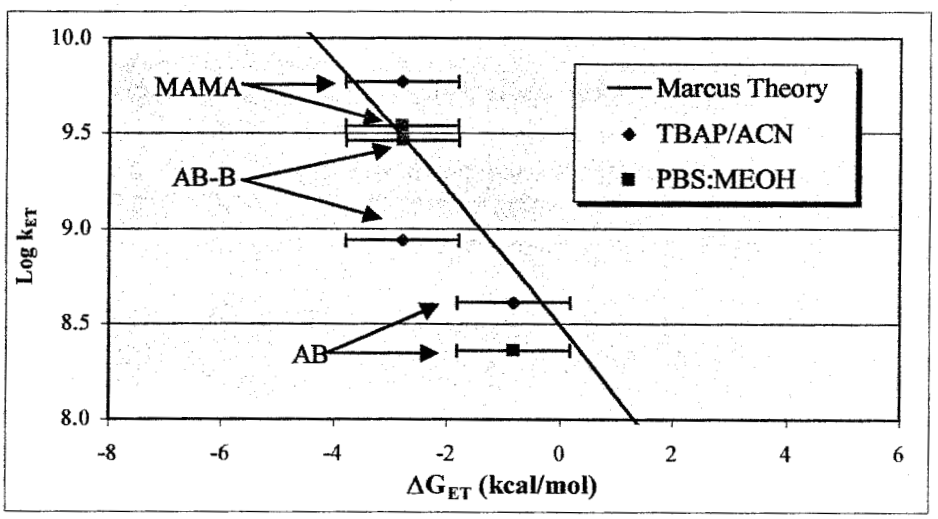

Figure 7.1 - Electron transfer rates versus the free energy of electron transfer.

Although the correlation between ΔG_{ET} and Log k_{ET} agrees well with Marcus theory, perhaps a more simple comparison can be made between the amine oxidation potential and the electron transfer rate. Figure 7.2 shows the correlation between $E^0(D/D^+)$ and Log k_{ET}. The amine oxidation potential, because it is only one measurement, unlike the free energy, which is a combination of multiple measurements, has a smaller margin of error.

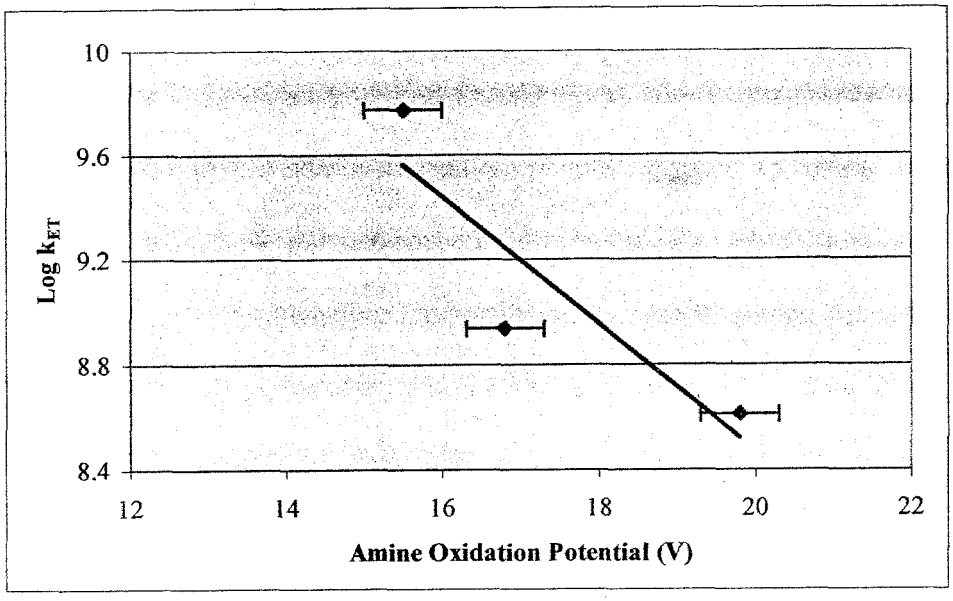

Figure 7.2 – Electron transfer rates versus amine oxidation potential.

More experiments need to be done to support or refute the use of the amine oxidation potential instead of the free energy of electron transfer as a means of predicting the success of a new sensor molecule.

7.2 Conclusion

7.2.1 Summary

Fluorescence lifetime and steady state measurements of MAMA and AB-B were made to understand the individual contributions from the components of AB (i.e. steric effects of the phenyl ring, and changes in PET rate with the N→B dative bond). MAMA showed the interaction between the fluorophore (electron acceptor) and the amine (electron donor). The phenyl ring of AB-B suggested directions in the trends of the pKa, lifetime values, and electron transfer rate without the added complication of the N→B

interaction. Finally, all of the pieces were put together and additional fluorescence steady state and lifetime measurements created a comprehensive picture of the original glucose sensor molecule, AB, as a function of pH, percent methanol in the solvent, as well as glucose concentration. Table 7.4 lists the measurements made for each molecule and whether the results are supported by theory.

Measurement	MAMA	AB-B	AB
Relative Fluorescence Intensity vs. pH (Steady-State)	X	X	X
Relative Fluorescence Intensity vs. Solvent (Steady-State)	X	X	-
Switching Fraction with Glucose	N/A	N/A	X
Relative Fluorescence Intensity vs. pH (Lifetime)	X	*	X
Fluorescence Lifetimes vs. pH	X	X	*
Fluorescence Lifetimes vs. Solvent	X	X	-
Fluorescence Lifetimes in ACN	X	X	X
Lifetime Change with Glucose	N/A	N/A	X
Electron Transfer Rate (Lifetime)	X	X	X
Electron Transfer Rate (Electrochemistry)	X	X	X

Table 7.4 - Summary of values measured for MAMA, AB-B, and AB. "X" indicates that measurement is explained by theory, and "*" indicates a lack of agreement with theory.

In most cases measurements agreed well with the expected theory. For the first time an in depth analysis of the fluorescence properties, both steady state and lifetime

have been completed on MAMA, AB-B, and AB. Characterization of the fluorescence over a range of pH values provided insight into the N→B interaction in AB, as well as evidence for 28% of molecules having enhanced N→B bonds where PET does not occur. These molecules are unable to change fluorescence properties with pH or glucose and therefore decrease the sensitivity of the sensor. Trends of decreasing pK_a, decreasing electron transfer rates, and increasing amine oxidation potential with the addition of the phenyl ring and the boronic acid were also discovered. These trends should be useful in identifying and evaluating new sensor molecules by predicting how a pK_a will change when components (i.e. boronic acid) are added to a potential sensor fluorophore. Using electrochemistry measurements on potential fluorophores, two novel sensor molecules were selected, synthesized and tested. COB and NIB have the potential for sensing glucose with the same mechanism as AB, yet with longer excitation and emission wavelengths. Initial measurements show these molecules to be less effective at sensing glucose than AB. Their steady state fluorescence intensity changed significantly with glucose concentration, however, their average fluorescence lifetime changed only slightly. Unfortunately, the amount of change in fluorescence lifetimes measured initially is not adequate for a glucose sensor. One possible reason for this is the rapid interconversion in the excited state. COB and NIB may be optimized to eliminate this, perhaps through the addition of certain stabilizing constituents. Another option may be to use the approach under investigation by Lakowicz, which uses a long lifetime fluorophore (that lacks glucose sensitivity) to change the average lifetime of the entire sensor and enhance the small change in sensor molecule lifetime.

7.2.2 Future Work

Using the knowledge gained from measurements of MAMA, AB-B, AB, COB and NIB, new sensor molecules should be synthesized. However, to avoid the problems seen with NIB and COB, more research should be done to understand why these two potential sensor molecules did not change their fluorescence lifetimes as predicted. They were chosen based on the similarity of the reduction potential of the new fluorophore and that of anthracene. Perhaps the amine oxidation potential is more important to the efficiency of the switching via PET. To understand how COB and NIB function, the pK_a as well as the fluorescence lifetimes in acetonitrile should be measured and compared to AB data. It may also be possible to adjust the THC of the boron atom by changing the constituents on the amine, thereby changing the N→B interaction and increasing the sensitivity to glucose.

REFERENCES

Seidel, C. Nucleic Acid Base Specific Quenching of a Coumarin-120-Derivative in Nucleotid-Conjugates – Photoinduced Electron Transfer? *SPIE Biomolecular Spectroscopy II* 1432: 91-104, 1991.

Appendix A

Frequency Domain Fluorescence Equations

Consider a light source with a sinusoidally modulated amplitude of the form

$$I(t) = a + b\sin\omega t \qquad \text{A-1}$$

where ω is the frequency of amplitude modulation. For an impulse (δ (t)) excitation the fluorescence decays exponentially in time as

$$f(t) = f_0 e^{-t/\tau} \qquad \text{A-2}$$

where τ is the lifetime of the excited state. Therefore, with sinusoidal excitation the fluorescence intensity is the correlation of Equations A-1 and A-2.

$$\begin{aligned} F(t) &= \int_0^t I(t')f(t-t')dt' \\ &= \int_0^t (a + b\sin\omega t')(f_0 e^{-(t-t')/\tau})dt' \\ &= af_0\int_0^t e^{-(t-t')/\tau}dt' + bf_0\int_0^t (\sin\omega t')e^{-(t-t')/\tau}dt' \end{aligned} \qquad \text{A-3}$$

Integrating Equation A-3 using

$$\int e^{Ax}\sin(Bx)dx = e^{Ax}\frac{[A\sin(Bx) - B\cos(Bx)]}{A^2 + B^2} \qquad \text{A-4}$$

results in the following equation for F(t).

$$\begin{aligned} F(t) &= af_0 e^{-t/\tau}[\tau e^{t'/\tau}]_0^t + bf_o e^{-t/\tau}[\frac{\tau e^{t'/\tau}(\sin\omega t' - \omega\tau\cos\omega t')}{1+\omega^2\tau^2}]_0^t \\ &= af_0\tau - af_0\tau e^{-t/\tau} + \frac{bf_0\tau(\sin\omega t - \omega\tau\cos\omega t)}{1+\omega^2\tau^2} + \frac{bf_0\omega\tau^2 e^{-t/\tau}}{1+\omega^2\tau^2} \end{aligned} \qquad \text{A-5}$$

Since the measurements are taken over times much greater than the average fluorescent lifetime ($t >> \tau$), the transient terms go to zero.

$$F(t >> \tau) = af_0\tau + \frac{bf_0\tau(\sin\omega t - \omega\tau\cos\omega t)}{1+\omega^2\tau^2} \quad \text{A-6}$$

Assuming the fluorescence is of the form

$$F(t) = A + B\sin(\omega t - \phi) \quad \text{A-7}$$

use of the trigonometric relation

$$\sin(\omega t - \phi) = \sin\omega t\cos\phi - \cos\omega t\sin\phi \quad \text{A-8}$$

allows for a direct comparison between Equations A-6 and A-7. This yields expressions for the DC and AC amplitudes, A and B.

$$A = af_0\tau \quad \text{A-9}$$

$$B = \frac{bf_0\tau}{\sqrt{1+\omega^2\tau^2}} \quad \text{A-10}$$

B is chosen with the square root such that

$$\cos\phi = \frac{1}{\sqrt{1+\omega^2\tau^2}} \quad \text{and} \quad \sin\phi = \frac{\omega\tau}{\sqrt{1+\omega^2\tau^2}} \quad \text{A-11}$$

These equations are well behaved in the limit of large ω, with cos $\phi \rightarrow 0$ and sin $\phi \rightarrow 1$, or in other words, $\phi \rightarrow 90°$. Note that if B had been chosen equal to $bf_0\tau$, both cos ϕ and sin ϕ go to zero at large ω.

Using the canonical definition for m, the modulation factor, the standard equations for the phase and modulation of a single exponential lifetime can be written using Equations A-9 and A-10.

$$m \equiv \frac{B/A}{b/a} = \frac{1}{\sqrt{1+\omega^2\tau^2}} \quad \text{A-12}$$

$$\tan\phi = \omega\tau \quad \text{A-13}$$

Appendix B

Error Analysis of Frequency Domain Measurements

Unlike error analysis in the time domain, the error of the lifetime measured in the frequency domain is not a simple function of the number of photons counted over time. (Beecham, 1998) The Globals Unlimited (GU) software program from the University of Illinois was used to calculate the error in the fluorescence lifetime measurements. GU employs three different methods for determining the errors. The first method uses the curvature matrix to estimate the error. This method was chosen for these experiments because it was typically the largest of the three errors. The second fixes all of the variable parameters except one, which it varies until the χ^2 value increases by a certain percentage (typically 67%). The third method holds one parameter fixed while varying all others until the χ^2 value is minimized. This is useful for determining if the fit has reached a global or a local minimum because the χ^2 values are plotted as a function of each fixed parameter in what is referred to as chi-squared plots (see Appendix C).

Recall from Chapter Four that the equation for χ^2 is given by

$$\chi^2 = \sum_{i=1}^{n} \frac{(data_i - fit_i)^2}{\sigma_i^2 (N - m - 1)} \qquad \text{B-1}$$

where σ_i is the standard deviation for each data point measured, N is the total number of data points, and m is number of fitting parameters. Experimental data points are represented as $data_i$ and values from the exponential fits are represented as fit_i. The least-squares fit is obtained by using a method developed by Marquardt (1963) and Levenberg

(1944). The user inputs an initial guess of the variable parameters (f_i and τ_i) in the exponential equation describing the observed average lifetime,

$$\langle \tau \rangle = \sum_i f_i \tau_i \qquad \text{B-2}$$

described by the initial parameter vector, P^0. Iterations (s) are performed varying the parameter improvement vector (δ) until a minimum χ^2 value is found.

$$\begin{aligned} P^1 &= P^0 + \delta^0 \\ P^2 &= P^1 + \delta^1 \\ &\vdots \\ P^{s+1} &= P^s + \delta^s \end{aligned} \qquad \text{B-3}$$

The vector δ is found by solving the matrix equation

$$\mathbf{C}\delta = \mathbf{B} \qquad \text{B-4}$$

where **C** is the curvature matrix

$$C_{jk} = \sum_{q=1}^{n_{exp}} \sum_{i=1}^{n(q)} \frac{1}{\sigma_{qi}^2} \frac{\partial fit_{qi}}{\partial param_j} \frac{\partial fit_{qi}}{\partial param_k} + \lambda \mathbf{I} \qquad \text{B-5}$$

and **B** is given by

$$B_k = \sum_{q=1}^{n_{exp}} \sum_{i=1}^{n(q)} \frac{(data_{qi} - fit_{qi})^2}{\sigma_{qi}^2} \frac{\partial fit_{qi}}{\partial param_k} \qquad \text{B-6}$$

where $param_j$ and $param_k$ are fitting parameters, λ is a scaling factor, **I** is the identity matrix, and the other symbols are as in equation B-1. The error matrix is found by inverting **C**.

$$\mathbf{E} = \mathbf{C}^{-1} \qquad \text{B-7}$$

The diagonal elements of E are equal to the square of the error for that parameter.

Five data trials (taken consecutively) from AB at pH 7.4 were analyzed using GU, without linking any parameters together. The following error values were obtained from the curvature matrix analysis.

File #	f_1	f_2	f_3	Error in f_1, f_2, f_3	τ_1	Error in τ_1	τ_2	Error in τ_2	τ_3	Error in τ_3	χ^2
1	0.526	0.424	0.050	0.021	11.559	0.261	3.498	0.264	0.875	0.347	0.863
2	0.536	0.423	0.041	0.025	11.571	0.303	3.262	0.310	1.019	0.490	1.000
3	0.589	0.392	0.019	0.011	10.755	0.119	2.897	0.099	0.265	0.358	1.675
4	0.523	0.407	0.070	0.043	11.514	0.45	3.593	0.551	1.137	0.393	1.008
5	0.545	0.404	0.051	0.024	11.243	0.287	3.408	0.265	0.736	0.243	0.835

Table B-1 – Results of GU analysis on individual trials with AB in pH 7.4 methanol and PBS (1:1 by volume).

The lifetime values and fractional contributions are plotted with the individual errors in Figures B-1 and B-2.

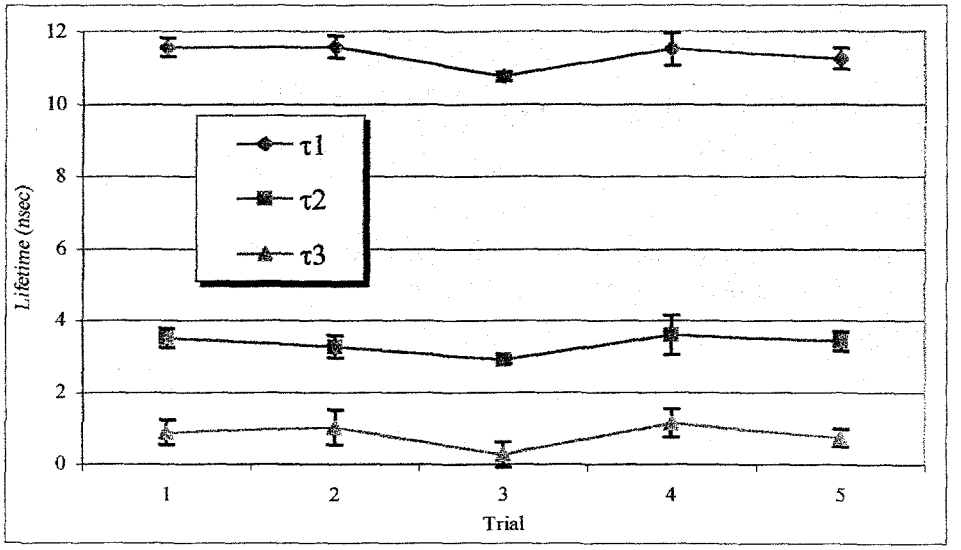

Figure B-1 – Lifetime values (and error) determined without linking trials.

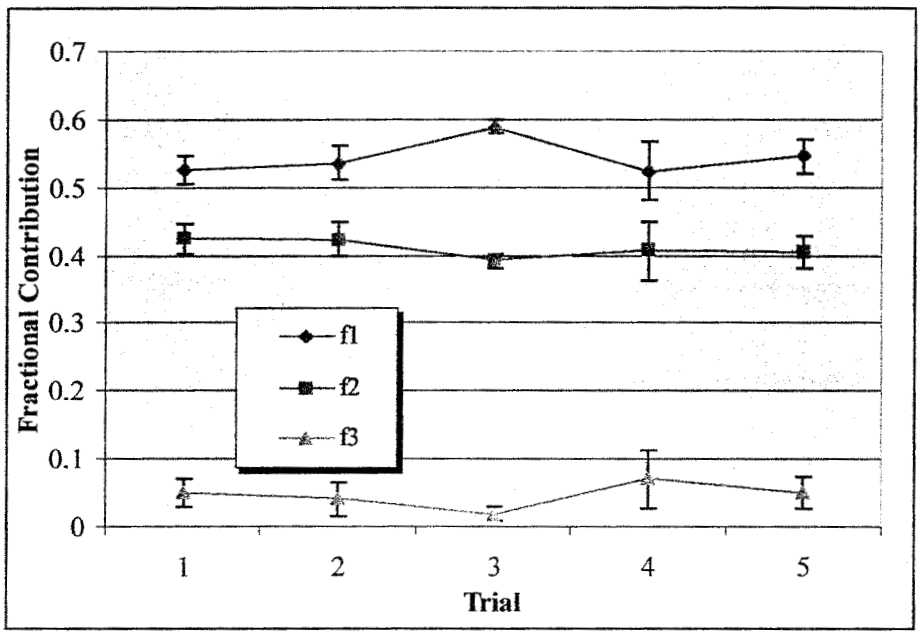

Figure B-2 – Fractional contributions (and error) determined without linking trials.

The five trials were performed in succession on a solution in steady state, and therefore the lifetime values can be linked together. This reduces the number of free variables and increases the total number of measurements at each modulation frequency, thereby reducing the error. The calculated error in the fractional contributions is reduced from an average of 0.025 to 0.009 when the five trials are linked together, yet the values remain approximately the same (Figure B-3).

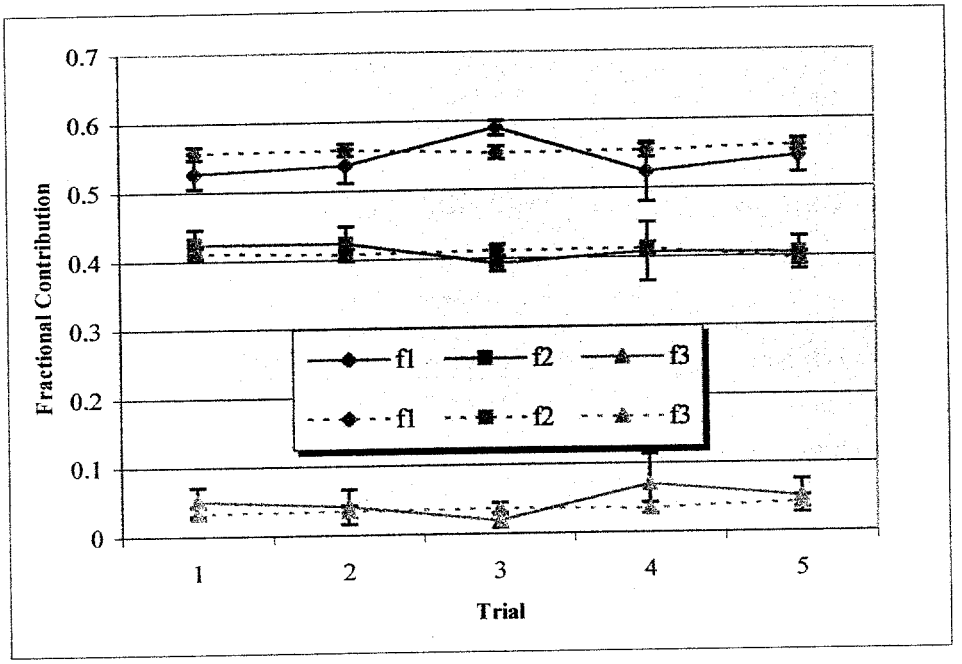

Figure B-3 – Comparison of fractional contributions and errors determined with (dashed lines) and without (solid lines) linking trials.

The lifetime values and corresponding errors are shown in Figure B-4 along with the values and errors found without linking the lifetimes together.

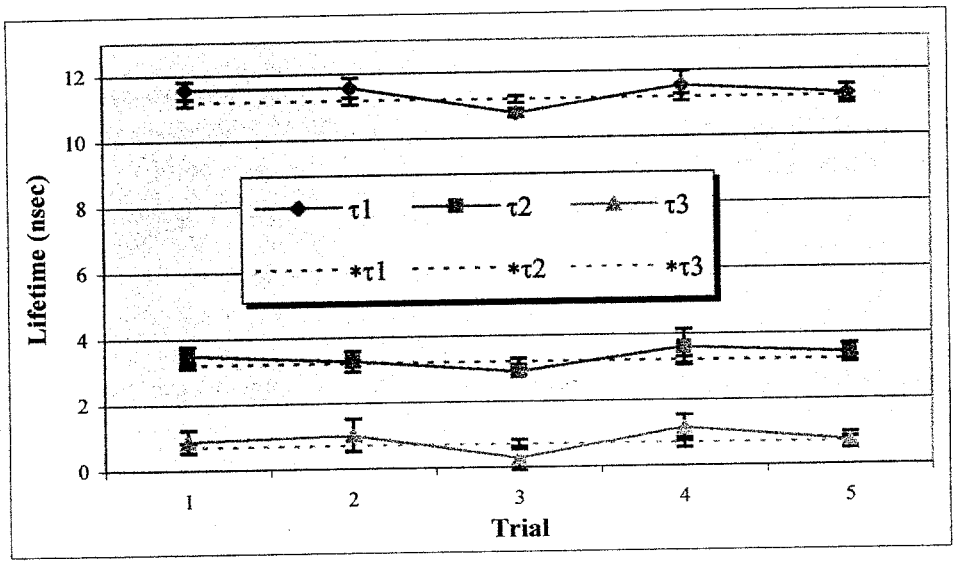

Figure B-4 – Comparison of lifetime values and errors determined with (dashed lines) and without (solid lines w/data points) linking trials.

As seen in Figures B-3 and B-4, the effect of linking the lifetime values is essentially to remove the statistical fluctuations between experimental trials.

REFERENCES

Beechem, J.M., E. Gratton, et al. Globals Unlimited, Technical Reference Manual, Revision 3. Board of Trustees, University of Illinois, 1998.

Appendix C

Example of Data Analysis

In this appendix a step-by-step example of the analysis of fluorescence lifetime measurements taken on AB in 50% methanol and 50% PBS solution (pH = 7.4) will be presented. Five successive trials (Figure C-1) were performed on the same sample held at 25°C.

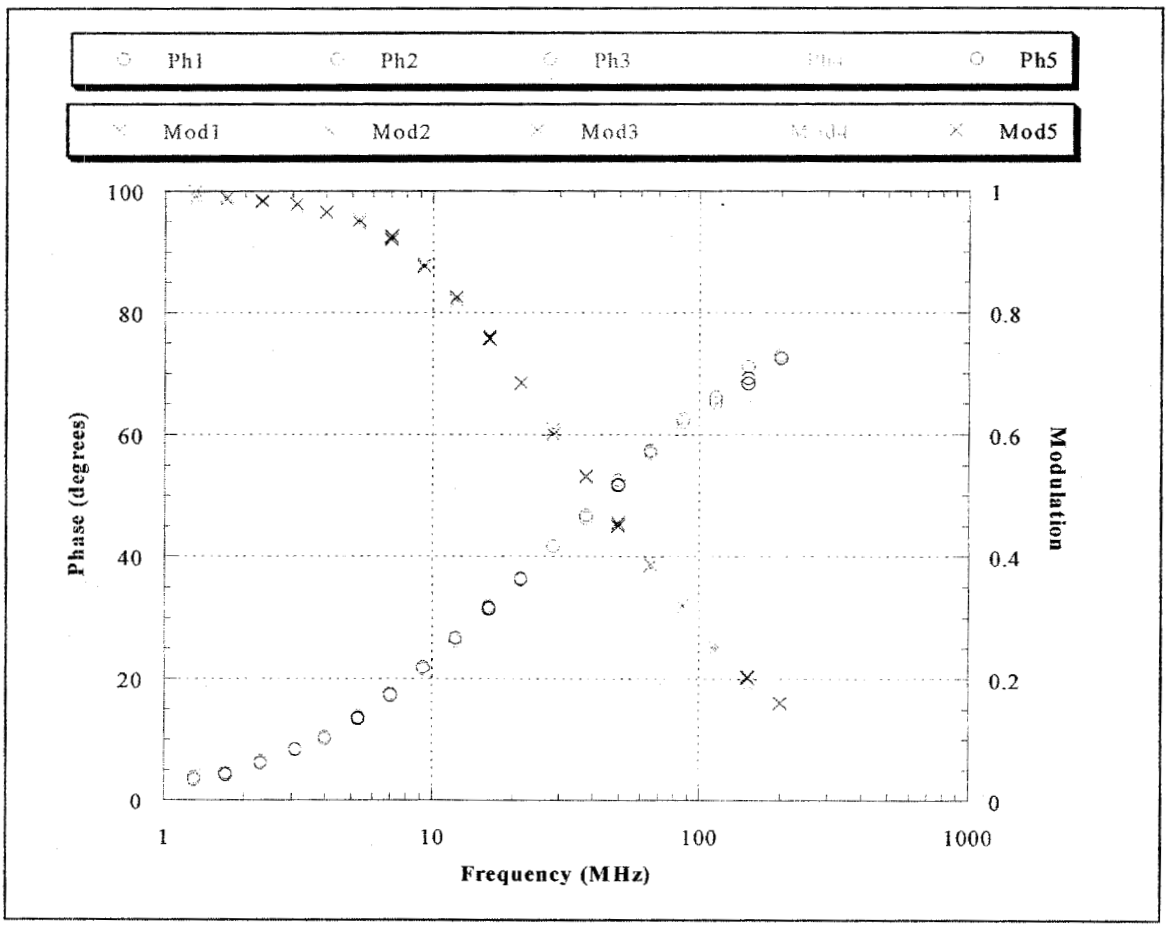

Figure C-1 – Data taken on AB in MeOH:PBS (1:1 by volume).

Globals Unlimited software (Beecham, 1988) was used to analyze the data, linking the lifetime values together. The results of the minimization are shown in Figure C-2.

```
Minimization started at 22 17 26
using Marquardt-Levenberg minimization algorithm

Number of iterations:  5  Global chisquare:    1.231    lamda M= 1.0E-0001

 1->0    life discrete  sas  0.557V  0.559V  0.553V  0.555V  0.561V
 1->0           lifetime  11.159V  11.159L  11.159L  11.159L  11.159L
 2->0    life discrete  sas  0.410V  0.407V  0.411V  0.412V  0.397V
 2->0           lifetime  3.192V  3.192L  3.192L  3.192L  3.192L
 3->0    life discrete  sas  0.032F  0.033F  0.036F  0.034F  0.042F
 3->0           lifetime  0.680V  0.680L  0.680L  0.680L  0.680L

Local chi-square values        0.975   1.428   1.758   0.999   0.975

exit because chisquare in a minimum within 0.00000010 Convergence reached.

Statistics:
Total minimization time =      0.65 sec.  Calls to function =       71
```

Figure C-2 – Screen of Globals Unlimited after running data analysis using a triple exponential decay function.

In Figure C-2, lamda M is the parameter λ described in Appendix B, sas is the fractional contribution to the total fluorescence by that lifetime component. Results from each trial are listed from left to right. If only two lifetimes are used to fit the data, the resulting χ^2 more than doubles (Figure C-3).

```
Minimization started at 22 15 38
using Marquardt-Levenberg minimization algorithm

Number of iterations:  8  Global chisquare:    3.264    lamda M= 1.0E-0006

 1->0    life discrete  sas  0.621V  0.629V  0.623V  0.624V  0.622V
 1->0           lifetime  10.446V  10.446L  10.446L  10.446L  10.446L
 2->0    life discrete  sas  0.379F  0.371F  0.377F  0.376F  0.378F
 2->0           lifetime  2.531V  2.531L  2.531L  2.531L  2.531L

Local chi-square values        2.718   1.906   2.231   1.776   7.658

exit because chisquare in a minimum within 0.00000010 Convergence reached.

Statistics:
Total minimization time =      0.50 sec.  Calls to function =       75
```

Figure C-3 – Screen of Globals Unlimited after running data analysis using a double exponential decay function.

To determine if the analysis is correct, the deviation between the measured values and theoretical values is plotted. A random distribution of errors about zero is desired. A periodic or regular trend in the deviation indicates that either the number of lifetime components is incorrect, or the analysis has found a local minimum. (Atzeni, 1997) The following five plots show the deviation found for each trial (Figures C-4 through C-8).

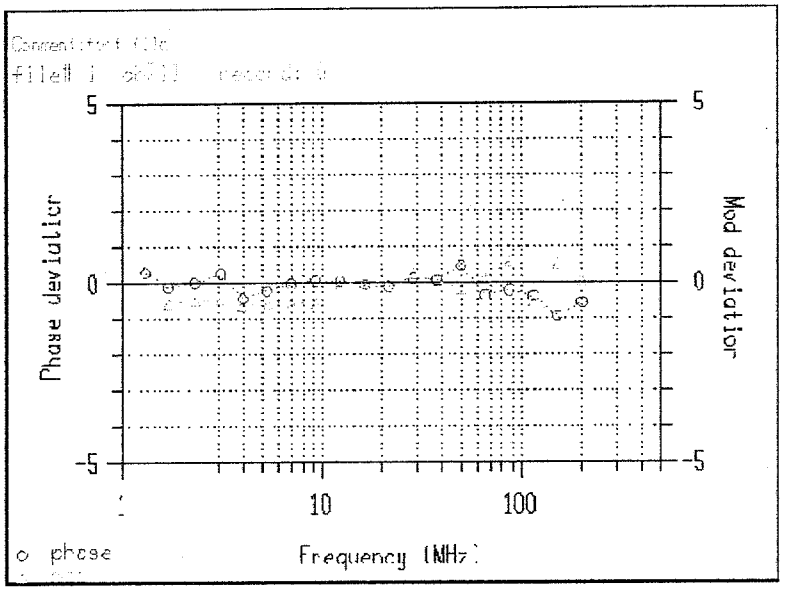

Figure C-4 – Deviation of phase (blue circles) and modulation (green triangles) for trial #1, fitting the data to a triple exponential decay.

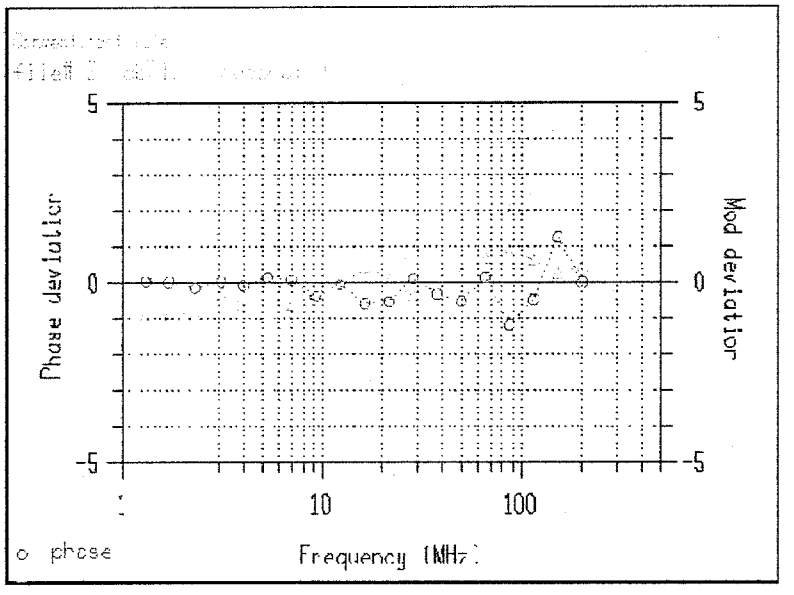

Figure C-5 – Deviation of phase (blue circles) and modulation (green triangles) for trial #2, fitting the data to a triple exponential decay.

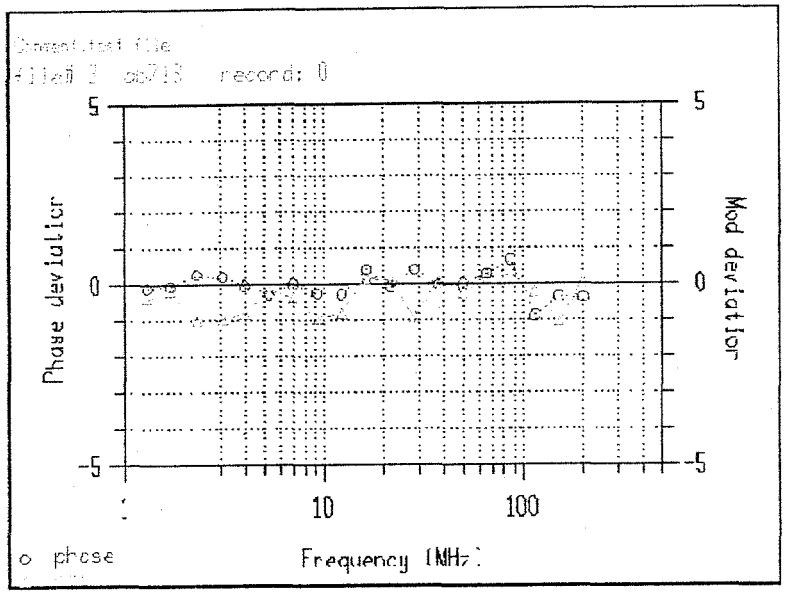

Figure C-6 – Deviation of phase (blue circles) and modulation (green triangles) for trial #3, fitting the data to a triple exponential decay.

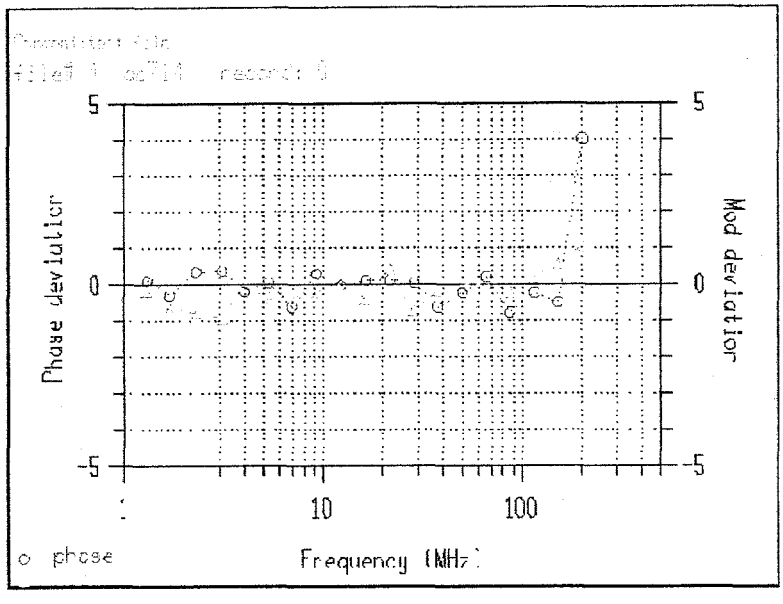

Figure C-7 – Deviation of phase (blue circles) and modulation (green triangles) for trial #4, fitting the data to a triple exponential decay.

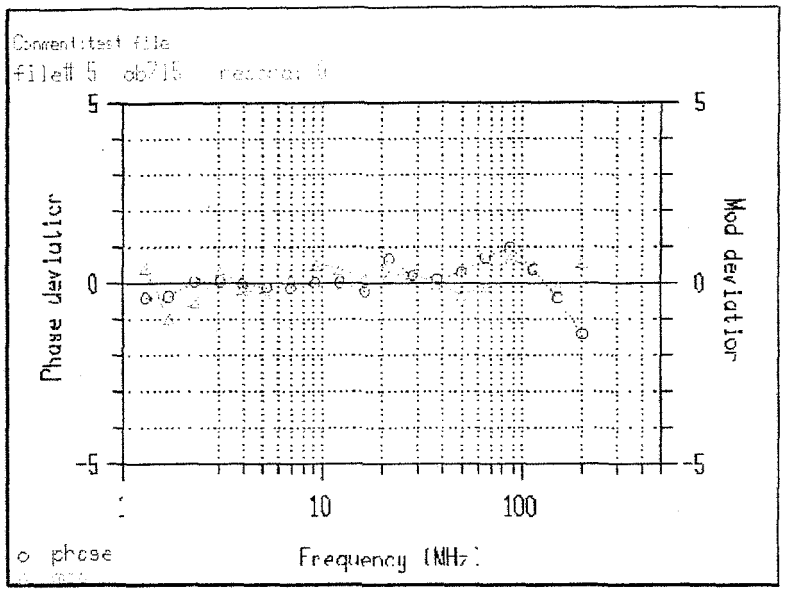

Figure C-8 – Deviation of phase (blue circles) and modulation (green triangles) for trial #5, fitting the data to a triple exponential decay.

A correlated error analysis was performed in order to see if the minimum found was local or global. The correlated error is found by fixing one parameter at values around the value found with the initial minimization, and the other parameters are varied to minimize χ^2. This produces chi-squared plots for each variable. If a global minimum is found, the plots should be parabolic in nature. Chi-squared plots for the parameters in this minimization are shown in Figures C-9 through C-21. The dashed red lines indicate the point at which the χ^2 value has increased by 67%. Note that $f_1+f_2+f_3 = 1$.

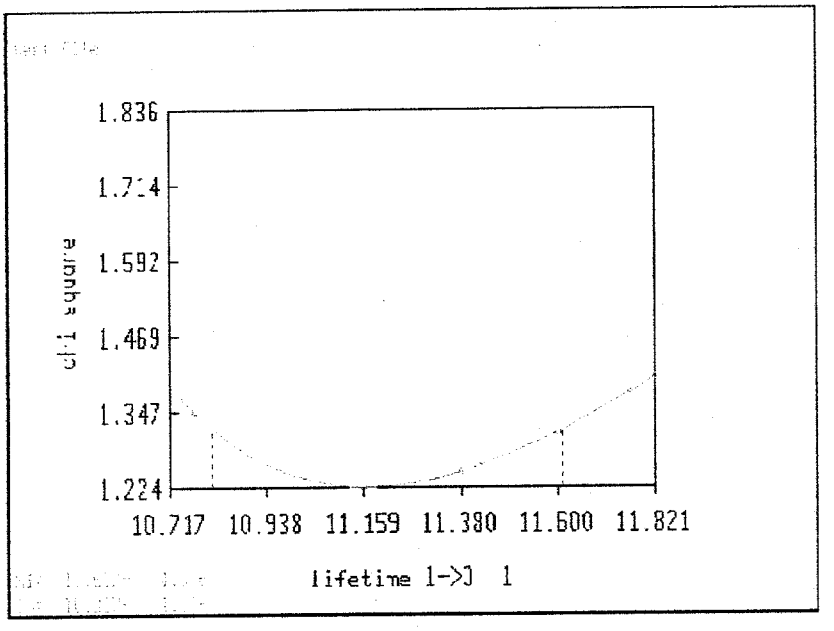

Figure C-9 – Chi-squared plot for the first lifetime (τ_1). The value of τ_1 ranges from 10.813 to 11.612 nsec.

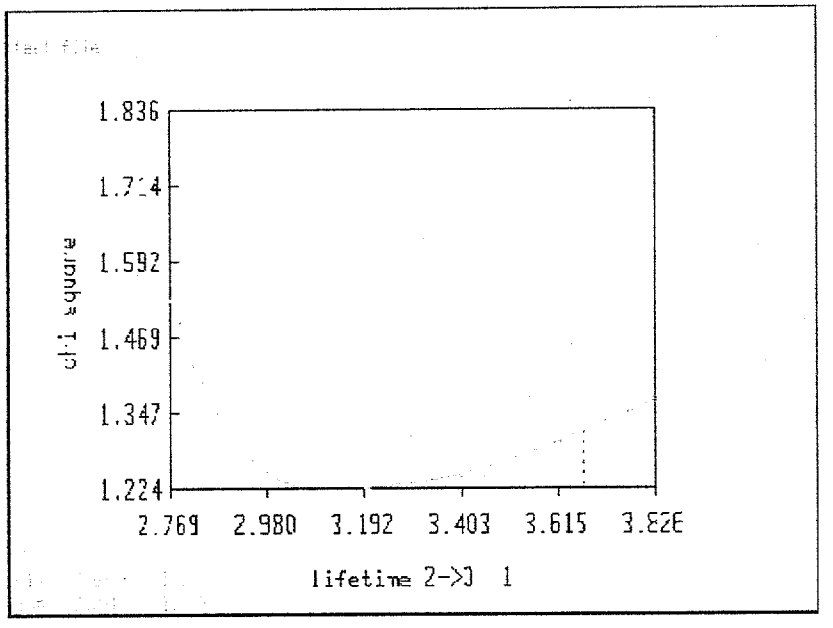

Figure C-10 – Chi-squared plot for the second lifetime (τ_2). The value of τ_2 ranges from 2.876 to 3.673 nsec.

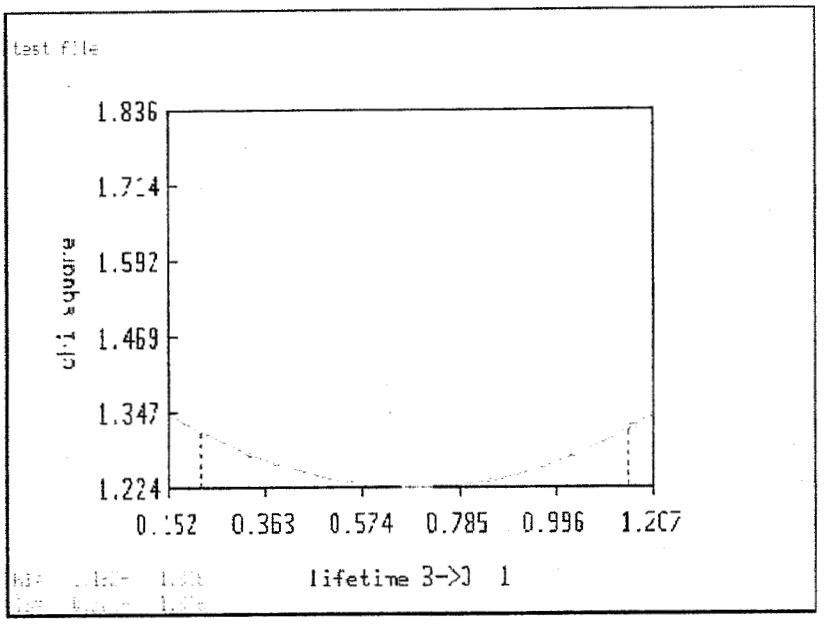

Figure C-11 – Chi-squared plot for the third lifetime (τ_3). The value of τ_3 ranges from 0.221 to 1.152 nsec.

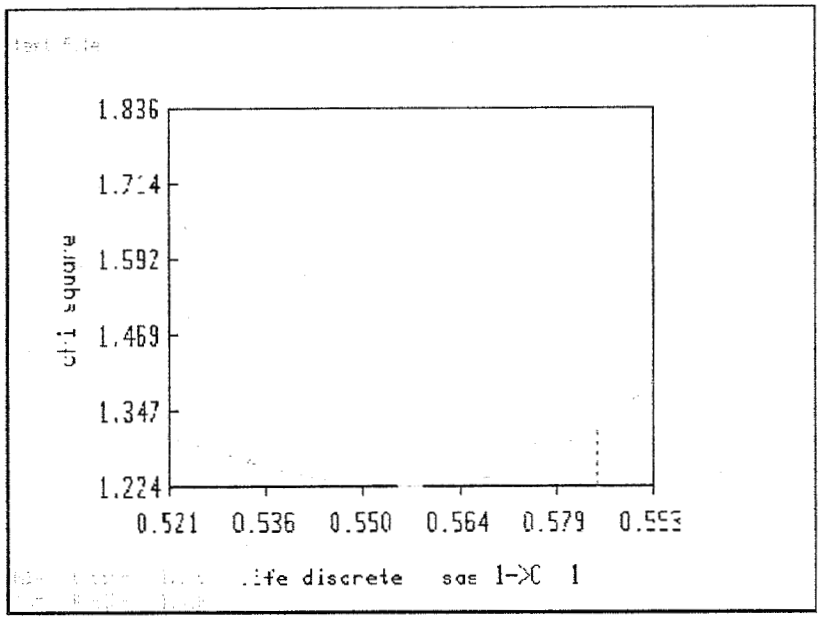

Figure C-12 – Chi-squared plot for the fractional contribution of the first lifetime (f_1) in trial #1. The value of f_1 ranges from 0.518 to 0.585.

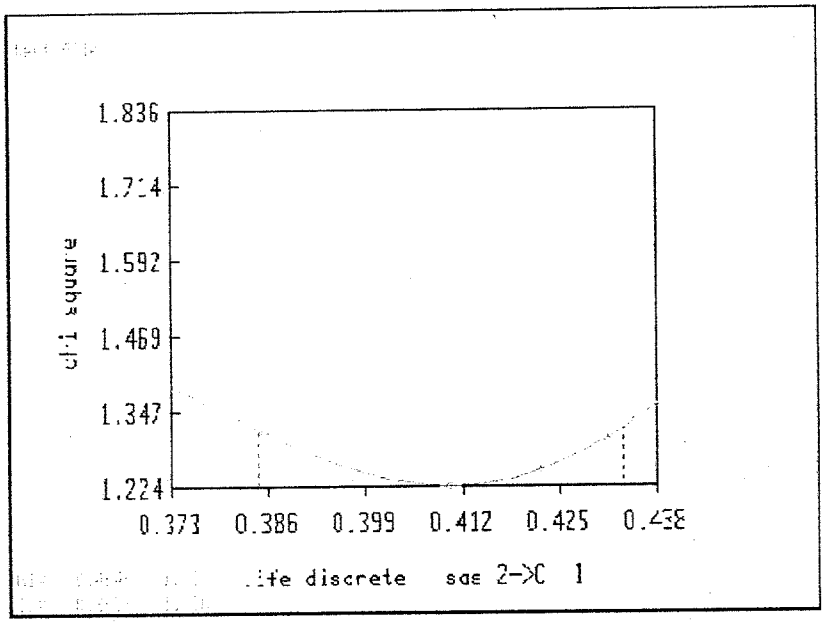

Figure C-13 – Chi-squared plot for the fractional contribution of the second lifetime (f_2) in trial #1. The value of f_2 ranges from 0.386 to 0.434.

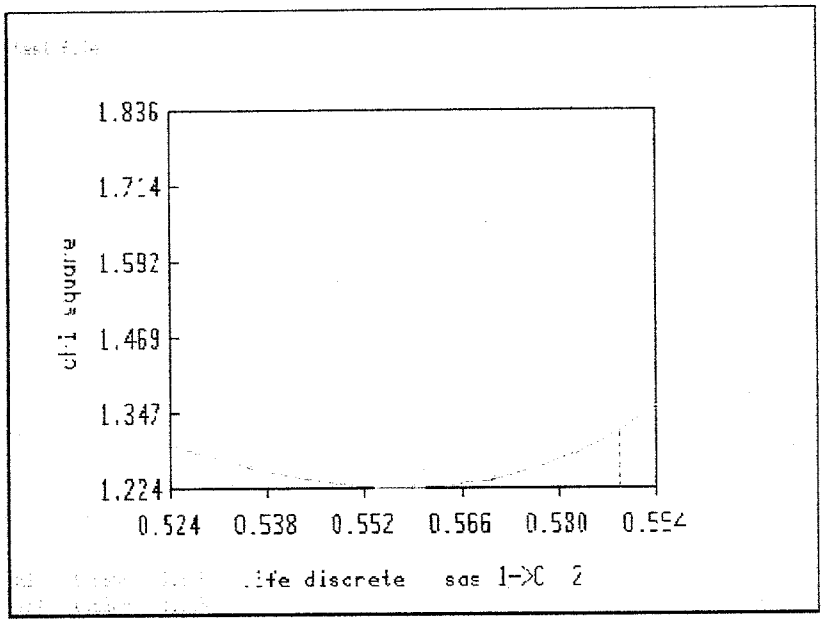

Figure C-14 – Chi-squared plot for the fractional contribution of the first lifetime (f_1) in trial #2. The value of f_1 ranges from 0.518 to 0.589.

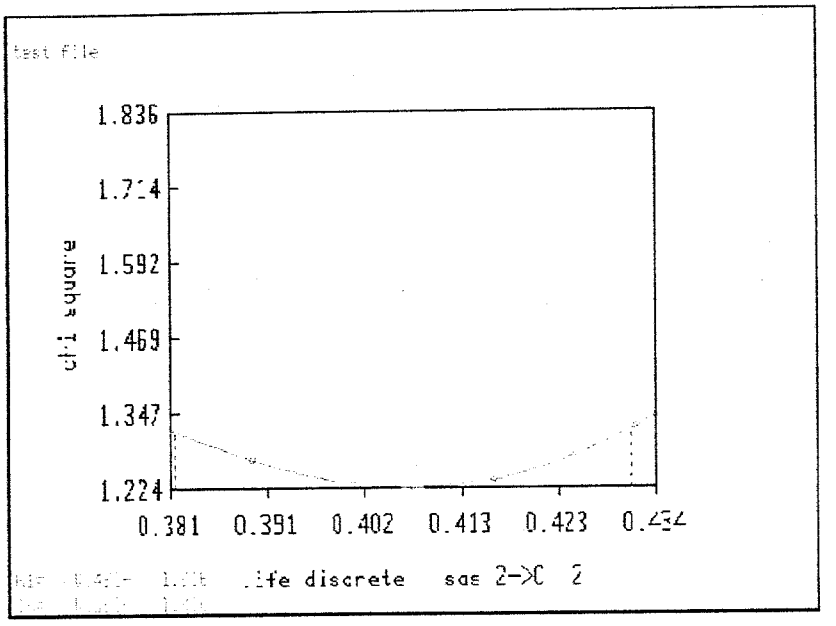

Figure C-15 – Chi-squared plot for the fractional contribution of the second lifetime (f_2) in trial #2. The value of f_2 ranges from 0.381 to 0.431.

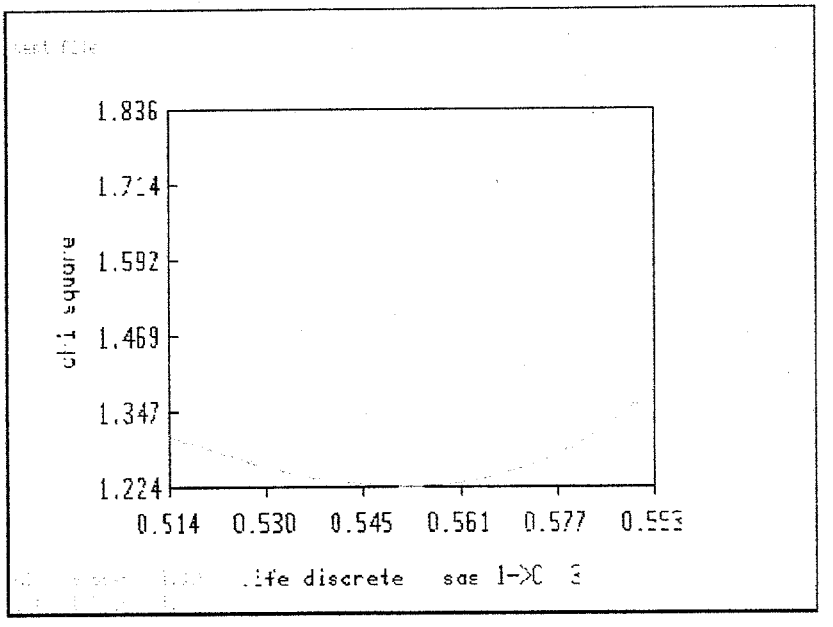

Figure C-16 – Chi-squared plot for the fractional contribution of the first lifetime (f_1) in trial #3. The value of f_1 ranges from 0.514 to 0.584.

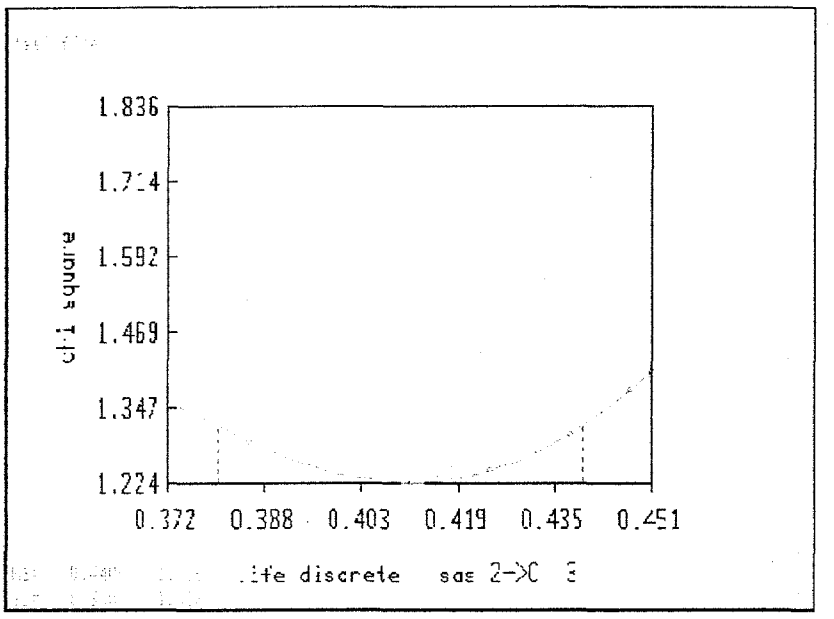

Figure C-17 – Chi-squared plot for the fractional contribution of the second lifetime (f_2) in trial #3. The value of f_2 ranges from 0.380 to 0.440.

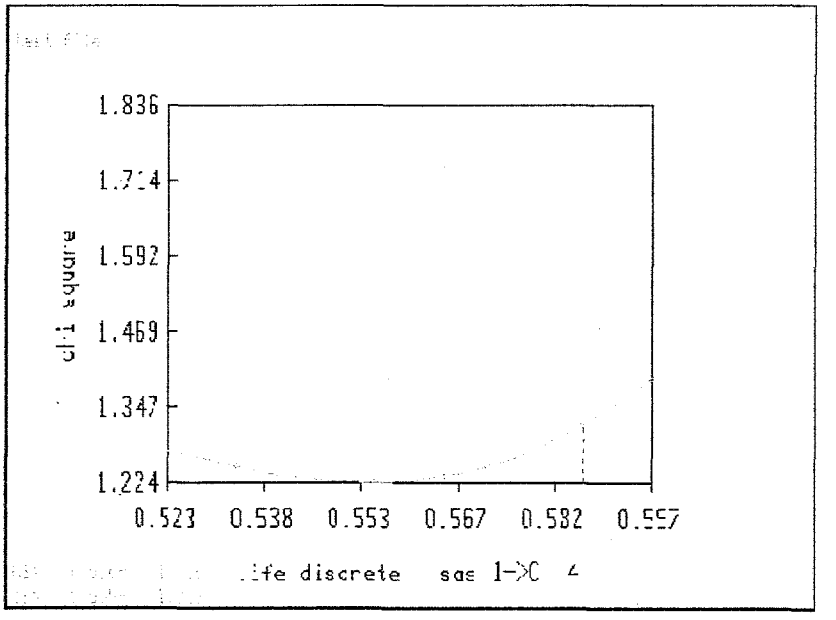

Figure C-18 – Chi-squared plot for the fractional contribution of the first lifetime (f_1) in trial #4. The value of f_1 ranges from 0.509 to 0.586.

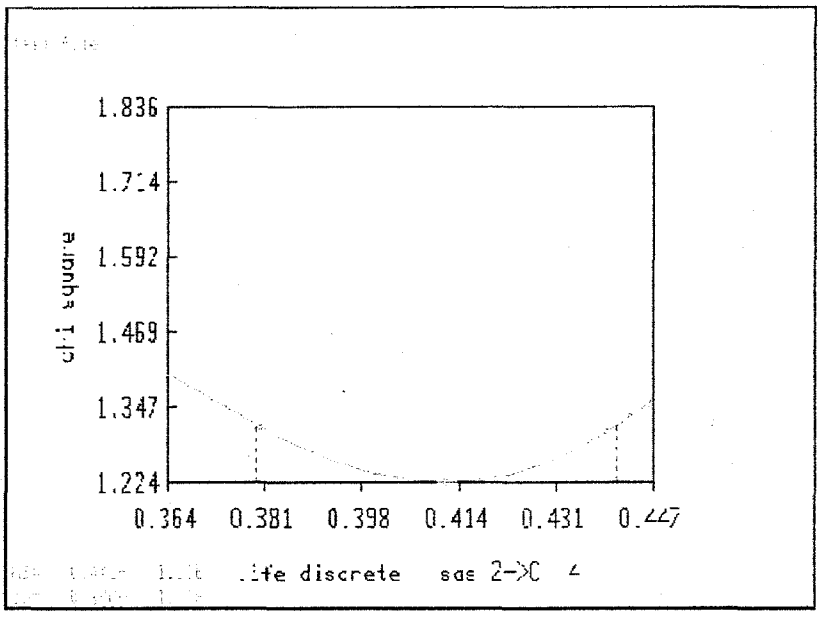

Figure C-19 – Chi-squared plot for the fractional contribution of the second lifetime (f_2) in trial #4. The value of f_2 ranges from 0.380 to 0.441.

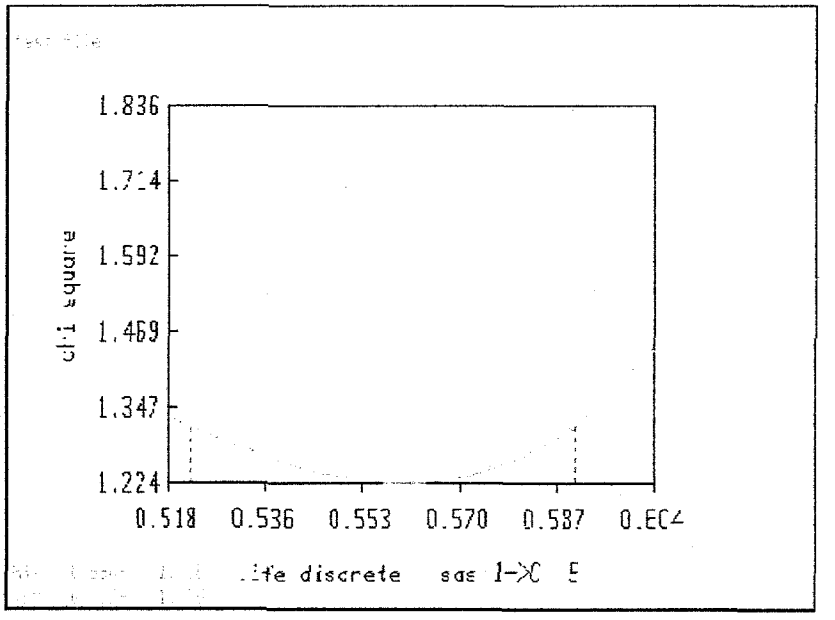

Figure C-20 – Chi-squared plot for the fractional contribution of the first lifetime (f_1) in trial #5. The value of f_1 ranges from 0.522 to 0.590.

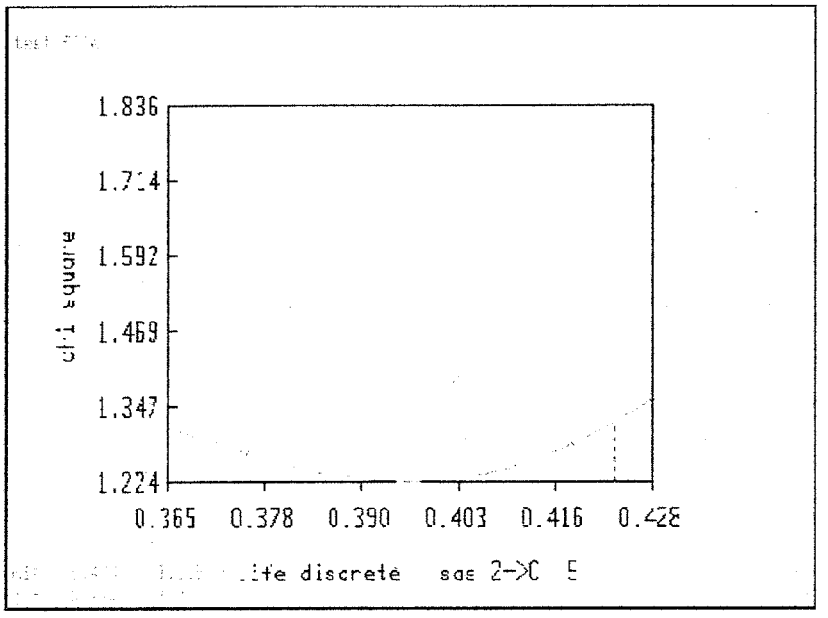

Figure C-21 – Chi-squared plot for the fractional contribution of the second lifetime (f_2) in trial #5. The value of f_2 ranges from 0.364 to 0.423.

REFERENCES

Atzeni, S.H., Ph.D. Jobin Yvon Horiba. *Personal communication*, 1997.

Beechem, J.M., E. Gratton, et al. Globals Unlimited, Technical Reference Manual, Revision 3. Board of Trustees, University of Illinois, 1998.